Evaluation of monsoon seasonality and the tropospheric biennial oscillation transitions in observations and CMIP models

Author:
Li, Yue

Publication Date:
2013

DOI:
https://doi.org/10.26190/unsworks/16193

Evaluation of monsoon seasonality and the tropospheric biennial oscillation transitions in observations and CMIP models

Yue Li

A thesis in fulfilment of the requirements for the degree of
Masters by Research

School of Biological, Earth and Environmental Sciences
Faculty of Science

March 2013

PLEASE TYPE

THE UNIVERSITY OF NEW SOUTH WALES

Thesis/Dissertation Sheet

Surname or Family name: **Li**

First name: **Yue** Other name/s:

Abbreviation for degree as given in the University calendar: **Master by Research**

School: **School of Biological, Earth and Environmental Sciences** Faculty: **Faculty of Science**

Title: **Evaluation of monsoon seasonality and the tropospheric biennial oscillation transitions in observations and CMIP models**

Abstract 350 words maximum: (PLEASE TYPE)

The Indian and Australian summer monsoon systems have considerable socioeconomic and environmental importance. Here we investigate monsoon seasonality, biennial variability and the interaction with Tropical sea surface temperatures (SST) in the Indo-Pacific sector. We consider a variety of observational and reanalysis products and also assess climate models from the Coupled Model Intercomparison Project Phase 3 and 5 (CMIP3 and CMIP5). In particular, the transitions between successive Indian and Australian monsoons, that form essential parts of the Tropospheric Biennial Oscillation (TBO) have been evaluated. We use Monte Carlo statistical techniques to examine the predictive skill that is inherent in these monsoon transitions and investigate the possible teleconnections between SST anomalies in the Indo-Pacific region, particularly associated with the El Niño-Southern Oscillation (ENSO).

Most climate models reproduce enhanced rainfall in the correct seasons for both the Indian and Australian monsoons. However, there are a number of biases in wet season duration and rainfall strength. While little improvement is seen in the overall strength of the monsoon rainfall from CMIP3 to CMIP5, there is a clear improvement in the seasonality particularly in simulating low rainfall rates outside of the monsoon season.

***Enhanced predictability* associated with the Indian-Australian monsoon in-phase transition is present in all observational and reanalysis datasets and most CMIP climate models, i.e. we have some skills in predicting whether an Australian monsoon will be stronger/weaker than normal, given information on the strength of preceding Indian monsoon. The SST anomalies in the Niño 3.4 region in December-March (DJFM) after the Indian monsoon season appear to be important for this transition. For the Indian-Indian monsoon out-of-phase transition, *enhanced predictability* only occurs in long-term observations but with little consistency across models. DJFM SST anomalies in the Niño 3.4 region over successive years appear to strongly affect this transition. The *enhanced predictability* for the other transitions shows little consistency between observational and reanalysis datasets, climate models and time periods. Multi-decadal variability in the TBO transitions is clearly seen in both observational and reanalysis products and climate models.**

Declaration relating to disposition of project thesis/dissertation

I hereby grant to the University of New South Wales or its agents the right to archive and to make available my thesis or dissertation in whole or in part in the University libraries in all forms of media, now or here after known, subject to the provisions of the Copyright Act 1968. I retain all property rights, such as patent rights. I also retain the right to use in future works (such as articles or books) all or part of this thesis or dissertation.

I also authorise University Microfilms to use the 350 word abstract of my thesis in Dissertation Abstracts International (this is applicable to doctoral theses only).

…… …… ……

Signature Witness Date

The University recognises that there may be exceptional circumstances requiring restrictions on copying or conditions on use. Requests for restriction for a period of up to 2 years must be made in writing. Requests for a longer period of restriction may be considered in exceptional circumstances and require the approval of the Dean of Graduate Research.

FOR OFFICE USE ONLY Date of completion of requirements for Award:

THIS SHEET IS TO BE GLUED TO THE INSIDE FRONT COVER OF THE THESIS

ORIGINALITY STATEMENT

‘I hereby declare that this submission is my own work and to the best of my knowledge it contains no materials previously published or written by another person, or substantial proportions of material which have been accepted for the award of any other degree or diploma at UNSW or any other educational institution, except where due acknowledgement is made in the thesis. Any contribution made to the research by others, with whom I have worked at UNSW or elsewhere, is explicitly acknowledged in the thesis. I also declare that the intellectual content of this thesis is the product of my own work, except to the extent that assistance from others in the project's design and conception or in style, presentation and linguistic expression is acknowledged.’

Signed .....

Date .....

Table of Contents Page

Acknowledgements

Foremost, I would like to express my greatest gratitude to my supervisor, Dr. Alex Sen Gupta, for his continuous support to my Master study and research. He patiently provided his encouragement, vision and advice for me to proceed through the master program. Without his guidance in all the time of research and writing-up, I couldn’t complete my project and thesis successfully.

Special thanks go to Dr. Nicolas Jourdain for his technique supports, guidance and helpful suggestions on research and thesis. I would like to acknowledge my co-supervisors, Dr. Andréa Taschetto and Dr. Caroline Ummenhofer. Their continuous guidance and support helped me comprehend my project. I owe them my heartfelt appreciation. I would also like to thank Dr. Wenju Cai, Dr. Jingjia Luo and Dr. Karumuri Ashok. The conversations with them inspired me with independent and critical thinking and broadened my horizons.

I would like to thank the ARC Centre of Excellence for Climate System Science (COECSS) and the Climate Change Research Centre (CCRC) for funding me to conduct my research and offering me opportunity of study and communicating with external experts. I also acknowledge the World Climate Research Programme's Working Group on Coupled Modelling, which is responsible for CMIP, and thank the climate modelling groups for producing and making available their model output for CMIP, the U.S. Department of Energy's Program for Climate Model Diagnosis and Intercomparison provides coordinating support and led development of software infrastructure in partnership with the Global Organization for Earth System Science Portals.

I would like to express my last special gratitude to my parents. Without their encouragement, unconditional support and immense love, I couldn’t finish this journal alone. I hope that this work makes them proud.

List of Abbreviations

AIR	All-Indian Rainfall
AMRI	Australian Monsoon Rainfall Index
AWAP	Australian Water Availability Project
CGCM	Coupled atmosphere-ocean General Circulation Model
CMIP3/CMIP5	Coupled Model Intercomparison Project Phase 3/ Phase 5
CMAP	Climate Prediction Center Merged Analysis of Precipitation dataset
DJFM/DJF	Austral summer, December-January-February-March/December-January-February
EEIO	Eastern Equatorial Indian Ocean
EMI_A	El Niño Modoki Index Region A (165°E-140°W, 10°S-10°N)
EMI_B	El Niño Modoki Index Region B (110°W-70°W, 15°S-5°N)
EMI_C	El Niño Modoki Index Region C (125°E-145°E, 10°S-20°N)
ENSO	El Niño -Southern Oscillation
EX-AMRI	Extended Australian Monsoon Rainfall Index
EX-IMRI	Extended Indian Monsoon Rainfall Index
GPCC	The Global Precipitation Climatology Centre dataset
GPCP	The Global Precipitation Climatology Project datasets
HadISST1	Hadley Centre Sea Ice and Sea Surface Temperature dataset version 1
IMRI	Indian Monsoon Rainfall Index
IOB	Indian Ocean Basin-wide
IOD	Indian Ocean Dipole
IPCC	Intergovernmental Panel on Climate Change
IPO	Interdecadal Pacific Oscillation
JJAS/JJA	Boreal summer, June-July-August-September/ June-July-August
MAM	March-April-May
MMM	Multi-Model Ensemble Mean
MJO	Madden-Julian Oscillation
NCEP/NCAR	The National Center for Atmospheric Prediction and the National Center for Atmospheric Research
NINO3	SST index from Niño-3 region (90°W-150°W, 5°S-5°N)
NINO3.4	SST index from Niño-3.4 region (5°N-5°S, 170°W-120°W)
RCP8.5	Representative Concentration Pathway with the highest global anthropogenic radiative forcing, reaching approximately 8.5 W/m^2 by 2100
SD	Standard Deviation
SON	September-October-November
SST	Sea Surface Temperature
TBO	Tropospheric Biennial Oscillation
WEIO	Western Equatorial Indian Ocean

List of Figures

List of Tables

Abstract

The Indian and Australian summer monsoon systems have considerable socioeconomic and environmental importance. Here we investigate monsoon seasonality, biennial variability and the interaction with Tropical sea surface temperatures (SST) in the Indo-Pacific sector. We consider a variety of observational and reanalysis products and also assess climate models from the Coupled Model Intercomparison Project Phase 3 and 5 (CMIP3 and CMIP5). In particular, the transitions between successive Indian and Australian monsoons, that form essential parts of the Tropospheric Biennial Oscillation (TBO) have been evaluated. We use Monte Carlo statistical techniques to examine the predictive skill that is inherent in these monsoon transitions and investigate the possible teleconnections between SST anomalies in the Indo-Pacific region, particularly associated with the El Niño-Southern Oscillation (ENSO).

Most climate models reproduce enhanced rainfall in the correct seasons for both the Indian and Australian monsoons. However, there are a number of biases in wet season duration and rainfall strength. While little improvement is seen in the overall strength of the monsoon rainfall from CMIP3 to CMIP5, there is a clear improvement in the seasonality particularly in simulating low rainfall rates outside of the monsoon season.

Enhanced predictability associated with the Indian-Australian monsoon in-phase transition is present in all observational/reanalysis datasets and most CMIP climate models, i.e. we have some skills in predicting whether an Australian monsoon will be stronger/weaker than normal, given information on the strength of preceding Indian monsoon. The SST anomalies in the Niño 3.4 region in December-February (DJFM) after the Indian monsoon season appear

to be important for this transition. For the Indian-Indian monsoon out-of-transition, *enhanced predictability* only occurs in long-term observations but with little consistency across models. DJFM SST anomalies in the Niño 3.4 region over successive years appear to strongly affect this transition. The *enhanced predictability* for the other transitions shows little consistency between observational/reanalysis datasets, climate models and time periods. Multi-decadal variability in the TBO transitions is clearly seen in both observational/reanalysis products and climate models.

Chapter 1. Introduction

1.1 Global monsoon

Monsoon is one of the most complex coupled atmosphere-land-ocean climate phenomena. They are characterized by seasonal reversals of prevailing surface winds and subsequent changes in precipitation. Many efforts have been made to distinguish the monsoon from other forms of climate variability. *Wang* [1994] delineated the tropical monsoon regime using outgoing long-wave radiation and monthly frequency of highly reflective cloud. *Wang and Ding* [2008] also derived a monsoon precipitation index that is the ratio of the annual range over the annual mean precipitation to identify the monsoon regions. *Wang and Ding* [2006] defined the monsoon domain by two criteria: 1) where the annual range of rainfall exceeds 180 mm, and 2) the local summer precipitation is more than 35% of annual rainfall. Based on their definition, eight regional monsoon systems have been recognized and documented (shown in Figure 1.1): the Indian monsoon [e.g. *Schott et al.*, 2009], the Western North Pacific monsoon [e.g. *Li and Wang*, 2005], the East Asian monsoon [e.g. *Wang et al.*, 2008b], the Australian monsoon [e.g. *Smith et al.*, 2008], the Northern African monsoon [e.g. *Okumura and Xie*, 2004], the Southern African monsoon [e.g. *Hastenrath et al.*, 1995], the North American monsoon [e.g. *Adams and Comrie*, 1997] and the South American monsoon [e.g. *Zhou and Lau*, 1998].

Monsoon-related variability significantly influences many countries at low-mid latitudes. In addition the associate release of energy drives changes to the local atmospheric circulation that can propagate away from the tropical region and influence climate in middle and high latitudes through teleconnection patterns. Thus, there is far-reaching importance for comprehensively understanding

monsoon dynamics and improving monsoon systems predictability.

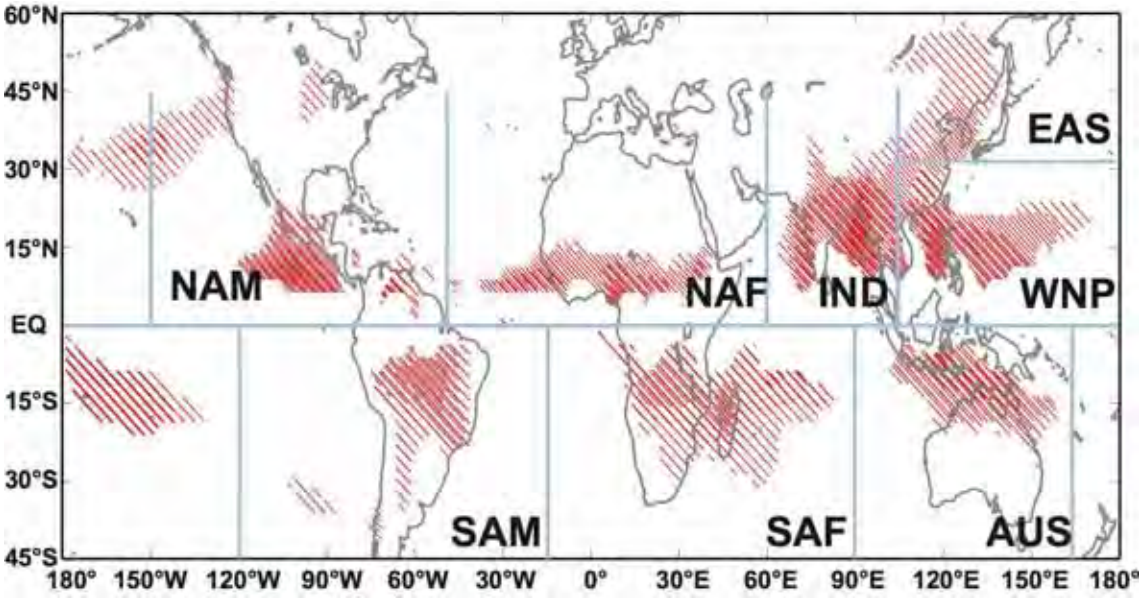

Figure 1.1 Global monsoon precipitation domains. The regional monsoons are the North and South American monsoon (NAM and SAM), the North and South African monsoon (NAF and SAF), the Indian monsoon (IND), the East Asian monsoon (EAS), the Western North Pacific monsoon (WNP) and the Australian monsoon (AUS). The monsoon domains are defined according to *Wang and Ding* [2006] (hatched in red). The annual range here is calculated as the absolute difference in rainfall between local summer and winter (June-July-August, JJA, for boreal summer/austral winter and December-January-February, DJF, for boreal winter/austral summer). Data used: Climate Prediction Center Merged Analysis of Precipitation (CMAP; 1979-2010) [*Xie and Arkin*, 1997].

1.2 Indian-Australian summer monsoon system

This study examines the complex interactions between two of the above monsoon systems, that is, the Indian and Australian monsoon systems. The Indian monsoon is typical continental monsoons, which is primarily driven by land-ocean temperature contrast [e.g. *Clark et al.*, 2000; *Kawamura*, 2002]. Figure 1.2 represents the rain-belt migration and surface wind reversal

associated with the monsoon season. In boreal summer (Figure 1.2a), the Asian land mass heats up faster than the surrounding ocean and a surface low pressure gradually develops over the land, resulting in a land-ocean pressure gradient. The pressure gradient leads to considerable moisture flow from the ocean, subsequently resulting in large-scale rainfall over the land. The latent heat release due to the strong convection provides an important feedback to enhance the monsoon circulation. This process is associated with the Indian summer monsoon. The thermal and pressure gradients between continent and ocean caused by the differential heat capacity of land and ocean are fundamental initial mechanisms of driving this monsoon cycle while the induced convections amplify the monsoon. The situation reverses in boreal winter (Figure 1.2b). The development of land-sea pressure gradient as the air over land is cooler and denser than that over ocean leads to wind blowing from the landmass, which drives the winter monsoon (the Australian summer monsoon). However, the Australian summer monsoon is not simply the reversal of the Indian summer monsoon. The land-sea thermal contrast favours but does not appear to be the fundamental driver to the Australian summer monsoon, and the role of land-sea contrast can be replaced by the longitudinal sea surface temperature (SST) gradient [*Chao and Chen*, 2001]. In addition, the monsoon cycle is also modified by moisture exchange between the ocean, atmosphere, and land [e.g. *Clark et al.*, 2000]. As summer monsoons show far-reaching importance to people living in those regions, this study attempts to examine the potential predictability of this complex system associated with the interaction between the Indian and Australian summer monsoons.

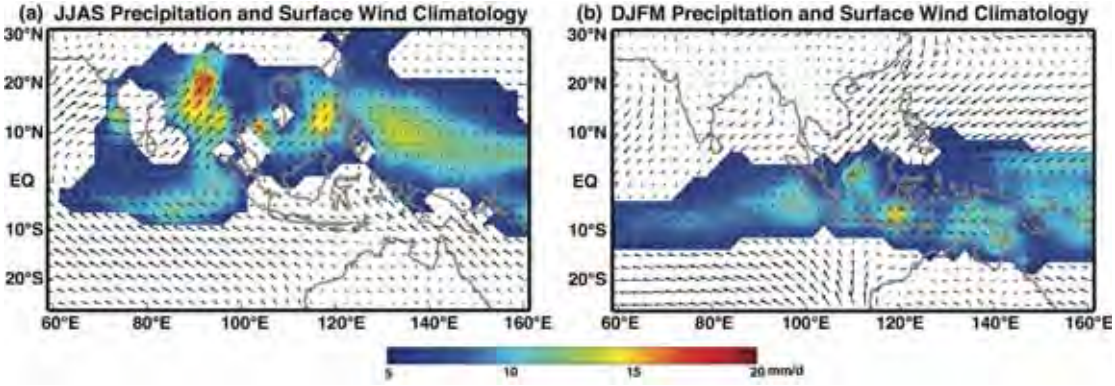

Figure 1.2 shows the precipitation and surface wind climatology composite in (a) boreal summer (JJAS) and (b) austral summer (DJFM). The Climate Prediction Center Merged Analysis of Precipitation data (CMAP; 1979-2010) [*Xie and Arkin*, 1997] were used to show the rain belt migration. Only the rainfall greater than 5.5 mm/day is shown. The surface wind is synthesized from 1000 hPa v-wind and u-wind with unit of m/s from the NCEP/NCAR Reanalysis Project (1948-2011) [*Kalnay et al.*, 1996].

1.3 Monsoon impacts

The Indian-Australian summer monsoon is very important for countries in the affected areas, especially on the agrarian-based countries that depend on abundant solar radiation and adequate rainfall brought by monsoons. A normal monsoon usually produces abundant rainfall that is necessary for successful crop growth. A failure in the monsoon can have a devastating impact on agriculture, fishery and societies. *Webster and Tomas* [1998], for example, showed a positive correlation between the Indian rice production and local rainfall. *McCreary et al.* [1996] showed a corresponding relationship between the prosperity of fisheries along the western Indian Ocean and Indian summer monsoon. This prosperity results from an intense phytoplankton bloom off Somalia due to nitrate input along coastal regions as a result of deep coastal upwelling associated with Indian summer monsoonal winds. Conversely, excessive anomalous monsoon rainfall may bring catastrophic floods to

monsoon regions. The austral summer of 2011 (December 2010 – February 2011) is an extraordinary example of strongly anomalous monsoon conditions triggered by strong La Niña conditions. During this season, Queensland experienced severe flooding. The Indian-Pakistan region also experienced its worst recorded flooding caused by the anomalous Indian summer monsoon during the La Niña episode in 2010 [*Mujumdar et al.*, 2012]. Thus, the correct forecast of monsoon rainfall is very important, and numerous attempts have been made to understand the variability of the Indian-Australian monsoon and the interactions among the components of this system.

1.4 Monsoon variability

The Indian-Australian monsoon regions not only show strong seasonality in wind and rainfall, but also exhibit large variability on intraseasonal, interannual, and interdecadal timescales. In terms of intraseasonal varability, *Hendon and Liebmann* [1990] examined the 850hPa zonal wind and rainfall in Darwin and revealed an intraseasonal oscillation pattern in summer monsoonal wind and rainfall. During boreal summer, Indian monsoon rainfall also exhibits a 40-day spectral peak that is associated with the Madden-Julian Oscillation (MJO) which is associated with “break” and “active” phases of the monsoon [*Hartmann and Michelsen*, 1989].

Numerous studies have examined the external drivers that contribute to the interannual and interdecadal variability of this monsoon system. These include the El Niño -Southern Oscillation (ENSO) [e.g. *Webster and Yang*, 1992; *Meehl and Arblaster*, 1998; *Wang et al.*, 2008a; *Boschat et al.*, 2010], the Indian Ocean Dipole (IOD) [e.g. *Ashok et al.*, 2001; *Schott et al.*, 2009], the Interdecadal Pacific Oscillation (IPO) [e.g. *Arblaster et al.*, 2002; *Meehl and Arblaster*, 2012] and Eurasian snow cover [*Vernekar et al.*, 1995]. *Suhas et al.*

[2012] argued that in addition to the aforementioned external drivers, the monsoon characteristics are also modulated by internal processes, such as the interaction between convection and the large-scale circulation, and the intraseasonal oscillation of the monsoon system.

1.5 Tropospheric Biennial Oscillation (TBO)

A biennial signal in the Indian-Australian summer monsoon system and the wider tropical Indo-Pacific region has been described in numerous studies in both observations and models [e.g. *Meehl*, 1987; 1994a; 1997; *Chang and Li*, 2000; *Meehl and Arblaster*, 2002; *Loschnigg et al.*, 2003; *Fasullo*, 2004; *Li et al.*, 2006]. This characteristic pattern has been named the Tropospheric Biennial Oscillation (TBO). *Meehl and Arblaster* [2002] defined the TBO as a tendency for a relatively strong monsoon to be followed by a relatively weak one, and vice versa one year later. Numerous studies have attempted to determine the mechanisms that might give rise to the TBO. *Meehl* [1993; 1994b; 1994a; 1997] depicted a complex TBO mechanism that consists of the coupled ocean-atmosphere and land-atmosphere biennial sub-mechanisms. Meehl's hypothesis is constructed on three premises: 1) at any given location in the Indian-Pacific region, there is only once when strong convection associated with summer monsoon reaches its maximum every year; 2) the corresponding air-sea coupling becomes strong at that time, and 3) the ocean and land have the capability to maintain the temperature condition for one year, and this persistent temperature condition could then feedback onto the monsoon system. *Chang and Li* [2000] were able to reproduce a TBO-like phenomenon using a simplified five-box tropical atmosphere-ocean-land model. Figure 1.3 illustrates the complex TBO mechanism synthesizing the mechanisms described in *Meehl* [*Meehl*, 1997; 2008] and *Chang and Li* [*Chang and Li*, 2000; 2009]. In Figure 1.3, during a strong Indian monsoon season, the monsoon heating and

convection over the Indian subcontinent induces anomalous westerlies in the Indian Ocean and also intensifies a large scale Walker Circulation that leads to easterly anomalies in the central Pacific. The westerly anomalies in the Indian Ocean help cool down the local SST, while the easterly anomalies in the central Pacific facilitate the deepening of the thermocline in the western Pacific thus increasing the surface temperature. The warm SST in the western Pacific persists to boreal autumn. The evaporation over the warm pool in the western Pacific is increased bringing enhanced convection and moisture convection convergence into the North Australia leading to a strong Australian summer monsoon. The warming in the western Pacific induces a stronger local Walker cell over the Indian Ocean and helps the cold SST anomalies (that developed after the strong Indian monsoon) to persist until the following boreal summer. This then leads to a weaker Indian summer monsoon. A new cycle starting from a weak Indian monsoon begins.

While the TBO is primarily associated with changes in the large-scale atmosphere-land-ocean circulation, there is some evidence that it is also modulated by the stratospheric Quasi-Biennial Oscillation (QBO). *Mohankumar and Pillai* [2008] found that the QBO in the lower stratosphere can modulate the monsoon winds and rainfall thereby affecting the TBO cycle.

The box model of *Chang and Li* [2000] shows highly biennial behaviour. However, in reality the biennial nature of the TBO and the associated transitions are quite irregular and varies on multi-decadal timescales (e.g. *Fasullo* [2004], *Yu and Janiga* [2007]). To address the causes of such an irregularity, *Li et al.* [2001] modified the simple 5-box model of *Chang and Li* [2000] by considering remote and local ocean-atmosphere-land interaction processes. Their results implied that the irregularity is likely to result from

nonlinear interactions with other time scale variability, such as MJO, ENSO or even synoptic disturbances.

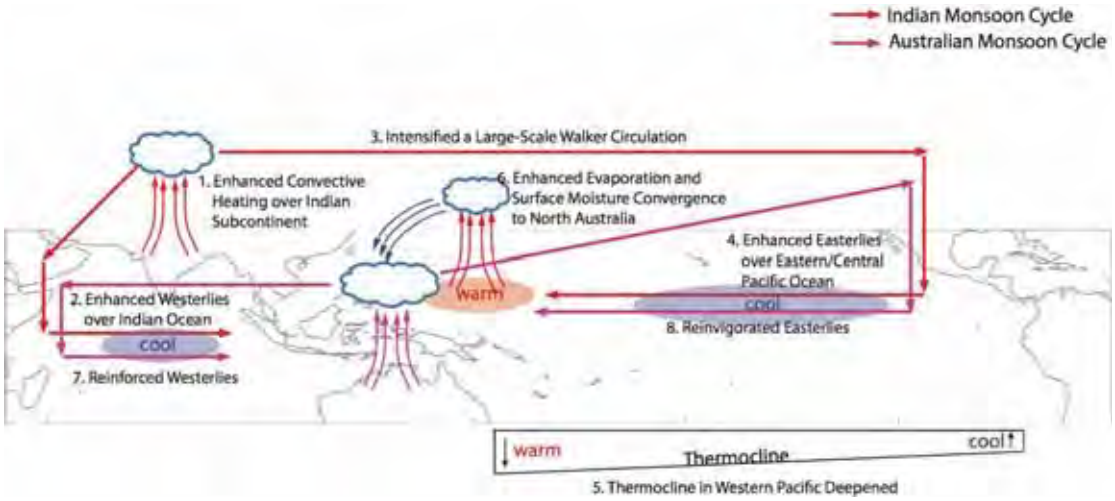

Figure 1.3 Diagram of the atmosphere-ocean-land mechanism of TBO. The red arrows represent the Indian monsoon cycle while the purple ones show the Australian monsoon cycle.

Many previous studies attempted to investigate a variety of external factors that influence the TBO and different TBO transition phases in the Indian-Australian summer monsoon system based on both observational analysis and model simulation. As described in previous studies (e.g. *Yu and Janiga* [2007], *Wu* [2008; 2009]), the monsoon transitions can be classified as “in-phase” and “out-of-phase”. In-phase transitions imply the transition from a strong/weak monsoon to a strong/weak monsoon. Out-of-phase transitions imply the transition from a strong/weak monsoon to a weak/strong monsoon. *Fasullo* [2004] found that the Indian-Indian monsoon out-of-phase transitions are related to ENSO conditions in observations. *Yu et al.* [2003] explored the independent roles of the Indian Ocean and the Pacific Ocean on TBO transitions by suppressing either the Indian Ocean or Pacific Ocean variability in a series of coupled atmosphere-ocean general circulation model (CGCM) experiments. They found that SST anomalies associated with ENSO-like patterns in the Pacific Ocean play an important role in the in-phase transitions

from a strong/weak Indian monsoon to a following strong/weak Australian monsoon. On the other hand, the basin-wide pattern of SST anomalies in the Indian Ocean is critical to the out-of-phase transition from a strong/weak Australian monsoon to a weak/strong Indian monsoon in the subsequent year. *Wu and Kirtman* [2004] mentioned that the roles of the Pacific SST anomalies in the TBO transitions are via either the Walker Circulation modulation or Rossby wave-type responses in surface winds over the Indian and Pacific Oceans. The SST anomalies in the Indian Ocean are primarily resulted from the response to the monsoon-ENSO system but contribute complementarily to TBO transitions. However, when the Pacific ENSO is suppressed in models, biennial transition between Indian monsoons, in-phase transition from Indian to Australian monsoon and out-of-phase transition from Australian to Indian monsoon can be accomplished through local air-sea interactions in the Indian Ocean [*Wu and Kirtman*, 2007; *Wu*, 2008; 2009]. In other words, there is some evidence that the TBO phenomena might be able to occur independently of ENSO variability at least in certain models.

The main scientific questions to be examined in this thesis are as follows:

1. Does the TBO mechanism improve seasonal forecasts of the Australian or Indian monsoon, either 6 months in advance or 12 months in advance?
2. How is the question above affected by the choice of dataset and the shortness of the observational record given the large natural variability in the tropical climate system?
3. Are the global climate models able to simulate the TBO? The question relates the evaluation of model skill for seasonal forecasts and our ability to identify robust mechanisms as models offer long time-series and better statistical significance.
4. Is the TBO more than just a response to ENSO variability?

Chapter 2. Methodology and datasets

For our examination of monsoon rainfall, we investigate the climatology and rainfall anomalies over four regions: the land-only Indian and the land-only Australian monsoon region (see the hatched areas in Figure 2.1), the extended Indian monsoon region (5°N-40°N, 60°E-100°E) and the extended Australian monsoon regions (20°S-5°N, 100°E-150°E, see the boxes in Figure 2.1). The land-only regions are considered for two reasons. Firstly, long-term land rainfall records are available for both Indian subcontinent and Australian landmass. For example, all-Indian monsoon rainfall index dates from 1871 [*Parthasarathy et al.*, 1994] and rainfall record from the Australian Water Availability Project traces back to 1900 [*Jones et al.*, 2009]. Secondly, land rainfall is a bigger concern than marine rainfall as human activities affected by rainfall are over land. As the oceans play important roles in monsoon processes, we also examine the extended monsoon regions. This is done as these larger regions may show more clear relationships with external drivers. In addition, previous studies (e.g. *Meehl* and *Arblaster* [2002], *Yu et al.* [2003], *Wu* [2008]) used these extended regions to identify the teleconnection of SST anomaly patterns in the Pacific to TBO transitions. To investigate the influence of the SST on summer monsoon rainfall, the SST anomalies in the Niño-3.4 region (5°N-5°S, 170°W-120°W) are examined. ENSO years in this study are defined using the classification of *Meyers et al.* [2007], updated by *Ummenhofer et al.* [2009]. These years were defined by comparing the filtered and adjusted SST indices to their ±1 standard deviation (SD) (See Appendix Table A.1).

2.1 Observations and reanalysis

In this study, we analyse two regional and four global observation-based and reanalysis precipitation products (see Table 2.1). The two regional

observation-based datasets are the homogeneous all-Indian monthly rainfall datasets (AIR) and the gridded high-quality daily rainfall data from Australian Water Availability Project (AWAP). The AIR time-series incorporates measurement from 306 rain-gauge stations over 30 meteorological subdivisions in India during the 1871-2009 period [*Parthasarathy et al.*, 1994]. The AWAP dataset is based on the Bureau of Meteorology daily recalibrated rain-gauge measurement, supplemented in data sparse areas by disaggregated monthly data [*Jones et al.*, 2009]. The AWAP rainfall is available from 1900 to 2009, on a 0.1°×0.1° latitude/longitude grid. In order to test the sensitivity of our results to the choice of dataset, we also employ four global observation and reanalysis gridded precipitation datasets: 1) the Climate Prediction Center Merged Analysis of Precipitation dataset (CMAP) with a

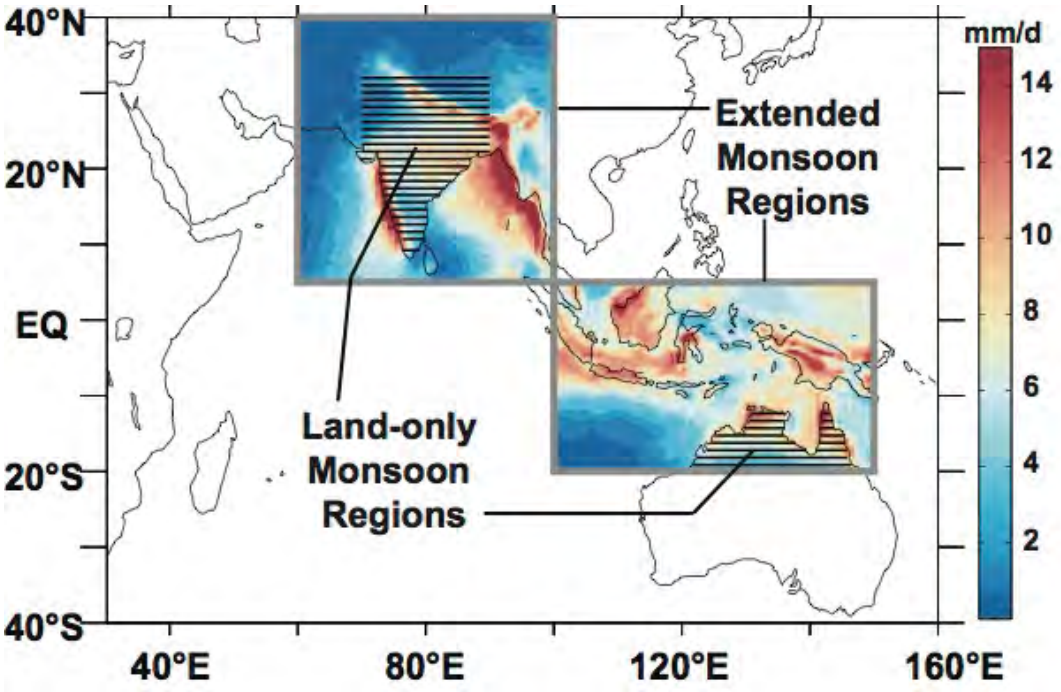

Figure 2.1 The hatched areas in the map show the land-only Indian and Australian monsoon regions that are used to calculate the IMRI and AMRI, and the boxes show the extended monsoon regions that are used to calculate the EX-IMRI and EX-AMRI. The colour bar indicates the mean JJAS rainfall for Indian monsoon and the mean DJFM rainfall for Australian monsoon in extended regions (from TRMM-3B43 data, averaged over 1998-2010 [*Adler et al.*, 2000]).

resolution of 2.5°×2.5° covering 1979-2008 [*Xie and Arkin*, 1996]; 2) the Global Precipitation Climatology Centre dataset (GPCC), land-only, with a resolution of 1°×1° from 1901 to 2010 [*Rudolf et al.*, 2010]; 3) the Global Precipitation Climatology Project datasets (GPCP) with a resolution of 2.5°×2.5° from 1979 to 2010 [*Adler et al.*, 2003]; and 4) the precipitation reanalysis from the National Center for Environmental Prediction and the National Center for Atmospheric Research (NCEP/NCAR) for the 1948-2010 period with a resolution of 2.5°×2.5° [*Kalnay et al.*, 1996]. GPCP and CMAP merge gauge and satellite observations, while GPCC is only based on rain gauge data. Rainfall from NCEP/NCAR is a model product (many observations are assimilated, but not rainfall).

Table 2.1 Precipitation and SST datasets used in this study.

	Data Acronym	**Period**	**Coverage**	**Resolution**	**References**
Observations	AIR	1871-2009	Indian Land		[*Parthasarathy et al.*, 1994]
	AWAP	1900-2009	Australian Land	0.1°×0.1°	[*Jones et al.*, 2009]
	GPCC	1901-2010	Global Land	1°× 1°	[*Rudolf et al.*, 2010]
	GPCP	1979-2010	Global	2.5°×2.5°	[*Adler et al.*, 2003]
Reanalysis	CMAP	1979-2008	Global	2.5°×2.5°	[*Xie and Arkin*, 1996]
	NCEP/NCAR	1948-2011	Global	2.5°×2.5°	[*Kalnay et al.*, 1996]
	HadISST1	1870-2010	Global Ocean	1°× 1°	[*Rayner et al.*, 2003]

The SST dataset used in this study is the Hadley Centre Sea Ice and Sea Surface Temperature dataset version 1 (HadISST1) from 1870 to 2011 with a resolution of 1°×1°. HadISST1 is reconstructed by a reduced-space optimal interpolation and then followed by a superposition of gridded SST observations onto the reconstruction [*Rayner et al.*, 2003]. The NINO3.4 index is derived from HadISST1 and used to examine the link between the monsoon rainfall and

ENSO (see section 3.1.4). The NINO3.4 index is defined as monthly SST anomalies averaged over the Niño-3.4 region (5°N-5°S, 170°W-120°W) from 1870 to 2010, with respect to the climatological seasonal cycle during the same period.

2.2 Model simulations

In sections 3.2.1 and 3.2.2, we investigate the rainfall from 24 CMIP3 models hindcast simulations (20c3m experiment) and 30 CMIP5 hindcast simulations (historical experiment). The CMIP3 simulations cover approximately the period of 1860-2000, while the CMIP5 simulations span approximately 1850-2005. Some models have several 'ensemble' historical simulations that vary only by the initial state. As tiny changes in the chaotic climate system will lead to different pathways for the system as a whole, model ensemble members with different starting states can take into account the influence of internal variability of the climate system. To examine the response of the TBO to anthropogenic forcing, there are 22 out of 30 CMIP5 models having outputs available from the highest representative concentration pathway RCP8.5 scenario [*Moss et al.*, 2010; *Riahi et al.*, 2011]. RCP8.5 is the scenario with the highest global anthropogenic radiative forcing used in the IPCC (Intergovernmental Panel on Climate Change) report, reaching approximately 8.5 W/m^2 by 2100. We consider the RCP8.5 scenario based on three reasons: 1) There are more model outputs available for RCP8.5 than other RCPs; 2) RCP8.5 is the highest emissions pathway so the forcing from RCP8.5 is stronger than other scenarios, so that the change in the monsoon due to anthropogenic forcing should be more manifest; and 3) the observed emission until 2012 is much closer to this scenario. In the final part, we compare the TBO predictability in a 50-year period between RCP8.5 and corresponding hindcast simulations of CMIP5. The RCP8.5 is chosen the year over 2051-2100 and the hindcast simulations cover

the period of 1956-2005.

The names of CMIP3 and CMIP5 models with the number of ensemble members used in this study are listed in Appendix Table A.2 and A.3. The CMIP5 models used to analyse the RCP8.5 scenario are marked in asterisk in Table A.3.

2.3 Monsoon rainfall indices

To evaluate the biennial variability of the Indian-Australian summer monsoon system, the land-only Indian monsoon rainfall index (IMRI), the land-only Australian monsoon rainfall index (AMRI) and the rainfall indices of extended monsoon regions (EX-IMRI and EX-AMRI) are constructed. Rainfall indices associated with Indian monsoon are calculated as the area averaged rainfall anomalies for JJAS while these associated with Australian monsoon are derived from the area averaged rainfall anomalies for DJFM. As the Australian monsoon starts around December and ends around March of the succeeding year, the year of indices that are associated with Australian monsoon is defined as the year of December. As such the length of the indices is one year shorter than the length of corresponding datasets (e.g. the AWAP dataset covers the period of 1900-2009, while AMRI-AWAP is 1900-2008). The reference IMRI is calculated from AIR dataset (Table 2.1), and therefore referred to as IMRI-AIR in the following. Other IMRIs, using the other datasets, are defined as the averaged JJAS rainfall anomalies over the Indian subcontinent (Figure 2.1). These indices are very similar to the IMRI-AIR. The only difference is that Himalaya is entirely included in our domain in order to be consistent with the various coarse model grids. Similarly, the reference AMRI is defined as the averaged DJFM rainfall anomalies over northern continental Australia (Figure 2.1) based on AWAP (Table 2.1) thus referred to as AMRI-AWAP in the

following. Other AMRIs, using the other datasets, are constructed using the same region. To answer the question of whether the variability of monsoon rainfall over ocean-included regions is different from the land-only regions, EX-IMRIs and EX-AMRIs are also derived from three global gridded precipitation datasets (GPCP, CAMP and NCEP/NCAR, see Table 2.1) over extended Indian and Australian regions, respectively.

The prefix of 'EX-' is added to IMRI or AMRI to distinguish the indices of extended regions from land-only regions, while the suffix of each index is to denote from which datasets the index is made. For instance, the IMRI-AIR represents the land-only Indian monsoon index derived from the AIR dataset; and EX-AMRI-CMAP represents the extended Australian monsoon index derived from the CMAP dataset. In order to focus in internal variability, rather than the long-term trend, all indices are detrended, and the climatological seasonal cycle, calculated over the entire dataset period, is removed.

Equivalent IMRI and AMRI indices for both CMIP3 and CMIP5 models are derived to examine the TBO transitions. NINO3.4 indices for the 30 CMIP5 models are also derived to investigate the teleconnection of SST in the tropical central Pacific to this monsoon system in the climate models. When presenting multi-model ensemble means we first average over ensemble members of individual models before averaging across models.

2.4 TBO transition definitions

A Monte Carlo technique is used to assess the significance of *enhanced predictability* of four transitions that are thought to be important for the TBO tendency. For a given year *t*, a successful TBO transition that consists of either positive or negative transitions are defined as follows:

(1) The Indian-Australian monsoon in-phase transition

Positive Transition: IMRI(t)>0 and AMRI(t)>0 or

Negative Transition: IMRI(t)<0 and AMRI(t)<0 ;

(2) The Indian-Indian monsoon out-of-phase transition

Positive Transition: IMRI(t)>0 and IMRI(t+1)<0 or

Negative Transition: IMRI(t)<0 and IMRI(t+1)>0;

(3) The Australian-Indian monsoon out-of-phase transition

Positive Transition: AMRI(t)>0 and IMRI(t+1)<0 or

Negative Transition: AMRI(t)<0 and IMRI(t+1)>0;

(4) The Australian-Australian monsoon out-of-phase transition

Positive Transition: AMRI(t)>0 and AMRI(t+1)<0 or

Negative Transition: AMRI(t)<0 and AMRI(t+1)>0.

The same definition is also applied on the extended monsoon regional indices EX-IMRIs and EX-AMRIs.

Figure 2.2 depicts the aforementioned definitions for land-only rainfall indices. We use blue and red bars to represent Indian and Australian monsoon rainfall indices, respectively. In Figure 2.2a & c, adjacent blue and red bars indicate the IMRI and AMRI in the same year. For Indian-Australian monsoon in-phase transitions (Figure 2.2a), we count the years when both colour bars are lower or higher than 0. If both blue and red bars in the same year are greater than 0, we count this year as a successful positive transition from the Indian to Australian monsoon. If both are lower than 0, that year is counted as successful negative Indian-Australian monsoon in-phase transition. For Australian-Indian monsoon out-of-phase transitions (Figure 2.2c), we compare a red-bar with a following blue-bar. If a red-bar is higher than 0 and the following blue-bar is lower than 0, we define this year as a successful positive Australian-Indian monsoon out-of-phase transition. If a negative red-bar is followed by a positive blue-bar,

this year is counted as a successful negative out-of-phase transition. In Figure 2.2b & d, we only need to compare the same colour bars in consecutive years. Positive transitions are counted when the positive bar is followed by a negative bar and counted vice versa for negative transitions. All successful positive and negative transition events are shaded in light blue and light red, respectively.

To determine the observed/simulated predictability associated with a given transition, we first count the number of successful transitions (denoted as N_o) in the observed time-series with N years, and then calculate the proportion of successful transitions (N_o/N). A Monte Carlo resampling technique is used to assess the significance of this proportion and assess how much *enhanced predictability* it implies over a random distribution. To do this, the time-series is randomly resampled 100,000 times (with replacement), and each time, we count the number of successful transitions (denoted as N_r) and calculate the proportion of successful transitions in the resampled time-series (N_r/N). The predictability of the monsoon resulting from a given transition is considered *enhanced* if the value of N_o/N is significantly higher than the median of all N_r/N values. Moreover, the *enhanced predictability* is considered significant at 90% if N_o/N lies in the upper decile of the N_r/N values (i.e. there is only a 10% probability getting a given *enhanced predictability* by chance). This method is also employed to assess the predictability associated with successful positive and negative transitions. First we count the number of successful positive and negative transitions, respectively (denoted as N_{PT} and N_{NT}) and the number of strong and weak monsoon years, respectively (denoted as N_S and N_W). The proportions of successful positive and negative transitions are defined as N_{PT}/N_S and N_{NT}/N_W. Then the time-series is randomly resampled 100,000 times (with replacement), and again each time, we count the number of successful positive and negative transitions (denoted as N_{PTr} and N_{NTr}) and calculate the

proportion of positive and negative successful transitions in the resampled time-series (N_{PTr}/N_S and N_{NTr}/N_W). The significant level is the same with integrated transitions.

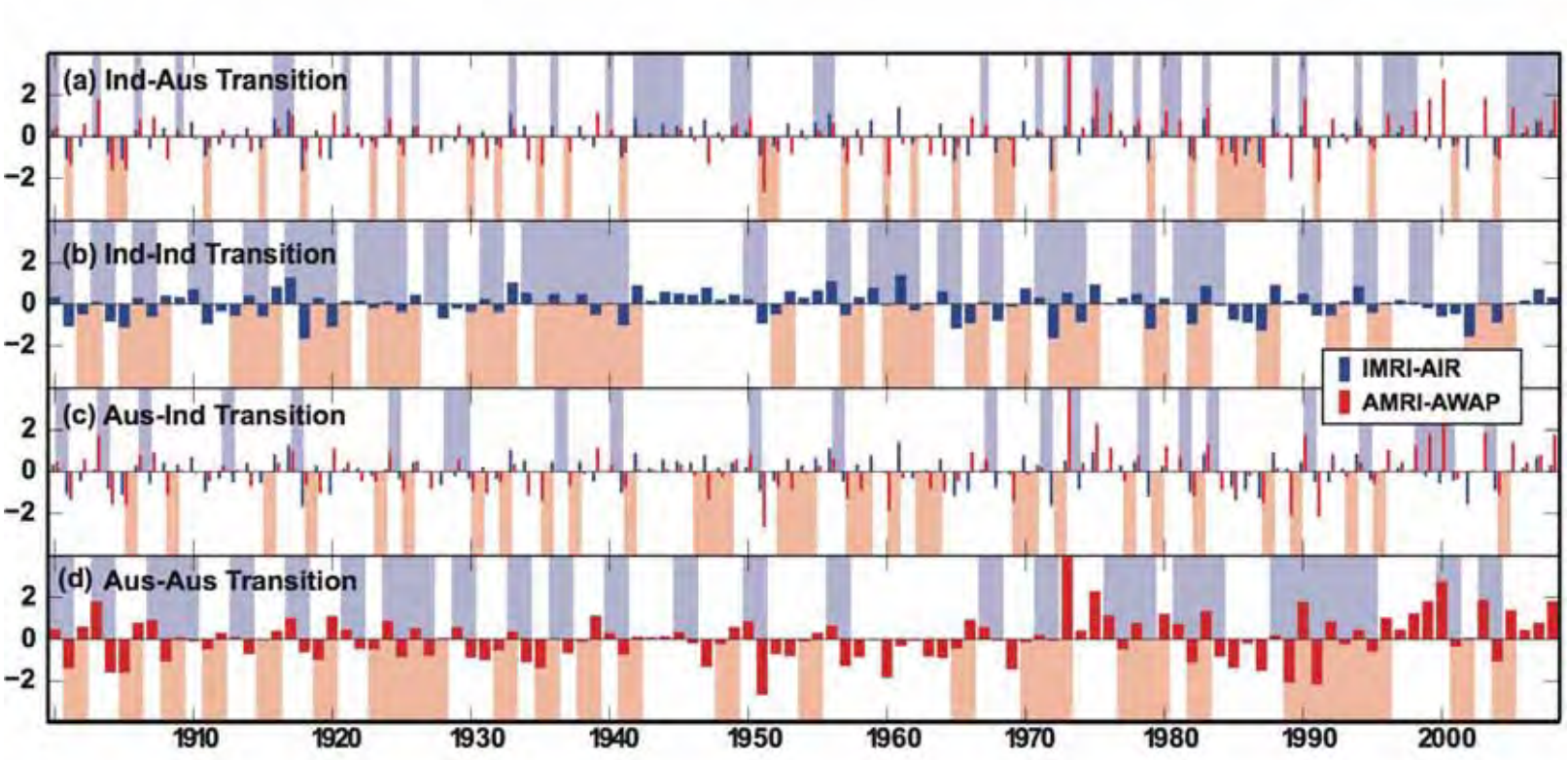

Figure 2.2 The time-series show IMRI-AIR (blue bars) and AMRI-AWAP (red bars) during the period of 1900-2008 with the successful positive and negative transitions marked in blue and red shadow for (a) Indian-Australian monsoon in-phase transition, (b) Indian-Indian monsoon out-of-phase transition, (c) Australian-Indian monsoon out-of-phase transition and (d) Australian-Australian monsoon out-of-phase transition. The unit is mm/d.

Chapter 3. Results

Here we examine the various transitions associated with the biennial tendency of Indian-Australian summer monsoon precipitation in land-only and extended regions defined in Figure 2.1. As the DJFM rainfall total accounts for approximately 78% of annual rainfall over northern continental Australia and the rainfall amount of JJAS accounts for approximately 81% of annual rainfall over Indian subcontinent, we consider only the DJFM for Australian monsoon season and JJAS for the Indian monsoon season. The results are divided into three major parts. In the first part, the precipitation and SST observations have been examined. The second part involves the assessment of CMIP3 and CMIP5 historical simulation with respect to TBO predictive capability and the correlation between the predictability and ENSO. The final part examines the change of predictability for four TBO transitions in the RCP8.5 future scenario.

3.1 Observations assessment

3.1.1 Monsoon seasonality: observation

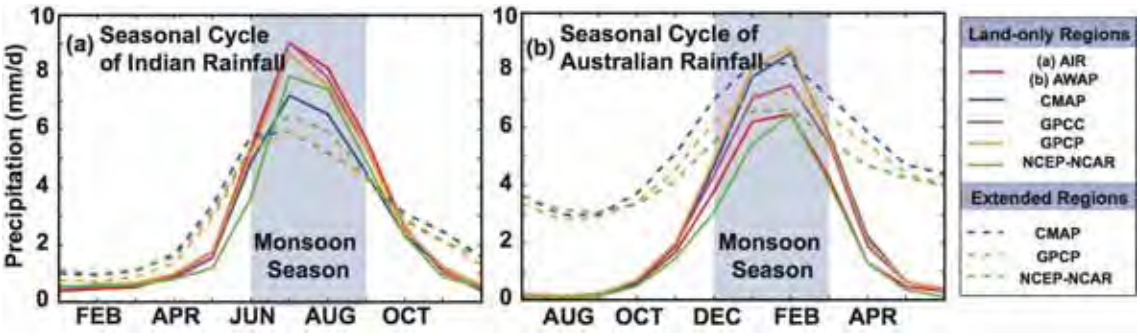

Figure 3.1 Seasonal cycle of rainfall over (a) Indian land-only (solid lines) and extended (dashed lines) regions and (b) Australian land-only (solid lines) and extended (dashed lines) regions. Different datasets using the common period from 1979 to 2008 are represented in different colours. The monsoon seasons are shown in grey shadow.

Figure 3.1 shows the seasonality of rainfall over four different monsoon regions and using the various datasets described in section 2.1. For monsoonal rainfall over Indian and Australian land-only regions, all observation and reanalysis data show a strong seasonality of monsoon rainfall. The Indian monsoon rainfall reaches its maximum in July, with peak climatological rainfall ranging from approximately 7.0 to 9.0 mm/d depending on the datasets. The Australian monsoon rainfall peaks in February with the range from about 7.0 to 8.5 mm/d. Rainfall in both extended regions shows less contrast between monsoon season and the rest of the year. In Indian monsoon regions, the maximum Indian rainfall in extended region is approximately from 6.0 to 6.5 mm/d depending on the datasets, which is lower than that over land-only region. This is because the extended Indian monsoon region contains large areas to the north and the west of the domain, where JJAS rainfall is relatively weak (less than 2 mm/d, see Figure 2.1). For the Australian monsoon, the annual rainfall range for extended region ranges from approximately 3.5 to 5.0 mm/d across the datasets, which is much less than the mean annual rainfall range (approximately 8 mm/d) for land-only region. For the extended region, outside the monsoon season the Maritime Continent which sites within the Indo-Pacific warm pool still receives considerable rainfall (i.e. approximately 3.0 mm/d rainfall across three datasets even in driest month August). In addition, the maximum convection migrate along the Maritime Continent area during the transition from Indian summer monsoon to the Australian summer monsoon, so the monsoon onset is variable from North to South of this region, leading to considerable rainfall outside of DJFM.

3.1.2 Monsoon indices assessment

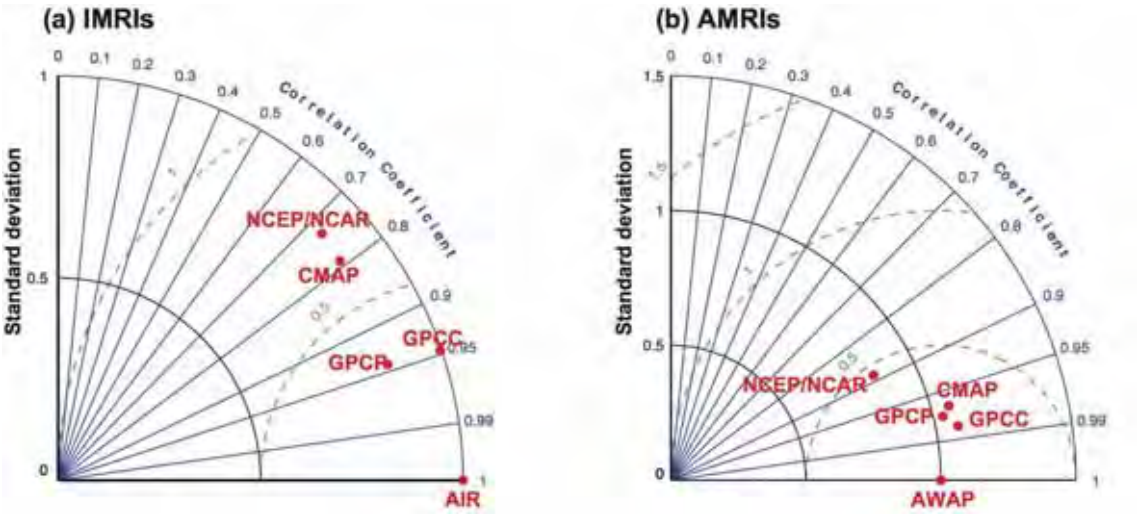

Figure 3.2 Taylor [2001] diagram for (a) the JJAS Indian monsoon rainfall indices (IMRIs) and (b) the DJFM Australian monsoon rainfall indices (AMRIs). The IMRIs are calculated based on the rainfall anomalies over Indian land-only monsoon region and the AMRIs are derived from the rainfall anomalies of Australian land-only monsoon region. The reference IMRI and AMRI are derived from (a) AIR and (b) AWAP, respectively. One standard deviation unit in the diagram represents one standard deviation of (a) AIR and (b) AWAP. All indices use the common period from 1979 to 2008. The green dash lines represent the centred root mean square error (RMSE) compared to the reference indices.

Figure 3.2 shows a comparison between monsoon indices calculated using different observational dataset over a common period of overlap. In general, IMRIs show larger variation across different datasets than AMRIs. The indices derived from the GPCC dataset shows the closest relationship with both reference indices. For the Indian monsoon (Figure 3.2 a), only IMRI-GPCC and IMRI-GPCP have a high correlation coefficient approximately 0.95 with reference IMRI-AIR. Both IMRI-NCEP/NCAR and IMRI-CMAP have correlations less than 0.8. However, the IMRI-GPCP shows approximately 75% of the variance of the reference IMRI-AIR. The AMRIs have correlations with

the reference above 0.95 and 0.99 except for the AMRI-NCEP/NCAR. As mentioned in section 2.3, the discrepancies between the different IMRIs are probably partly related to differences in defining the regions (i.e. the reference index does not include the Himalaya, while other indices do), while all AMRIs are based on the same region.

3.1.3 Predictability of transitions: observation

We define the *enhanced predictability* of the various TBO transitions using a Monte Carlo resampling technique detailed in section 2.4. This Monte Carlo method is employed on all the Indian and Australian monsoon indices. Figure 3.3 to Figure 3.6 show the predictability for the four transitions and the various observational and reanalysis datasets in comparison to the associated cumulative probability distribution based on randomly resampled data. Each figure is arranged as three columns: Integrated (all successful positive and negative) transitions, successful positive transitions and successful negative transitions. The definitions of positive and negative transitions are given in section 2.4. In positive/negative Monte Carlo experiments, we calculate the percentage of successful positive/negative transitions compared to the total number of possible positive/negative transitions. The integrated transition columns take both positive and negative transitions into account. The *enhanced predictability* (shown as a red dashed line in each plot) is represented as the departure of the observed predictability from the median of the randomized distribution.

Indian-Australian monsoon in-phase transition

All the observational reanalysis datasets show statistically significant *enhanced predictability* at 90% level of confidence for the integrated Indian-Australian monsoon in-phase transition (Figure 3.3). In addition, both positive and

negative components of each dataset show consistent significant results with the integrated transition except for NCEP/NCAR, for which the *enhanced predictability* for the individual positive-only or negative-only transitions are not significant. Interestingly, there is a tendency for higher predictability for the negative transitions across all datasets except CMAP, compared to the positive ones. For the reference monsoon indices AIR/AWAP, the *enhanced predictability* is approximately 16.5% with a p-value of 0.0004, which means we can improve our predictive capability by ~16.5% over chance of predicting if the next Australian monsoon will be anomalously strong or weak given information about whether the current Indian monsoon is anomalously strong or weak. The results for GPCC are similar to AIR/AWAP (~14% *enhanced predictability*), as they share the same temporal period with a 109-year length. The indices of GPCP and CMAP (start from 1979 and finish in 2009 and 2007, respectively) show considerable higher *enhanced predictability*, i.e. approximately 25%. The NCEP/NCAR dataset that runs from 1948 to 2010 shows about 14% *enhanced predictability*. It appears that differences in *enhanced predictability* exist in different periods and different datasets, which suggests that the TBO is subject to multi-decadal variability.

To investigate the multi-decadal variability of the TBO, we also conduct the Monte Carlo experiments based on the common period of 1979-2007 for all datasets (Table 3.2). For integrated Indian-Australian monsoon in-phase transitions, the *enhanced predictability* from AIR/AWAP and GPCC is increased to 27.6% and consistent with that from GPCP and CMAP. The *enhanced predictability* for NCEP/NCAR increases from approximately 14% to 17% over the 1979-2007, but this is still much lower than other datasets. We also calculate the *enhanced predictability* from AIR/AWAP for the period of 1900-1978 and the *enhanced predictability* from GPCC for the period of

1901-1978. The *enhanced predictability* of AIR/AWAP is 11.4% for the period of 1900-1978 with a p-value of 0.02, while that of GPCC is 9.0% with a p-value of 0.07. This indicates that the occurrence of successful TBO transitions from Indian to Australian monsoon is considerable higher in the last 30 years.

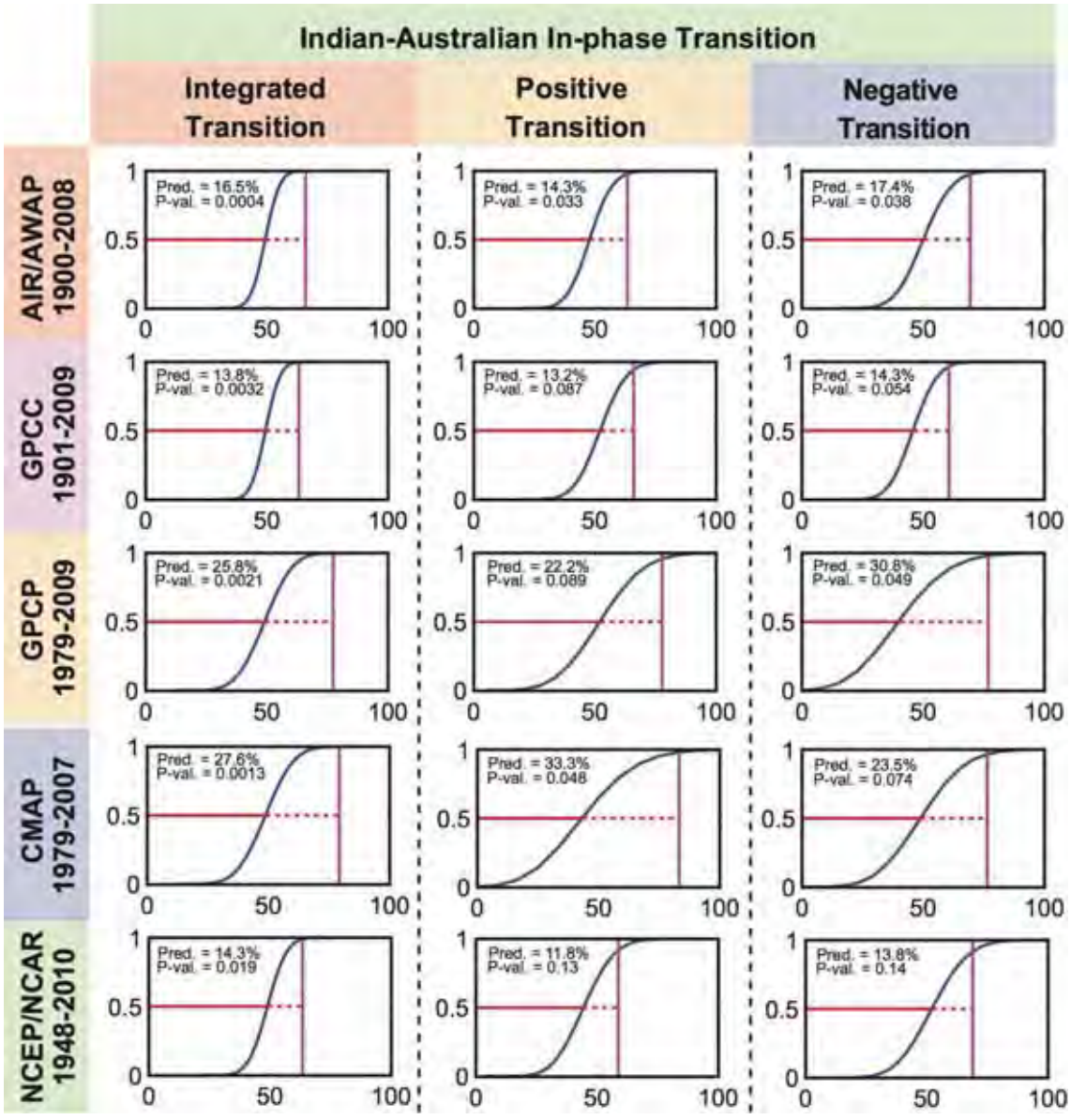

Figure 3.3 The Monte Carlo results for Indian-Australian monsoon in-phase transitions (first column), Indian-Australian positive transitions (second column) and Indian-Australian negative transitions (third column) based on IMRIs and AMRIs that are calculated from different observational and reanalysis precipitation datasets. The datasets are AIR/AWAP (1900-2008), GPCC (1901-2009), GPCP (1979-2009), CMAP (1979-2007) and NCEP/NCAR (1948-2010).

The numbers on x-axis are percentage. The purple vertical lines mark the percentage of the observed successful TBO transition events in total possible TBO transition events. The blue curves represent the Cumulative Distribution Function (CDF) of the randomized distribution with horizontal red solid lines showing its median. The red dash lines represent the *enhanced predictability*. The values of *enhanced predictability* and p-value are shown in each plot.

Indian-Indian monsoon out-of-phase transition

For Indian-Indian monsoon out-of-phase transitions (Figure 3.4), only the reference IMRI-AIR shows significant *enhanced predictability* of 7.3% with a p-value of 0.06 (for the integrated transitions). Other datasets show both predictability values above and below the median value, but the results are not significant at 90% confidence level. Over the shorter common period of 1979-2007, the *enhanced predictability* becomes negative for all except for IMRI-NCEP/NCAR (where *enhanced predictability* is 0, Table 3.2) although none of the values are statistically significant. As the decreased predictability from the period of 1979-2007 might arise from multi-decadal variability of the TBO, we also calculate the predictability from pre-1978 period based on the two long IMRIs. The *enhanced predictability* for IMRI-AIR (1871-1978) is increased from 7.3% to 10.3% (p~0.026) while the one for IMRI-GPCC (1901-1978) is from 5.5% to 9.1% (p~0.083). This suggests that in contrast to the results from the Indian-Australian monsoon in-phase transition, the biennial tendency from a strong/weak Indian monsoon to a following weak/strong Indian monsoon has weakened in the past 30 years. This result might be related to the recent weakening of the El Niño-Indian monsoon relationship ([*Kumar et al.*, 1999; *Ummenhofer et al.*, 2011], see Appendix Article II).

Australian-Indian monsoon out-of-phase transition

For the Australian-Indian monsoon out-of-phase transition (Figure 3.5), there are no significant *enhanced predictability* appearing among different monsoon indices except for the GPCC integrated Australian-Indian monsoon

out-of-phase transition which shows the *enhanced predictability* of 8.3% with p-value of 0.05. Similarly, there is no significant *enhanced predictability* for this transition when considering just the last 30 years (Table 3.2).

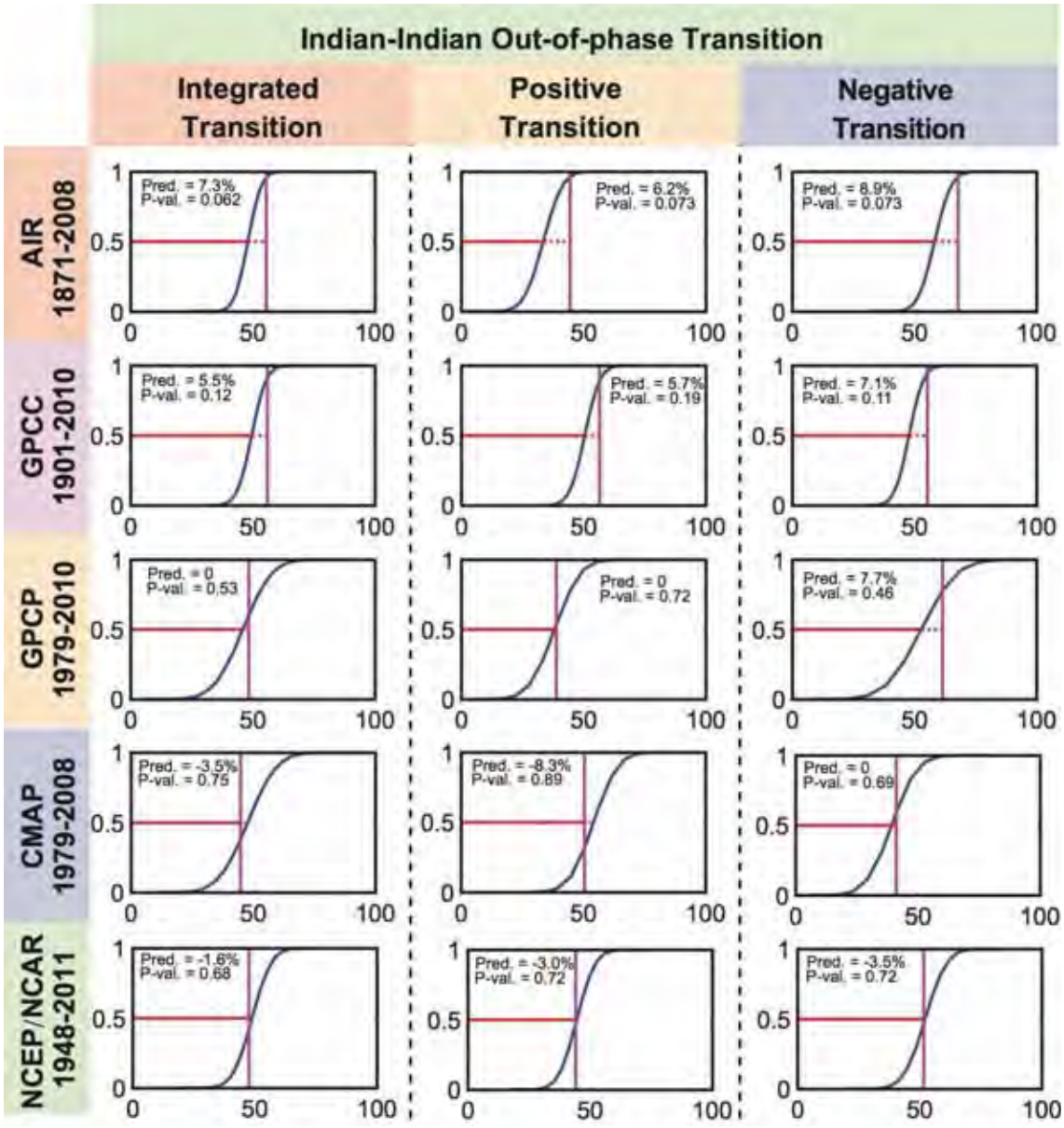

Figure 3.4 As Figure 3.3, but for Indian-Indian monsoon out-of-phase transition.

Australian-Australian monsoon out-of-phase transition

For the longer datasets (i.e. AMRI-AWAP, AMRI-GPCC and AMRI-NCEP/NCAR) the Australian-Australian monsoon out-of-phase transitions (Figure 3.6), do not show significant enhanced predictability. However, all indices except AMRI-CMAP show significant *enhanced predictability* (>14%) in recent 30 years. The time-series from 1979 to 2007 for

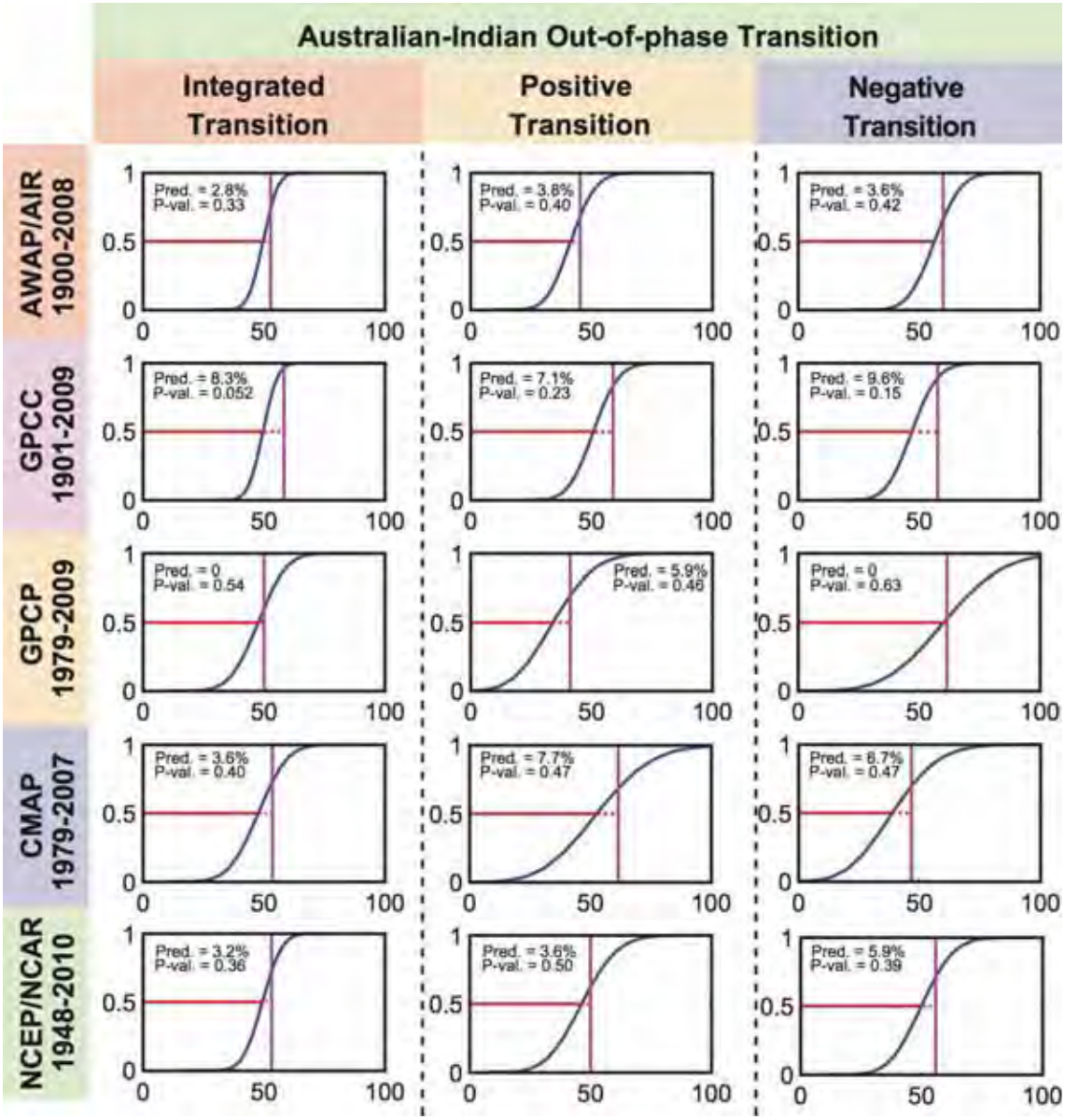

Figure 3.5 As Figure 3.3, but for Australian-Indian monsoon out-of-phase transition.

all Australian monsoon indices are plotted in Figure 3.7. The correlation coefficients between AMRI-CMAP and other AMRIs are 0.97 (AMRI-AWAP), 0.97 (AMRI-GPCC), 0.98 (AMRI-GPCP) and 0.81 (AMRI-NCEP/NCAR). As the variability of AMRI-CMAP is strongly coherent with other AMRIs, the lack of significant *enhanced predictability* for AMRI-CMAP in last 30 years might be attributed to small discrepancies in the rainfall anomalies in a few years. As we use 0 mm/d as the threshold to define whether an Indian-Indian or Australian-Australian monsoon transition is successful, small differences between datasets in years where rainfall is close to the average can lead to

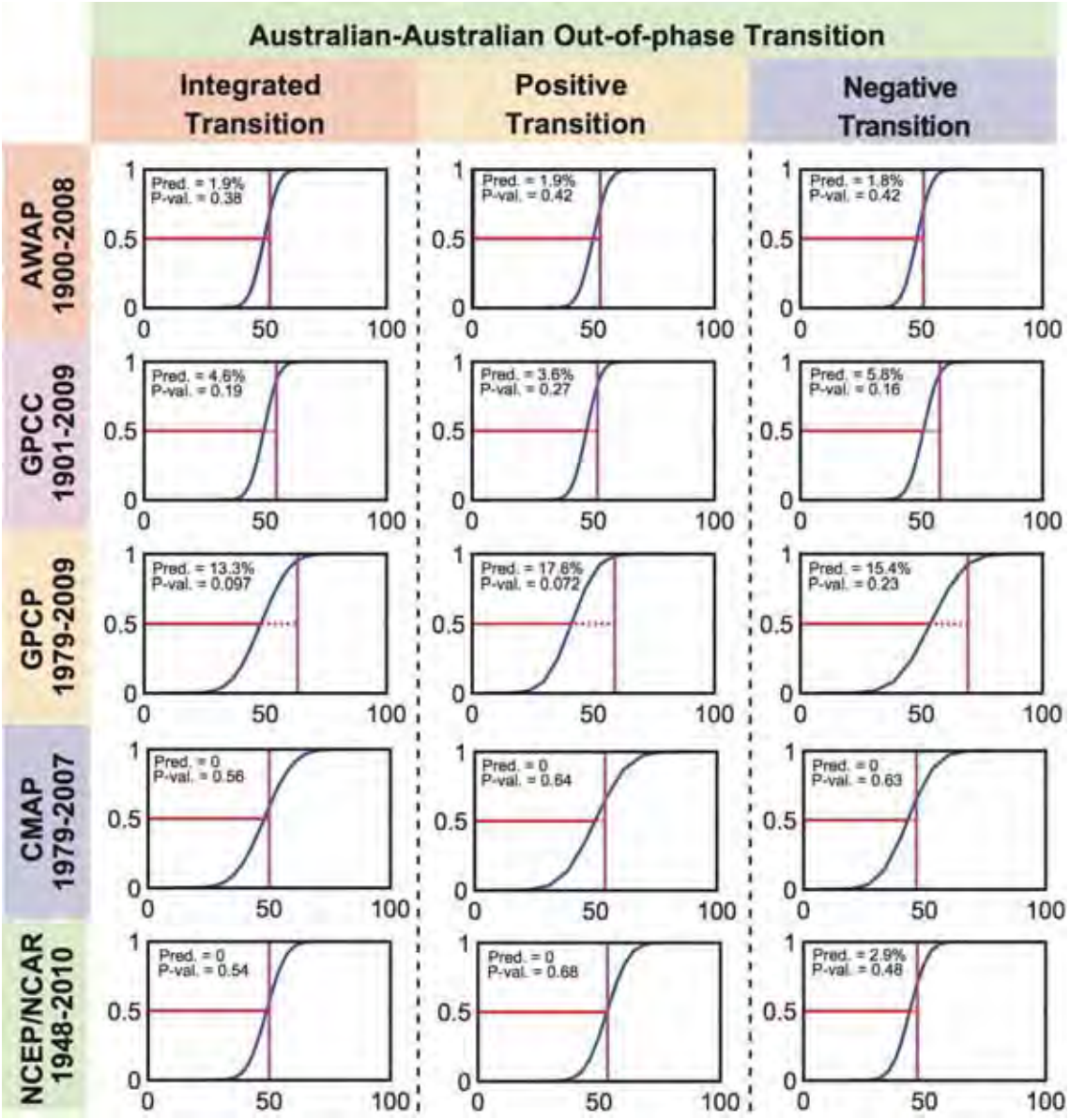

Figure 3.6 As Figure 3.3, but for Australian-Australian monsoon out-of-phase transition.

datasets producing different results with respect to transition success. For example, the Australian monsoon rainfall anomaly in 1991 in AMRI-CMAP is approximately -3 mm/d, while that in 1992 is below but close to the threshold 0 mm/d. As such, although the monsoon rainfall in 1992 is considerably greater than that in 1991 the transition is not counted as successful (Figure 3.7). For all the other datasets 1992 has slightly positive monsoon rainfall anomally and the transition is considered successful. This problem is evident for a number of different years for the Australian-Australian transition (Figure 3.7). This highlights a potential problem with the definitions used for the transitions.

Another definition proposed by *Meehl and Arblaster* [2002] takes the strength of the preceding monsoon into account as follows:

(1) The Indian-Indian monsoon out-of-phase transition

Positive Transition: IMRI(t-1) < IMRI(t) > IMRI(t+1) or

Negative Transition: IMRI(t-1) > IMRI(t) < IMRI(t+1);

(2) The Australian-Australian monsoon out-of-phase transition:

Positive Transition: AMRI(t-1) < AMRI(t) > AMRI(t+1) or

Negative Transition: AMRI(t-1) > AMRI(t) < AMRI(t+1);

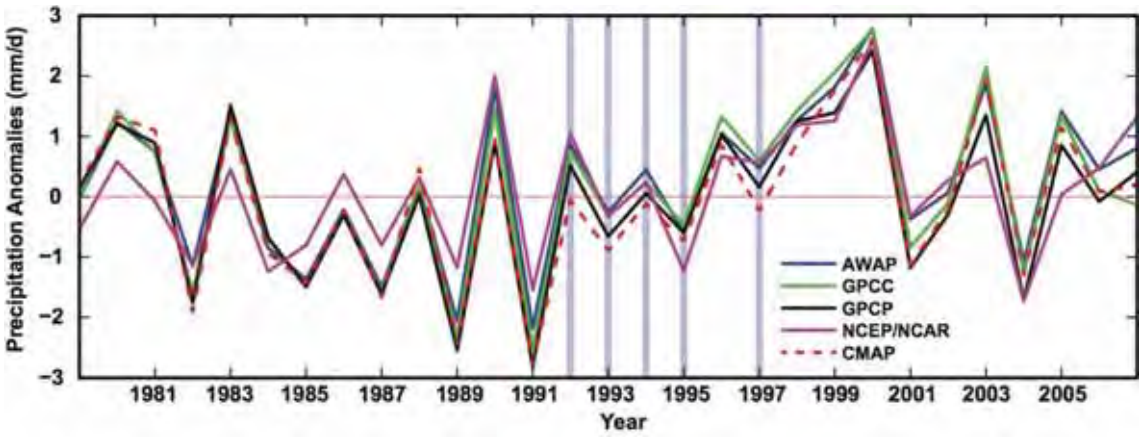

Figure 3.7 AMRI derived from five different datasets over the common period from 1979 to 2007. The blue vertical lines show the years that are not counted as successful Australian-Australian transition years in AMRI-CMAP but are included in successful TBO years for other four AMRIs.

However, the problem with this definition is that it involves two successive transitions. For instance, according to this definition, 1981 is not a successful TBO year as the monsoon in 1980 is stronger than 1981 despite a dramatic drop in monsoon strength that occurs from 1981 to 1982. Another example is seen from 1985 to 1987. These years will be considered as having successful TBO transitions according to *Meehl and Arblaster*'s definition although the difference of monsoon strength between these years is only 1 mm/d. As a result, 1981 should be considered as a successful TBO year while 1985, 1986 and

Table 3.1 The years of positive transition and negative transition for four different TBO transitions. Years are selected from the period of 1871-2010 for Indian-Indian transition, while other transitions are available from 1900 to 2008. Years that are associated with El Niño events are marked in red and the La Niña events are marked in blue according to the classification from *Ummenhofer et al.* [2009]listed in Appendix Table A.1.

	Indian-Australian Transition	**Indian-Indian Transition**	**Australian-Indian Transition**	**Australian-Australian Transition**
Positive Transition	1900, 1903, 1906, 1909, 1916, 1917, 1921, 1924, 1926, 1933, 1936, 1940, 1942, 1943, 1944, 1945, 1949, 1950, 1955, 1956, 1967, 1971, 1973, 1975, 1976, 1978, 1980, 1981, 1983, 1988, 1990, 1994, 1996, 1997, 1998, 2003, 2005, 2006, 2007, 2008	1872, 1875, 1879, 1884, 1887, 1890, 1894, 1898, 1900, 1903, 1906, 1910, 1914, 1917, 1919, 1922, 1924, 1927, 1931, 1934, 1936, 1938, 1940, 1950, 1956, 1959, 1961, 1964, 1967, 1971, 1973, 1978, 1981, 1983, 1990, 1994, 1998, 2003, 2008	1900, 1903, 1906, 1912, 1917, 1924, 1928, 1929, 1936, 1940, 1950, 1956, 1967, 1971, 1973, 1978, 1981, 1983, 1990, 1994, 1998, 1999, 2000, 2003	1900, 1903, 1907, 1909, 1913, 1917, 1921, 1924, 1926, 1929, 1933, 1936, 1940, 1945, 1950, 1956, 1967, 1971, 1976, 1978, 1981, 1983, 1988, 1990, 1992, 1994, 2000, 2003
Negative Transition	1901, 1904, 1905, 1911, 1915, 1918, 1923, 1925, 1930, 1932, 1935, 1937, 1941, 1951, 1952, 1957, 1960, 1962, 1965, 1968, 1969, 1972, 1979, 1982, 1984, 1985, 1986, 1987, 1991, 1995, 2001, 2004	1873, 1877, 1880, 1885, 1888, 1891, 1896, 1899, 1902, 1905, 1907, 1913, 1915, 1918, 1920, 1923, 1925, 1930, 1932, 1935, 1937, 1939, 1941, 1952, 1957, 1960, 1962, 1966, 1969, 1972, 1974, 1979, 1982, 1987, 1992, 1995, 2002, 2004, 2010	1905, 1908, 1915, 1918, 1923, 1925, 1930, 1932, 1935, 1937, 1941, 1946, 1947, 1948, 1952, 1953, 1954, 1957, 1958, 1960, 1962, 1963, 1969, 1970, 1972, 1977, 1979, 1982, 1987, 1989, 1993, 1995, 2004	1901, 1905, 1908, 1911, 1915, 1919, 1923, 1925, 1927, 1932, 1935, 1938, 1941, 1948, 1954, 1965, 1970, 1972, 1977, 1979, 1982, 1987, 1989, 1991, 1993, 1995, 2001, 2004

1987 should not be considered. Thus, unlike the definitions from *Meehl and Arblaster* [2002], the definition used in this study is not based on any precondition and just focuses on the strength of the relationship in rainfall

between two years. While neither definitions is ideal, and other definitions are possible that include alternative thresholds, our method is still useful for assessing individual transitions making up the TBO.

In conclusion, significant *enhanced predictability* is seen across most datasets for Indian-Australian monsoon in-phase transitions, the pre-1978 period for Indian-Indian monsoon out-of-phase transitions and the post-1978 period for Australian-Australian monsoon out-of-phase transitions. The predictive capability for Australian-Indian monsoon out-of-phase transition is unclear. Additionally, multi-decadal variability appears to be important in all TBO transitions except in Australian-Indian monsoon transition. In the last 30 years, the occurrence of successful Indian-Australian and Australian-Australian monsoon transitions has increased while the occurrence of successful Indian-Indian monsoon transitions has decreased.

Table 3.2 The Monte Carlo results for all transitions based on the common period of 1979-2007 for all datasets.

Indian-Australian Monsoon In-phase Transition (1979-2007)									
	Integrated Transition			**Positive Transition**			**Negative Transition**		
	Observed Percentage	**P-value**	***Enhanced Predictability***	**Observed Percentage**	**P-value**	***Enhanced Predictability***	**Observed Percentage**	**P-value**	***Enhanced Predictability***
AIR/AWAP	79.3	0.002	27.6%	86.7	0.114	26.7%	71.4	0.027	35.7%
GPCC	75.9	0.004	27.6%	83.3	0.107	25.0%	70.6	0.058	23.5%
GPCP	75.9	0.005	24.1%	76.5	0.113	23.5%	75.0	0.068	33.3%
NCEP/NCAR	69.0	0.031	17.2%	78.6	0.242	14.3%	60.0	0.098	20.0%
CMAP	79.3	0.001	27.6%	83.3	0.049	33.3%	76.5	0.075	23.5%
Indian-Indian Monsoon Out-of-phase Transition (1979-2007)									
	Integrated Transition			**Positive Transition**			**Negative Transition**		
	Observed Percentage	**P-value**	***Enhanced Predictability***	**Observed Percentage**	**P-value**	***Enhanced Predictability***	**Observed Percentage**	**P-value**	***Enhanced Predictability***
AIR	46.4	0.701	-3.6%	42.9	0.858	-7.1%	50.0	0.632	0
GPCC	46.4	0.670	-3.6%	54.5	0.837	-9.1%	41.2	0.600	0
GPCP	46.4	0.619	0	37.5	0.799	-6.3%	58.3	0.551	0
NCEP/NCAR	46.4	0.714	-3.6%	46.2	0.868	-7.7%	46.7	0.644	0
CMAP	46.4	0.671	-3.6%	54.5	0.837	-9.1%	41.2	0.602	0

----------Continued----------

Australian-Indian Monsoon Out-of-phase Transition (1979-2007)									
	Integrated Transition			Positive Transition			Negative Transition		
	Observed Percentage	P-value	*Enhanced Predictability*	Observed Percentage	P-value	*Enhanced Predictability*	Observed Percentage	P-value	*Enhanced Predictability*
AWAP/AIR	53.6	0.396	3.6%	50.0	0.554	0	58.3	0.373	8.3%
GPCC	60.7	0.187	10.7%	66.7	0.345	6.7%	53.8	0.314	15.4%
GPCP	50.0	0.545	0	40.0	0.555	0	61.5	0.555	0
NCEP/NCAR	50.0	0.575	0	50.0	0.651	0	50.0	0.482	8.3%
CMAP	53.6	0.404	3.6%	61.5	0.475	7.7%	46.7	0.471	6.7%
Australian-Australian Monsoon Out-of-phase Transition (1979-2007)									
	Integrated Transition			Positive Transition			Negative Transition		
	Observed Percentage	P-value	*Enhanced Predictability*	Observed Percentage	P-value	*Enhanced Predictability*	Observed Percentage	P-value	*Enhanced Predictability*
AWAP	60.7	0.125	14.3%	50.0	0.280	6.3%	75.0	0.095	16.7%
GPCC	64.3	0.090	14.3%	60.0	0.128	13.3%	69.2	0.129	15.4%
GPCP	64.3	0.091	14.3%	60.0	0.129	13.3%	69.2	0.130	15.4%
NCEP/NCAR	67.9	0.029	21.4%	56.3	0.095	12.5%	83.3	0.021	25.0%
CMAP	50.0	0.564	0	53.8	0.634	0	46.7	0.633	0

3.1.4 SST anomalies evolution

In order to investigate the possible roles of the Indian and Pacific Ocean SST anomalies on the four different transitions and their positive and negative transition components, we analyse lagged SST anomaly composites for all successful TBO transitions. In general, most of the four transitions are accompanied by significant ENSO-like signals, and in some cases, the SST in the Indian Ocean seem to be important for the transitions.

Figure 3.8 shows lagged SST anomaly composites for years when there is a successful Indian (JJA(0)) to Australian (DJF(0)) monsoon transition. There are 40 positive and 32 negative transition events involved in this composite. For the case of successful positive transitions, a relatively strong Indian monsoon (Figure 3.8-a7) is followed by a relatively strong Australian monsoon half a year later (Figure 3.8-a9). Interestingly, before the strong Indian monsoon starts, there are no significant SST signals in either the Indian Ocean or Pacific Ocean. It might be changes in the Walker Circulation that are more important for the enhanced Indian monsoon rainfall rather than local SST in the case of this transition. During the Indian monsoon season, a cool pool develops from the central to eastern Pacific in JJA(0) (Figure 3.8-a7), which helps the strong Indian monsoon. The La Niña-like signal peaks in SON(0)–DJF(0) (Figure 3.8-a8 & a9) and then begins to decay accompanied by an Indian Ocean basin-wide cooling during the strong Australian monsoon (Figure 3.8-a9). For the case of successful negative transitions, prior to weak Indian monsoon, a large cool anomaly develops in the Indian Ocean that migrates eastwards (Figure 3.8b1-b6). Decreased SST anomalies in the Indian Ocean are able to suppress the upward motion of air and lead to lower moisture availability to the Indian subcontinent. Given the atmosphere responds quickly to changes in SST,

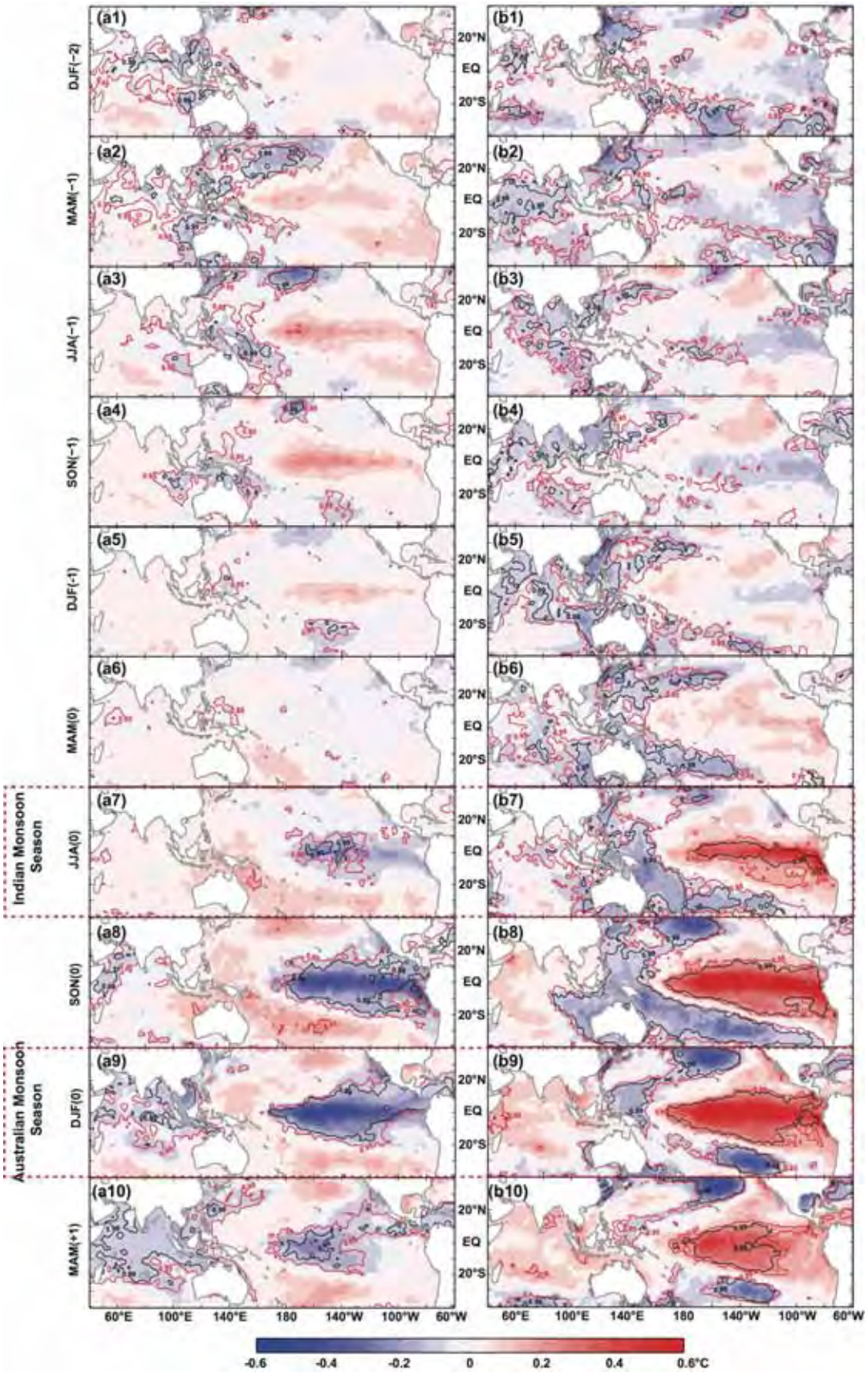

Figure 3.8 The composites of evolution of seasonal averaged SST anomalies for Indian-Australian monsoon (a1-a10) positive transition and (b1-b10) negative transition. The

years of composites are referred to Table 3.1. The monsoon seasons are marked in red dashed boxes. In each plot, the red and black contours represent the results of two-tailed t-test at 95% and 99% level of confidence, respectively.

the Indian monsoon may be influenced by the SST anomalies in JJA(0) (Figure3.8-b8). Surprisingly, the cool SST anomalies have weakened substantially and are only significant to the south of India during weak Indian monsoon season. By contrast, a strong El Niño-like signal appears in the Pacific that thus facilitating the weakening of Indian monsoon rainfall (Figure 3.8-b7). The transition from weak Indian monsoon to weak Australian monsoon is accompanied by the development of El Niño-like signal. The large cool SST anomalies are developed in the western Pacific in SON(0) (Figure 3.8-b8), thus decreasing evaporation and reduction of moisture convergence into the North Australia, which leads to weak Australian monsoon (Figure 3.8-b9). In the meantime, the warm pool in the central and eastern tropical Pacific Ocean leads to anomalous Walker Circulation with strength of easterly trade winds decreasing, which facilitates the weakening of Australian monsoon. During the transition from Indian monsoon (JJA(0)) to Australian monsoon (DJF(0)), it appears that the Pacific Ocean plays an important role for both positive and negative transitions. Our result is consistent with *Yu et al.* [2003] who used a series of CGCM experiments by suppressing either the Indian Ocean or the Pacific Ocean variability in each experiment. They found that the Indian-Australian monsoon in-phase transition is indeed dependent on an interactive Pacific Ocean in the CGCM. In addition, the ENSO-type pattern in Pacific and basin-wide cooling in the Indian Ocean are featured in their CGCM experiments. However, when they conducted the CGCM experiments on Australian-Indian monsoon out-of-phase transition, they found that it was interactions with the Indian Ocean that were particularly important. Such a result is only observed in Australian-Indian positive transition (Figure 3.9a7-a10)

in this study.

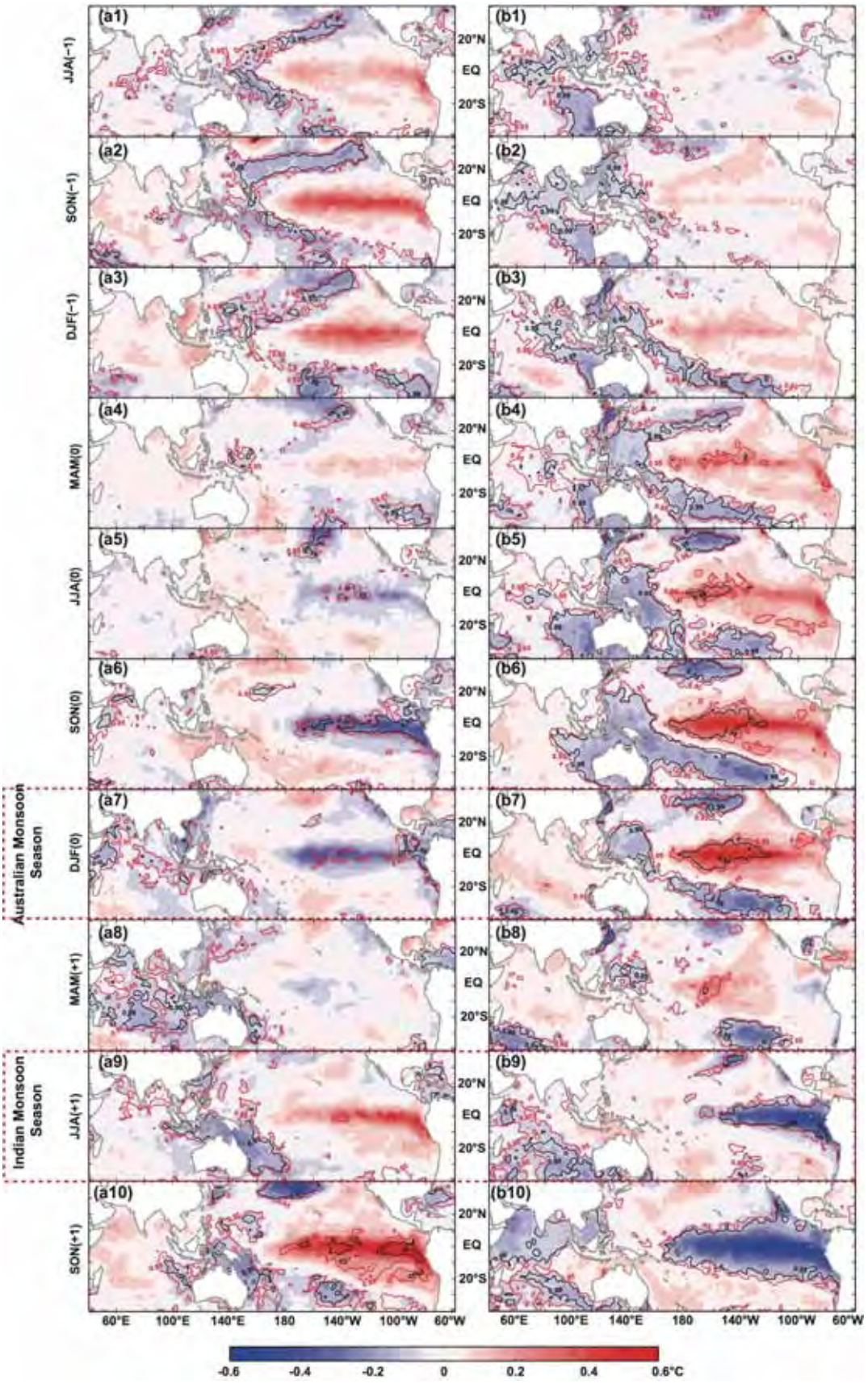

Figure 3.9 As Figure 3.8, but for Australian-Indian monsoon out-of-phase transition.

Significant SST anomalies are seen in the Indian Ocean before (Figure 3.9b1-b6) but not during (Figure 3.9b7-b10) the negative transition. The significant SST anomalies appear in the Indian Ocean and then migrate to the western Pacific with the development of SST anomalies associated with El Niño in the central Pacific. This might suggest that in reality different mechanisms exist in positive and negative components of this transition, and there is an asymmetry in the drivers affecting the Australian-Indian transition.

Figure 3.10 shows the evolution of SST anomaly composites for successful Indian-Indian monsoon out-of-phase transition. Both positive and negative transitions are characterized by the Pacific ENSO-type pattern. For the positive transition, the timeframe can be divided into two stages. The first stage is dominated by SST anomalies associated with La Niña in the Pacific Ocean (Figure 3.10a5-a7). This ENSO-type pattern maintains its amplitude and reverses the sign in JJA(+1) (Figure 3.10-a9). In the second stage, the significant SST anomalies in the Indian Ocean appear in SON(0) and become basin-wide cooling in DJF(0) (Figure 3.10 a6-a8). This cool condition in the Indian Ocean persists to MAM(+1) (Figure 3.10-a8), which leads to decreased evaporation and helps suppress the weak Indian monsoon (JJA(+1), Figure 3.10-a9). Similar to the Indian-Australian positive transition (Figure 3.8-a6), there is no significant SST anomalies in either the Indian Ocean or Pacific Ocean before the strong Indian monsoon for the Indian-Indian positive transition (Figure 3.10-a4). For the negative transition, the El Niño-like signal starts in MAM(0) (Figure 3.10-b4), a season before weak Indian monsoon, and reverses its sign during the subsequent strong Indian monsoon (JJA(+1), Figure 3.10-b9). SST in the Indian Ocean is warmer than normal in MAM(+1) (Figure 3.10-b8) and JJA(+1) (Figure 3.10-b9), although not statistically significant. The asymmetry in the SST anomalies evolution between the

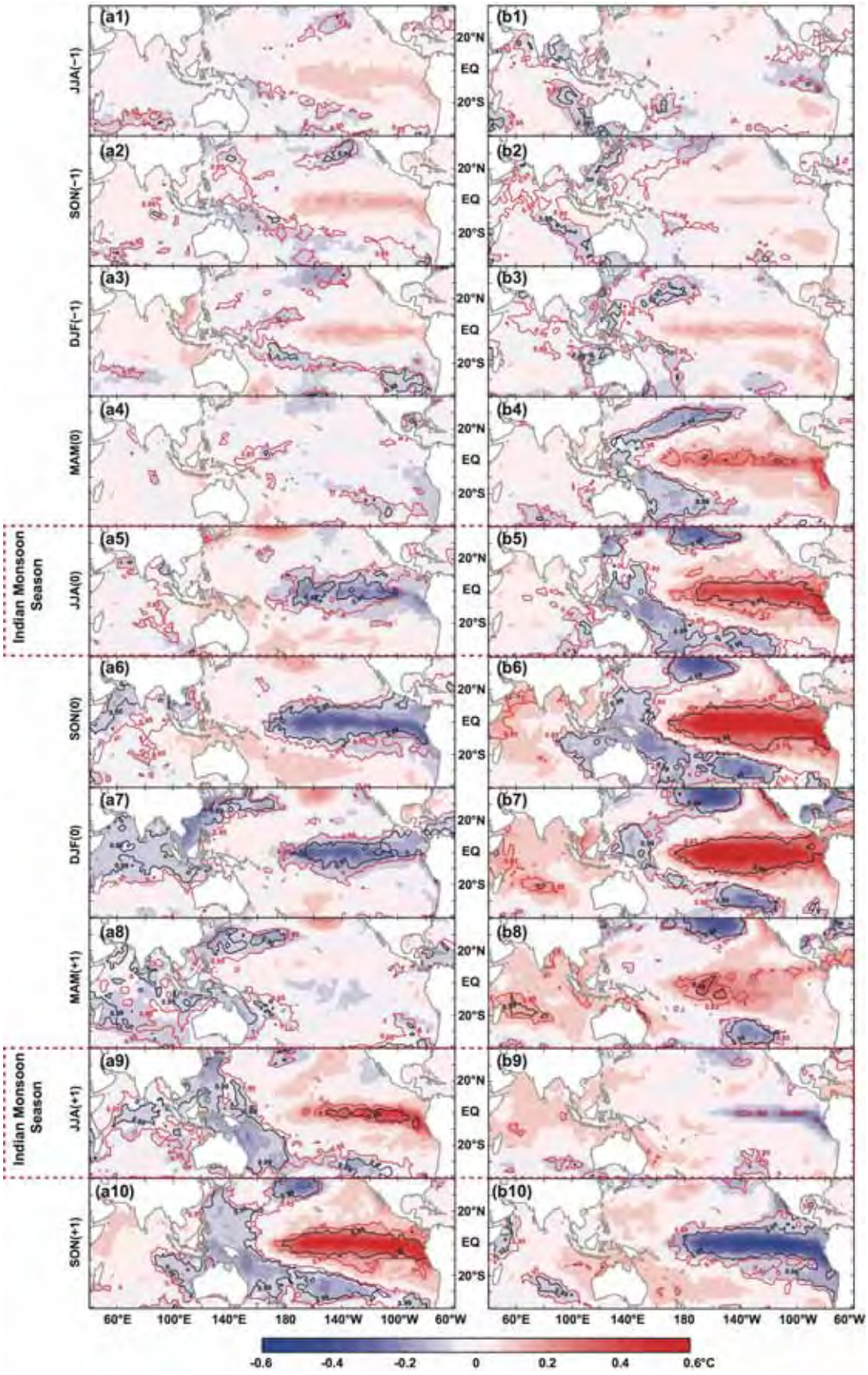

Figure 3.10 As Figure 3.8, but for Indian-Indian monsoon out-of-phase transition.

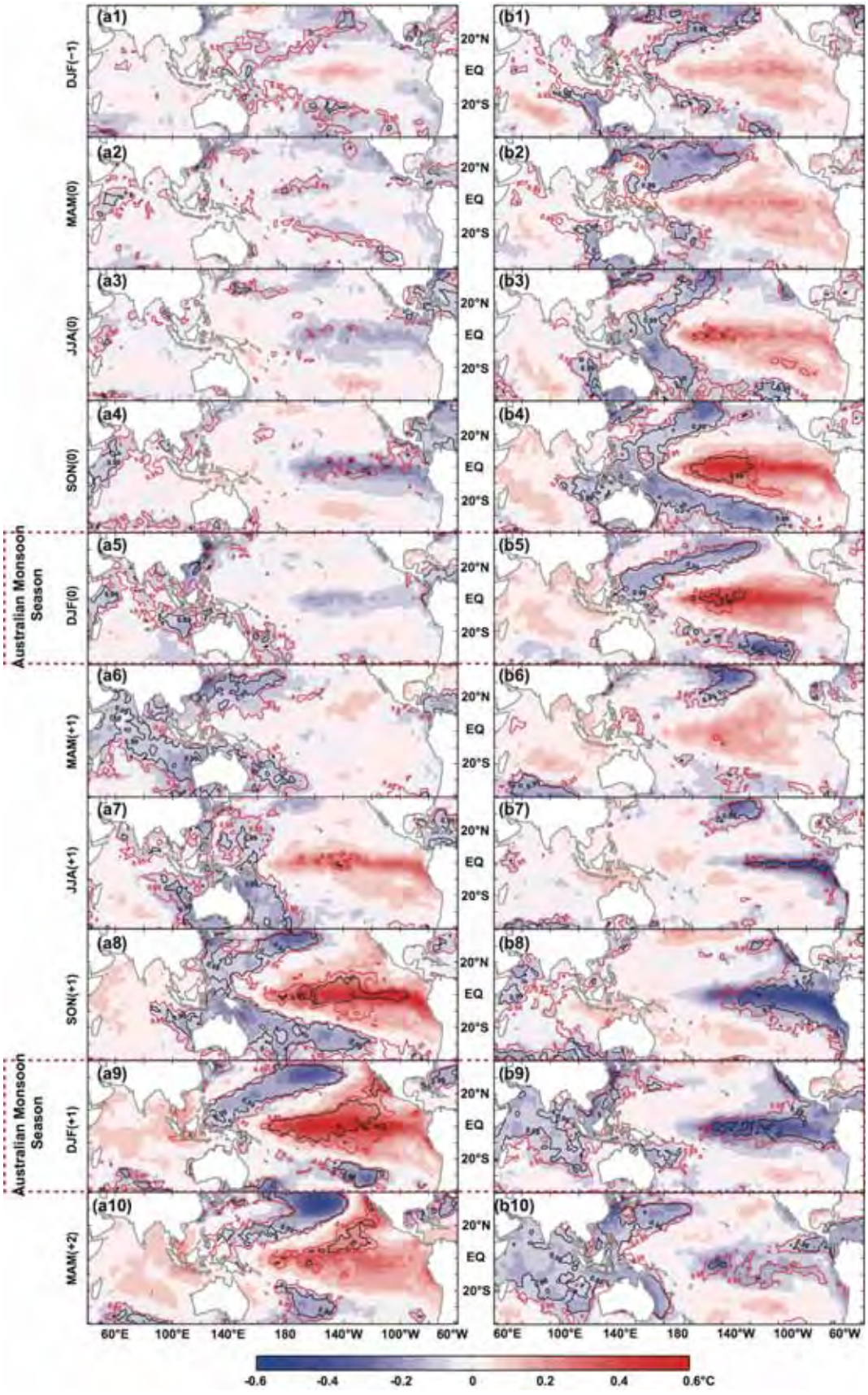

Figure 3.11 As Figure 3.8, but for Australian-Australian monsoon out-of-phase transition.

positive and negative transitions might suggest that the mechanisms that drive

the Indian-Indian positive and negative transitions are also different. While SST anomalies in both the Pacific and Indian Ocean are important to the positive transition, the SST anomalies associated with ENSO play a dominant role in the negative transition.

The positive and negative transitions for Australian-Australian monsoon out-of-phase transitions exhibit a high degree of asymmetry in their SST anomalies evolutions (Figure 3.11). The positive transition shows an Indian-to-Pacific SST migrating pattern from strong Australian monsoon (DJF(0), Figure 3.11-a5) to subsequent weak Australian monsoon (DJF(+1)). For the negative transition, before the weak Australian monsoon (DJF(0), Figure 3.11-b5) there is a significant El Niño that persists to DJF (0), possibly causing a weak Australian monsoon.

We also examine SST composites for the years when all the four transitions co-occurred successfully (Figure 3.12). Here, the successful positive transitions are years of strong Indian monsoons that are followed by a strong Australian monsoon half a year later, which are then followed by a weak Indian monsoon half a year later and finally a weak Australian monsoon half a year later. The successful negative transition occurs when a weak Indian monsoon is followed by a weak Australian monsoon, which itself is followed by a strong Indian monsoon and a strong Australian monsoon in the following year. There are 16 years with successful positive transitions (1900, 1903, 1917, 1924, 1936, 1940, 1950, 1956, 1967, 1971, 1978, 1981, 1983, 1990, 1994, 2003), 7 out of which are La Niña years, and there are 7 in 16 years are followed by El Niño years. Twelve years (1905, 1915, 1923, 1925, 1932, 1935, 1941, 1972, 1979, 1982, 1987, 2004) have successful negative transitions, 6 out of which are El Niño years, and 7 out of 12 years are followed by La Niña years.

In Figure 3.12, the positive transition and negative transition are characterized by a strong asymmetry of SST evolution in the Pacific and Indian Oceans, particularly during the first year (from MAM(0) to MAM(+1), Figure 3.12 a1-a5). The SST anomalies evolution for the negative transitions are consistent with the mechanisms developed by *Meehl* [1997] and *Chang and Li* [2000]. Prior to the weak Indian monsoon (MAM(0), Figure 3.12-b1), there are no significant SST anomalies occurring in the Indian Ocean, but an ENSO-like anomaly is developing from the eastern Pacific. During the weak Indian monsoon (Figure 3.12-b2), the relatively weak surface winds and latent heat flux help the formation of warm SST anomalies in the Indian Ocean in JJA(0) and into SON(0), which in turn will facilitate increased moisture to the Indian monsoon in the following year. *Meehl* [1997] mentioned that the "memory" provided by the high ocean heat content at the end of weak monsoon season helps to maintain the SST anomalies for some time. In addition, atmospheric circulation anomalies associated with the developing El Niño facilitates keeping the water warm in the Indian Ocean until the following Indian monsoon season. In the Indian Ocean, a positive IOD develops peaking in the boreal autumn (SON(0), Figure 3.12-b3). After SON(0), a basin-wide warming in the Indian Ocean co-occurs with the decaying phase of the El Niño until boreal spring in the following year (MAM(+1), Figure 3.12-b5). This result is consistent with many previous studies (e.g. *Chowdary et al.* [2007], *Hong et al.* [2010], and *Taschetto et al.* [2011]). The uniform basin-wide warming in the Indian Ocean enhances the convection via increasing evaporation when the convective maximum arrives at the Indian subcontinent. Consequently, there are stronger surface winds and a strong Indian monsoon in JJA(+1) (Figure 3.12-b6) with corresponding increased monsoonal rainfall and higher latent heat flux to the atmosphere. Simultaneously, the La Niña signal and negative IOD begin to

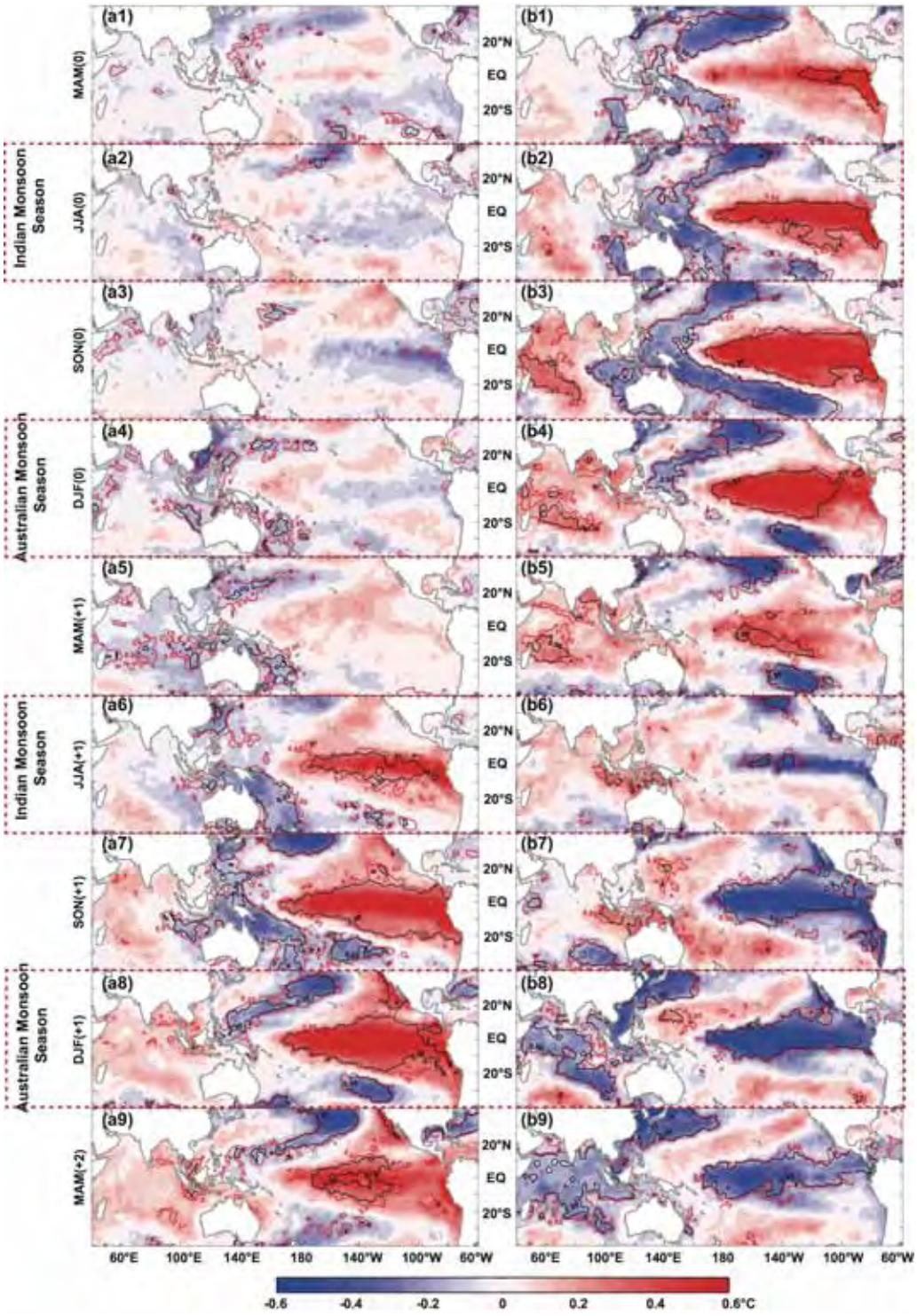

Figure 3.12 As Figure 3.8, but for the years when all four TBO transitions co-occurs.

develop and peak in SON(+1) (Figure 3.12-b7). Significant basin-wide cooling then occurs in the Indian Ocean when the La Niña signal is weakening. The significant positive IOD (Figure 3.12-b3), which is characterized by decreased SST in the eastern Indian Ocean, contributes to a weak Australian monsoon in DJF(0) (Figure 3.12-b4) by evaporation-wind feedback over northern Australia.

One year later, the relatively warm SST in the eastern Indian Ocean associated with the negative IOD (Figure 3.12-b7) and La Niña circulation anomalies favour a strong Australian monsoon (Figure 3.12-b8).

The SST anomalies evolution for the positive transition is quite different from the negative transition. Significantly cool SST anomalies start to appear south of Maritime Continent, north and east coast of Australia in DJF(0) when the strong Australian monsoon occurs, and peak in SON(+1) (Figure 3.12-a7). Interestingly, unlike the years when only successful Indian-Australian positive transitions occur (Figure 3.8 a7-a9), there is no significant La Niña-like signal seen during the Indian-Australian positive transitions when all four TBO transitions are successful (Figure 3.12 a2-a4). The difference between these two composites can be explained as follows: La Niña included in Figure 3.8-a seems to be filtered out from the composite shown in Figure 3.12-a. This happens due to the asymmetric nature of ENSO evolution, where La Niña tends to last longer than El Niño events, thus modulating monsoonal rainfall for consecutive years. In the boreal spring (MAM(+1), Figure 3.12-a5), basin-wide cooling in the Indian Ocean contribute to the subsequent weak Indian monsoon due to the decreased heating convection caused by weakened evaporation. Significantly warm SST anomalies develop in the central and eastern Pacific Ocean with a significant decrease in the western Pacific SST. In SON(+1) (Figure 3.12-a7), the El Niño-type pattern peaks and a positive IOD develops. The El Niño signal decays with the basin-wide warming in the Indian Ocean during the weak Australian monsoon (Figure 3.12-a8).

.

To further examine the asymmetry during the years with all four successful transitions, we derive five SST anomaly indices from different regions to investigate the phase relationship among SST anomalies in different parts of

ocean. We calculate the region-averaged monthly SST anomalies from selected years. The regions we use are illustrated in Figure 3.13a with their details listed in Table 3.3. In Figure 3.13, we present composites for these anomalies for positive and negative transitions. The composites start from Mar(0) that is three-month prior to the Indian monsoon season and end at May(+2) that is three-month after the responding Australian monsoon, i.e. over a period of 27 months. In both positive and negative transitions, NINO3 and NINO3.4 indices follow each other closely.

Table 3.3 Information on indices that are used in Figure 3.13. $\overline{SSTA}_x$ in the table represents the SST anomalies averaged over region *x*.

Index	Mode	Regions	Definition	References
NINO3	ENSO	Niño-3 Region, NINO3 (90°W-150°W, 5°S-5°N)	$\overline{SSTA}_{NINO3}$	[*Trenberth*, 1997]
NINO3.4		Niño-3.4 Region 3.4, NINO3.4 (120°W-170°W, 5°S-5°N)	$\overline{SSTA}_{NINO34}$	
IOD	Indian Ocean Dipole	Western Equatorial Indian Ocean, WEIO (50°E-70°E, 10°S-10°N,)	$\overline{SSTA}_{WEIO} - \overline{SSTA}_{EEIO}$	[*Saji et al.*, 1999]
		Eastern Equatorial Indian Ocean, EEIO (10°S-0, 90°E-110°E)		
EMI	El Niño Modoki	EMI_A (165°E-140°W, 10°S-10°N)	$\overline{SSTA}_{EMI\_A} - 0.5\times \overline{SSTA}_{EMI\_B} - 0.5\times \overline{SSTA}_{EMI\_C}$	[*Ashok et al.*, 2007]
		EMI_B (110°W-70°W, 15°S-5°N)		
		EMI_C (125°E-145°E, 10°S-20°N)		
IOB	Indian Ocean Basin Warming /Cooling	Indian Ocean Basin, IOB (40°E-120°E, 20°S-20°N)	$\overline{SSTA}_{IOB}$	

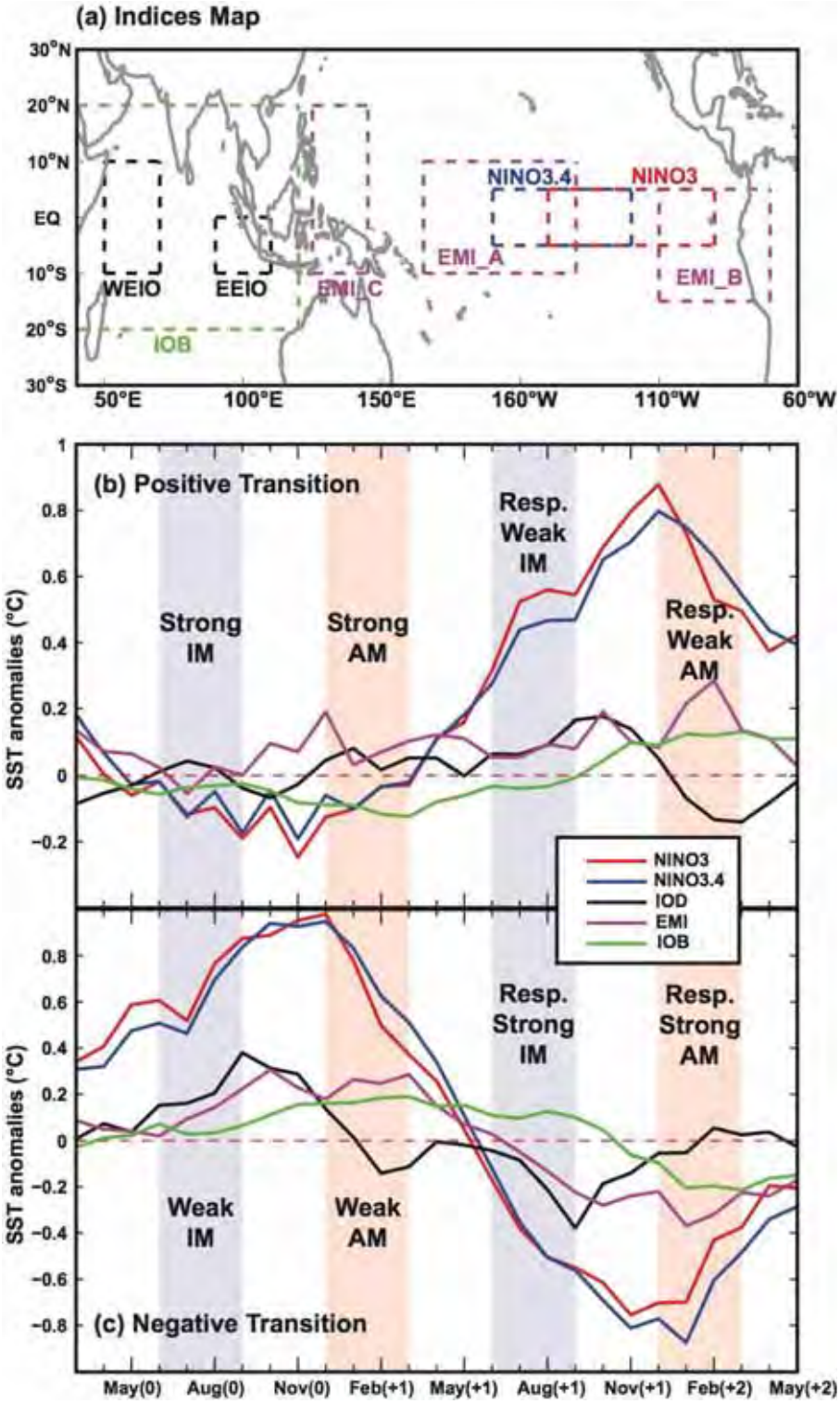

Figure 3.13 Lagged composite monthly SST anomalies indices derived from regions shown in (a), which are named NINO3, NINO3.4, IOD, EMI and IOB (see Table 3.3 for details). The years selected in (b) positive transitions and (c) negative transitions are consistent with Figure 3.12 when all four transitions co-occur. Blue shadows mark the Indian monsoon seasons while the red ones mark the Australian monsoon seasons.

For the in-phase transition (Figure 3.13b) for the period between the strong Indian monsoons to strong Australian monsoons, SST anomalies in the eastern and central Pacific are almost neutral or weakly negative, with lowest SST anomalies in the break (Nov(0)) between two strong monsoon seasons. The SST anomalies begin to increase during the strong Australian monsoons becoming positive at the end of the strong Australian monsoons (Mar(+1)). Pacific SST anomalies peak almost a year later at the onset of weak Australian monsoons. As such the weak Indian monsoons and Australian monsoons are co-occurring with relatively high SST anomalies in the Pacific. Here we employ the similar method with Australian monsoon rainfall index in section 2.3 to calculate the standardized DJFM averaged NINO3.4 index for the period of 1870-2010, and then compare the index in each year with ±1 SD. Surprisingly, during the 16 years of successful positive transitions, 10 events occur when the DJFM averaged NINO3.4 index is within ±1 SD (ENSO neutral years) and only 4 events occur when the DJFM averaged NINO3.4 index is lower than -1 SD (La Niña events). Half of these successful positive transition years are followed by the years with DJFM averaged NINO3.4 index greater than +1 SD (El Niño events). The IOB shows a small magnitude and low-frequency variation with approximately three months lag to NINO3 and NINO3.4. The variability for other indices in positive transition is less clear.

The evolution during the negative transition is quite different. Unlike the positive transition, high SST anomalies in the Pacific Ocean (El Niño events) are followed by low SST anomalies (La Niña events) in both NINO3 and NINO3.4 indices. The weak Indian and Australian monsoons are accompanied by strongly positive SST anomalies, and the subsequent strong Indian and Australian monsoons occur when SST anomalies are strongly negative. Seven out of 12 weak Indian to weak Australian monsoon transitions co-occur with El

Niño events, 71.4% of which are followed by La Niña events. The IOD index peaks at the withdrawal of Indian monsoon, three month ahead of ENSO peaking, while the IOB index peaks approximately three months after the peak of ENSO. Both IOD and IOB indices are significant at the 95% level according to a two-tailed Student's *t* test, although their magnitudes are much smaller than NINO3 and NINO3.4 indices. This may suggest that the basin-wide change of SST in the Indian Ocean is a response to the forcing of ENSO and IOD plays a complementary role in the transitions.

3.2 CMIP3 and CMIP5 models

Some of the work presented in this section has been published in Li Y., Jourdain N.C., Taschetto A.S., Ummenhofer C.C., Ashok K., and Sen Gupta A. (2012), Evaluation of monsoon seasonality and the tropospheric biennial oscillation transitions in the CMIP models, *Geophysical Research Letters, 39*, L20713, doi:10.1029/2012GL053322 (see Appendix Article I).

3.2.1 Monsoon seasonality: models

The Indian-Australian monsoon system is characterized by intensive rainfall over the Indian subcontinent in boreal summer (JJAS) and North Australia in austral summer (DJFM). A realistic simulation of the unique monsoon seasonal cycle of this system gives us some measure of the realism of the simulated monsoon before further evaluation of *enhanced predictability* of the TBO transitions. The seasonal cycles of land-only regions for 24 CMIP3 and 30 CMIP5 models are illustrated in Figure 3.14, while the seasonal cycles of the extended regions are shown in Figure 3.15. Models and observations/reanalysis are sorted according to the average monsoon rainfall amount (i.e. average JJAS rainfall for the Indian monsoon and average DJFM

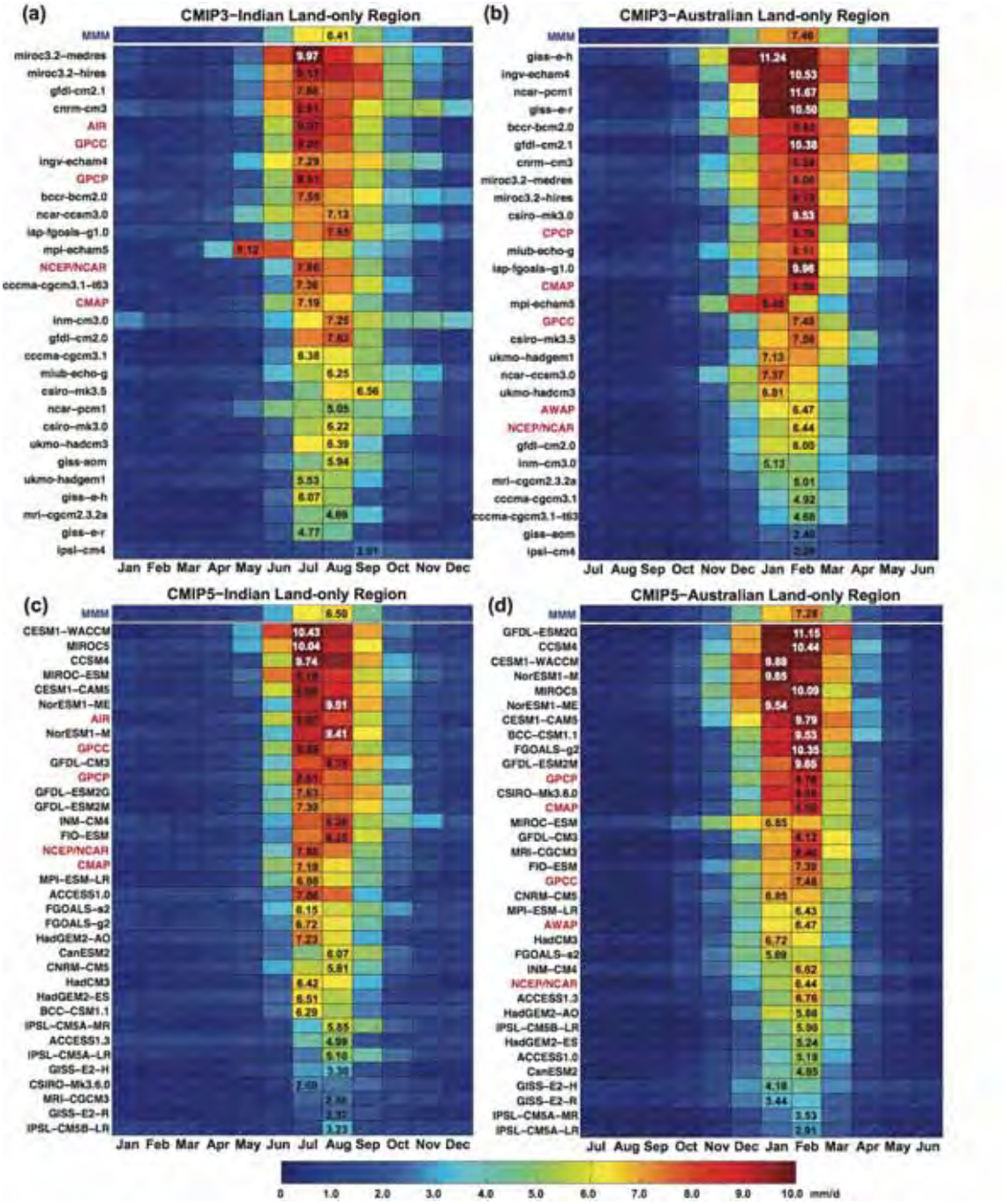

Figure 3.14 Seasonal cycle of the Indian (a,c) and Australian (b,d) land-restricted rainfall for observations, reanalysis and CMIP3 (a,b) and CMIP5 (c,d) models. Models (names in black), observations and reanalysis (names in red) are sorted according to the average monsoon rainfall amount (JJAS rainfall for Indian monsoon and DJFM rainfall for Australian monsoon). The top row shows the multi-model mean (MMM, names in blue) of CMIP3 or CMIP5 models for Indian and Australian rainfall. Internal numbers show the maximum rainfall (mm/d) in the month of greatest rainfall (numbers in white are just to contrast with background box colour).

rainfall for the Australian monsoon) with the highest value on top.

In this study, the months with averaged rainfall more than 3.5 mm/d are considered as wet months. For all five observational/reanalysis Indian rainfall datasets, the four wettest months in the Indian subcontinent extend from June to September with maximum rainfall in July (Figure 3.14a & c). The length of distinct wet months for CMIP3 models ranges from two (e.g. giss-e-r) to eight (e.g. cnrm-cm3), with ipsl-cm4 failing to capture a monsoon season cycle (based on the 3.5 mm/d threshold). Fourteen out of 30 CMIP5 models correctly simulate JJAS as the four wettest months (e.g. CESM1-CAM5), nine models underestimate the length of the wet season and five models lack a distinct monsoon season (GISS-E-H, CSIRO-Mk3.6.0, MRI-CGCM3, GISS-E2-R and IPSL-CM5B-LR). In terms of maximum rainfall, 11 out of 24 (46%) CMIP3 and 16 out of 30 (53%) CMIP5 models manage to simulate the peak rainfall in July, with a large number of the remaining models delayed by one month. Three CMIP3 models show significant bias in the timing of the monsoon. For example, mpi-echam5 peaks two months early and two models (csiro-mk3.5 and ipsl-cm4) have a peak that is delayed by two months. There is also considerable spread in the amplitude of seasonal cycle. While rainfall in the peak monsoon month across observational/reanalyzed datasets ranges from 7.2 to 9.1 mm/d, both CMIP3 and CMIP5 models range from about 3 to 10 mm/d. Multi-model means for CMIP3 and CMIP5 models are similar with approximately 6 mm/d in July, indicating that overall the simulated monsoon rainfall is too weak. For a number of models (particularly CMIP3), there is too much rainfall outside of the monsoon season. This is particularly obvious for the cnrm-cm3 and inmcm3-0 models.

The wet season for the North Australia occurs from December to March, with maximum rainfall in February in the five observational/reanalysis datasets used

here. Observed rainfall ranges from 6.4 mm/d to 8.8 mm/d (Figure 3.14b & d). There are 18 out of 24 CMIP3 models (75%) and 21 out of 30 CMIP5 (70%) models correctly simulating the timing of maximum rainfall in February, with maximum rainfall of the multi-model means in February (7.5 mm/d for CMIP3 and 7.3 for CMIP5) lying within the observational range. Models show a wide range of wet-month duration. In CMIP3 models, the length of wet months ranges from three (e.g. mri-cgcm2.3.2a) to seven (e.g. bccr-bcm2.0). Two CMIP3 models essentially show no monsoon seasonality, i.e. giss-aom and ipsl-cm4. Sixteen out of 24 (67%) CMIP3 models have more than four wet months and only three (12.5%) models correctly simulate four wet months. For CMIP5 models, the percentage that correctly simulate wet season in DJFM increased to 37% (11 out of 30 CMIP5 models). Eight CMIP5 models overestimate the duration of the wet season with more than four wet months (e.g. CCSM4 has six wet months), while eleven models show short duration of wet months (e.g. GISS-E2-H has two wet months). With respect to the monsoon strength, the three CMIP3 models (ukmo-hadcm3, gfdl-cm2.0 and inm-cm3.0) that correctly simulate the wet season apparently underestimate the monsoon strength compared to observations. However, most CMIP5 models with correct wet seasons show stronger monsoon rainfall than observations.

In general, CMIP5 models show an overall improvement in simulating low rainfall rates outside of monsoon season and less bias in the seasonal cycle compared to CMIP3 models. In terms of monsoon strength, most CMIP3 (14 out of 24) and CMIP5 (18 out of 30) models underestimate the strength of the Indian land-only monsoon rainfall, with the multi-model ensemble means of rainfall lower than the range of observations. Both CMIP3 and CMIP5 models correctly simulate the strength of Australian land-only monsoon rainfall. Thus, little improvement is shown from CMIP3 to CMIP5 models in simulating the

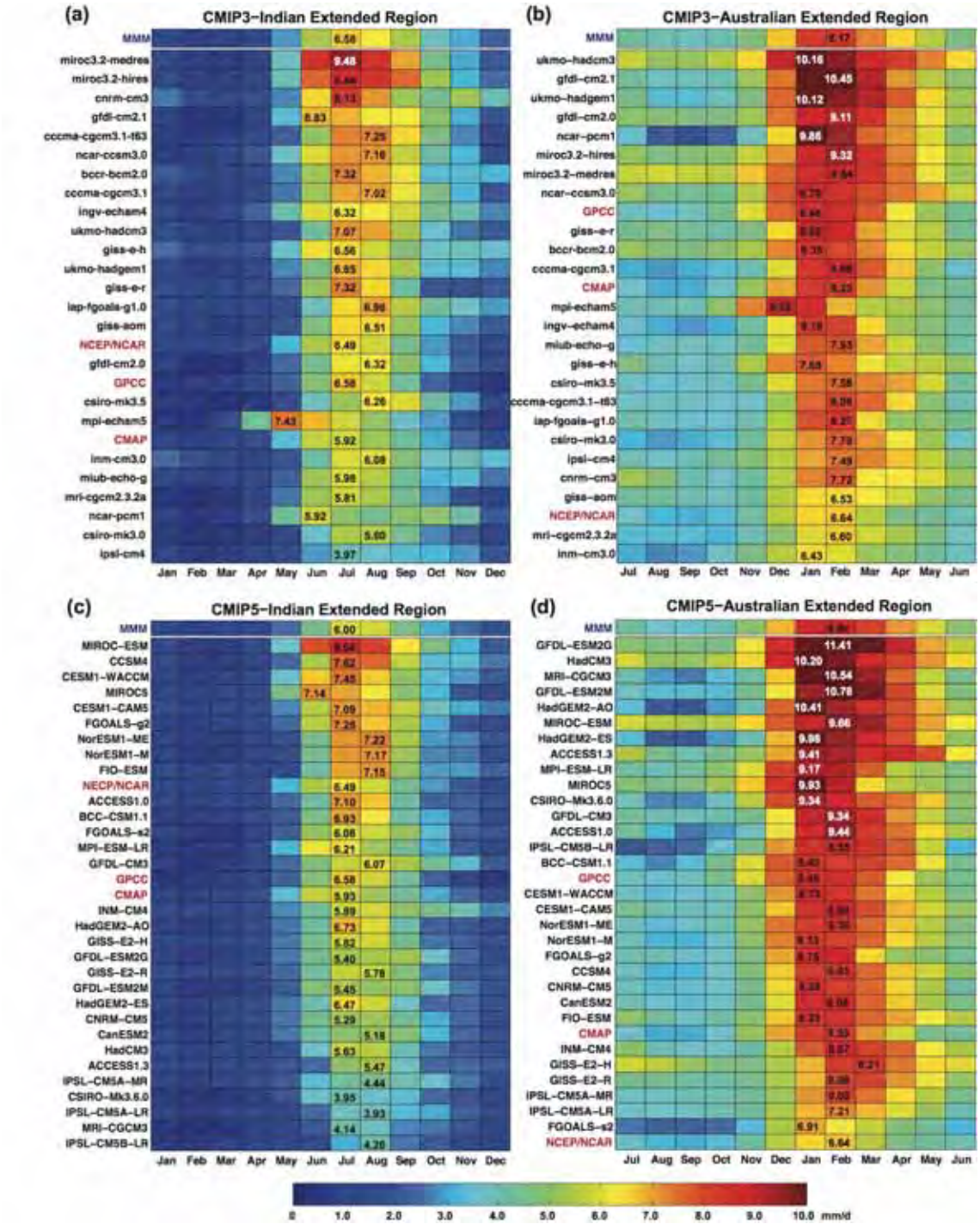

Figure 3.15 As Figure 3.14, but based on the rainfall of extended regions.

monsoon strength. With respective to the monsoon seasonality, more CMIP3 models show longer wet season duration and too much rainfall outside of wet seasons in both Indian and Australian land-only monsoons, and CMIP5 models show apparent improvement in these two aspects over CMIP3 models. However, 2 out of 24 (8%) CMIP3 models (ipsl-cm4 and giss-aom) have no

clear monsoon rainfall seasonal cycle either over India or Australia, and 5 out of 30 (17%) CMIP5 models fail to capture the monsoon seasonal cycle. Thus, with respect to models with extremely weak monsoon seasonality, CMIP5 has a larger proportion of poor models than CMIP3.

Figure 3.15 shows the simulated seasonal cycles of Indian and Australian rainfall in extended regions. For Indian rainfall seasonality (Figure 3.15a & c), both CMIP3 and CMIP5 models show peak rainfall lying within the observational range and occurring in the correct month in terms of the multi-model mean. CMIP3 models show a larger range of behaviours for both monsoon season length and rainfall peak month. Nineteen out of 30 CMIP5 models correctly simulate the maximum rainfall in July, while the peak rainfall in other models is shifted by one month. However, compared to the Indian subcontinent, the extended Indian region exhibits weaker monsoon strength for both observations and models. In the extended Australian monsoon region (Figure 3.15b & d), seasonality is relatively weak with considerable rainfall even outside of the monsoon season. This is because the extended Australian monsoon region contains the Maritime Continent. On the one hand, the Maritime Continent is interspersed among lots of ocean area, where there is almost constant rain during the year. On the other hand, this area bridges the Indian summer monsoon and Australian summer monsoon temporally and spatially. Monsoon onset varies from North to South of this area, so that the wet season integrated rainfall over the extended region prolongs compared to the wet season when we only average the rainfall over North Australian continent. The three global observational and reanalysis products show different wet-month duration. For example, the GPCC dataset has six distinct wet months from November to April; the CMAP has its four wettest months in DJFM; while monsoon seasonality in the NCEP/NCAR dataset is less clear. Most

models exhibit prolonged wet months until April or May. In general, the monsoon seasonality of rainfall in extended regions is not as apparent as in land-only monsoon regions.

3.2.2 Predictability of transitions: models

The same Monte Carlo technique described in section 3.1.3 is employed to calculate the *enhanced predictability* for all TBO transitions in the CMIP3 and CMIP5 simulations. The results are summarised in Figure 3.16. Models for which no ensemble member shows a significant *enhanced predictabilit*y in any of the transitions are not shown, thus 18 out of 24 CMIP3 models and 23 out of 30 CMIP5 models are presented in Figure 3.16. For Indian-Australian monsoon in-phase transition, there are 12 out of 24 (50%) CMIP3 and 20 out of 30 (67%) CMIP5 models for which at least one ensemble member has significant *enhanced predictability* (i.e. at least one red circle shown in Figure 3.16a), consistent with observations/reanalysis. Even when considering just individual ensemble members with significant *enhanced predictabilities*, values for CMIP5 models range between about 5%-15%. They therefore underestimate the observed *enhanced predictability* which is at or above ~15% depending on the datasets. For CMIP3 models, the range in *enhanced predictability* is much larger, ranging from approximately 5% to 30%. In Figure 3.16a, many models with multiple ensemble members show contrasting results for their different members. For example, the CMIP3 model giss-e-r has 9 ensemble members, five of which show *enhanced predictability* while four of which show *negative predictability*. This suggests that there is a substantial multi-decadal or centennial variability in the efficacy of this transition, which is consistent with the results drawn from observations [*Meehl and Arblaster*, 2011]. Nevertheless, when considering concatenated ensemble members, the Indian-Australian monsoon transition shows significant predictability for 11 of 24 CMIP3 models,

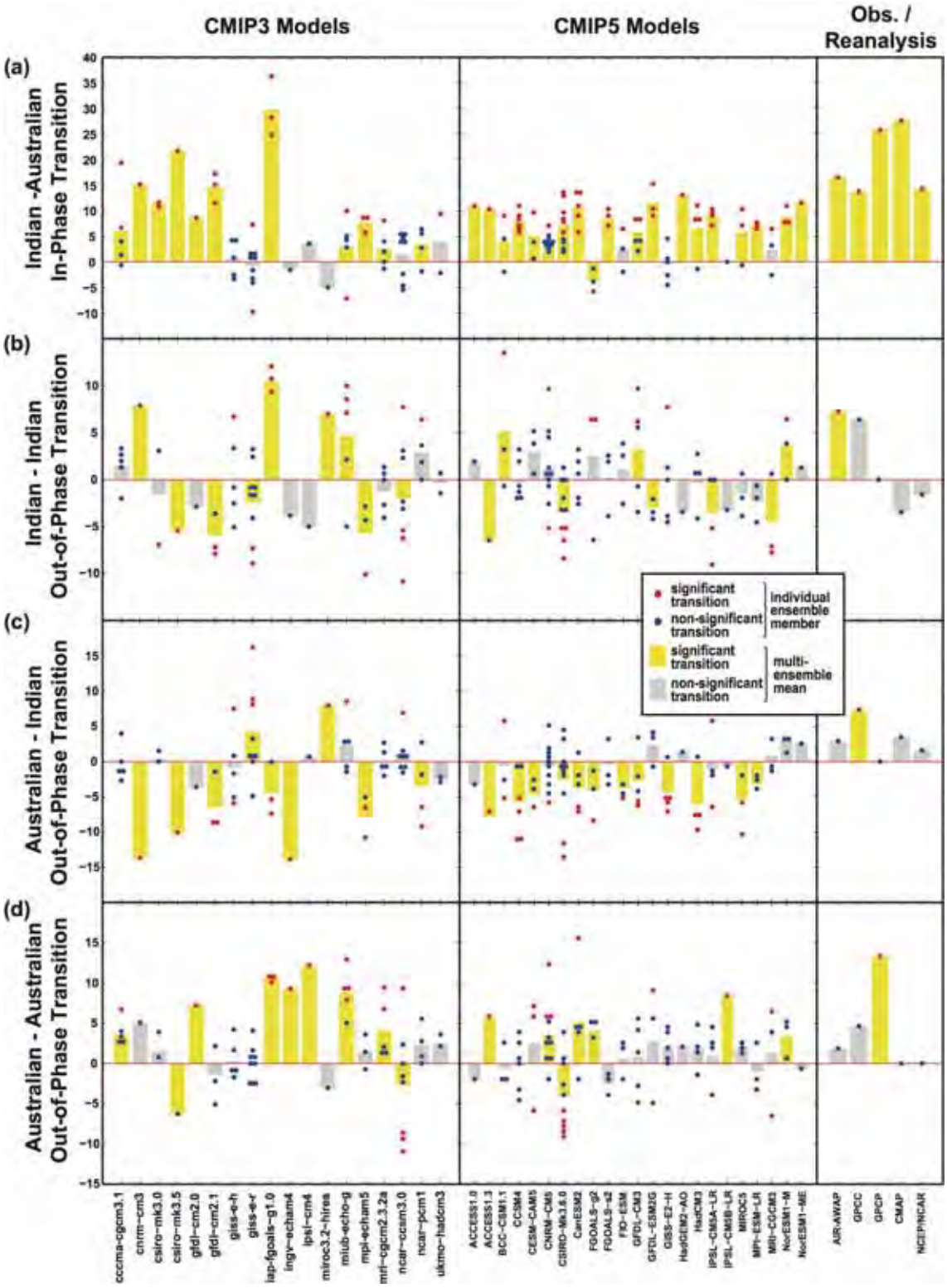

Figure 3.16 Percentage *enhanced predictability* for the (a) Indian-Australian, (b) Indian-Indian, (c) Australian-Indian and (d) Australian-Australian transitions based on land-restricted regions for observations/reanalysis and CMIP3 and CMIP5 models for which at least one ensemble member for that model and for at least one of the transitions shows a significant increase in

predictability. Circles represent individual ensemble members (marked in red are significant, p<0.1). Bars represent the multi-ensemble mean percentage *enhanced predictability* for each model with yellow indicating significant changes. The multi-ensemble mean predictability was calculated by concatenating time-series for all ensemble members prior to Monte Carlo resampling (Results of individual model ensemble members are listed in Appendix Table A.4&A.5).

and for 18 of 30 CMIP5 models (yellow bars in Figure 3.16a). In summary, while this transition appears to be robust for observational records, only about half of the models exhibit significant *enhanced predictability*.

As mentioned earlier in section 3.1.3, the significant enhanced predictability of the Indian-Indian monsoon out-of-phase transition is only found in the long-term reference observations (e.g. AIR/AWAP), but the predictability has decreased over the last 30 years (Table 3.2). With regard to models (Figure 3.16b), 7 out of 24 (29%) CMIP3 models and 6 out of 30 (20%) CMIP5 models show at least one ensemble member with significant enhanced predictability (at the 90% statistical level of confidence). However, individual models with multi-ensemble members often show contrasting results with regards to predictability, indicating multi-decadal variability in this transition. The model results suggest no robust *enhanced predictability* for this transition. Only a small proportion of multi-ensemble means of CMIP3 and CMIP5 models exhibit significant *enhanced predictability* (4 for CMIP3 and 3 for CMIP5). Moreover, some CMIP3 and CMIP5 models actually exhibit significant *negative predictability*. This means that for those models a strong Indian monsoon tends to be followed by a strong Indian monsoon in the following year, opposite to the sequence of events expected as part of a TBO.

For Australian-Indian monsoon out-of-phase transition (Figure 3.16c), only five

CMIP3 models and two CMIP5 models have at least one ensemble member with significant positive *enhanced predictability*, although again different ensemble members produce conflicting results. Surprisingly, the majority of models show significant *negative predictability*, in particular when considering concatenated ensemble members (10 out of 24 CMIP3 models and 18 out of 30 CMIP5 models). This means that a strong Australian monsoon will often be followed six months later by a strong Indian monsoon, opposite to the response expected for a successful Australian-Indian monsoon out-of-phase transition. This behaviour is not found in any of the observational datasets. This simulated response might be related to a longer than observed duration of ENSO in the CMIP simulations [*Taschetto et al.*, submitted]. For example, a La Niña event that persists too long into a second year would be expected to lead to a strong Australian monsoon followed by a strong Indian monsoon [*Jourdain et al.*, 2013]. In this way, differences in ENSO behaviour can affect the Australian-Indian monsoon in-phase transition.

Finally, the Australian-Australian monsoon out-of-phase transition (Figure 3.16d) has a variety of behaviours shown in observations/reanalysis. In particular only the short GPCP shows significant *enhanced predictability*. For this transition, there are some model/ensemble members with statistically *enhanced predictability*. However, there is little agreement across the models. Eight out of 24 CMIP3 models and 7 out of 30 CMIP5 models have at least one ensemble member with significant *enhanced predictability*. When considering concatenated ensemble members, there are 7 out of 24 CMIP3 models and 6 out of 30 CMIP5 models exhibiting significant *enhanced predictability*.

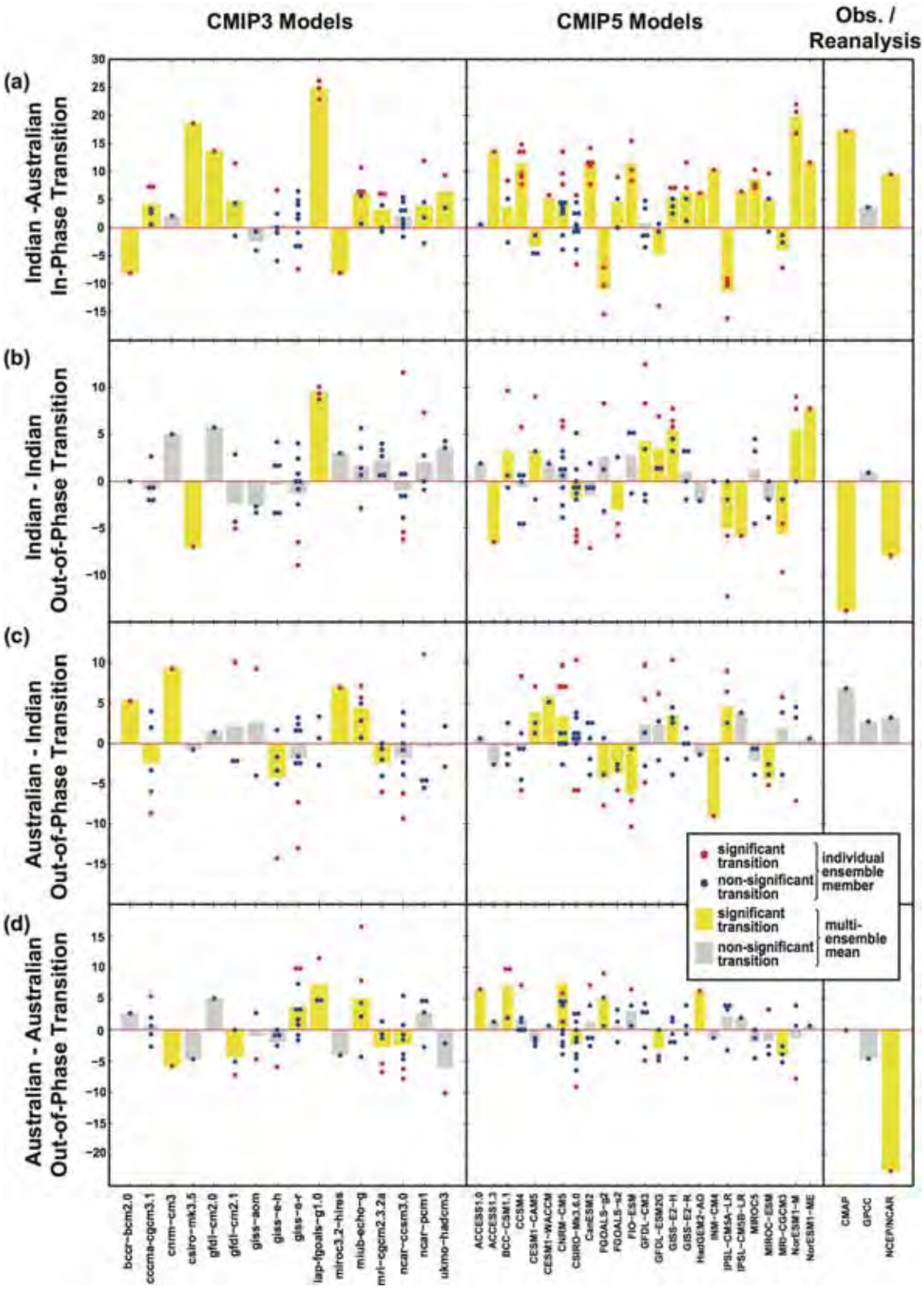

Figure 3.17 As Figure 3.16, but for the predictability of TBO transitions based on extended regions (Results of individual model ensemble members are listed in Appendix Table A.6&A.7).

In section 3.2.1, the seasonality of rainfall in the Indian and Australian extended monsoon regions was evaluated: there is less difference between monsoon and non-monsoon seasons compared to the land-only based rainfall. For the purpose of comparison, the Monte Carlo results calculated from EX-IMRIs and EX-AMRIs are shown in Figure 3.17. For Indian-Australian monsoon in-phase transition, significant *enhanced predictability* occurs in observation/reanalysis (CMAP and NCEP/NCAR) when the short-term is considered. There are 10 out of 24 CMIP3 models and 18 out of 30 CMIP5 models showing significant *enhanced predictability* in at least one ensemble member (red circles) for this transition (Figure 3.17a). When considering the predictability of concatenated ensemble members (yellow bars), CMIP3 models show a similar behaviour between land-only and extended regions. However, for CMIP5 models, the predictability of concatenated ensemble members demonstrates a larger range (5%-20%) with higher variance (SD is 7.3%), compared to their land-only counterparts (range is 5%-15% with a SD of 4.2%). For Indian-Indian monsoon out-of-phase transition (Figure 3.17b), the short-term observation/reanalysis (CMAP and NCEP/NCAR) surprisingly show significant negative predictability. There is little consensus across models. Unlike for the land-only indices, the large proportion of models with significant negative predictability is not seen in the predictability of the Australian-Indian monsoon out-of-phase transition from the extended-region indices (Figure 3.17c). It might suggest that the link between the Indian and Australian monsoon with respect to the extended regions is not that clear [*Neale and Slingo*, 2003]. The contrasting results among observations and models with different monsoon indices suggest that there is no robust process driving an Australian-Indian monsoon out-of-phase transition and as such this transition does not provide additional predictability for the Indian monsoon.

Given that overall there are fewer models showing *enhanced predictability* when using the extended regions, we will focus our analysis below on teleconnections of SST anomalies in the tropical Pacific to the monsoonal rainfall in land-restricted regions. In particular, we examine ENSO variability in the CMIP5 model simulations, and attempt to understand how the SST anomalies in the Pacific Ocean could exert an influence on TBO transition predictability.

3.2.3 Influence of ENSO

As documented in numerous previous studies and also in section 3.1.4, the strength of Indian/Australian monsoon rainfall can be modulated by ENSO (e.g. *Holland* [1986], *Webster and Yang* [1992]). In this section, we will evaluate the teleconnection between ENSO and Indian/Australian monsoon rainfall in CMIP5 models, and evaluate whether the TBO transition can be related to ENSO characteristics in the CMIP models.

The JJAS (for Indian land region) and DJFM (for Australian land region) averaged rainfall are correlated with the NINO3.4 indices at different leads and lags for all CMIP5 models (Figure 3.18) to show the relationship between ENSO and Indian/Australian monsoons. In Figure 3.18a, we calculate the lagged correlations with the averaged JJAS Indian rainfall in year(0) leading the NINO3.4 index by 29 months to the averaged JJAS Indian rainfall in year(0) lagging the NINO3.4 index by 15 months. Thus, the peak of NINO3.4 indices in year(0) lags the JJAS Indian rainfall in year(0) by 3 months. The models have been sorted by the correlation between with the reference AIR/HadISST1 (top, name in red) and simulated lagged correlation time-series. In Figure 3.18a,

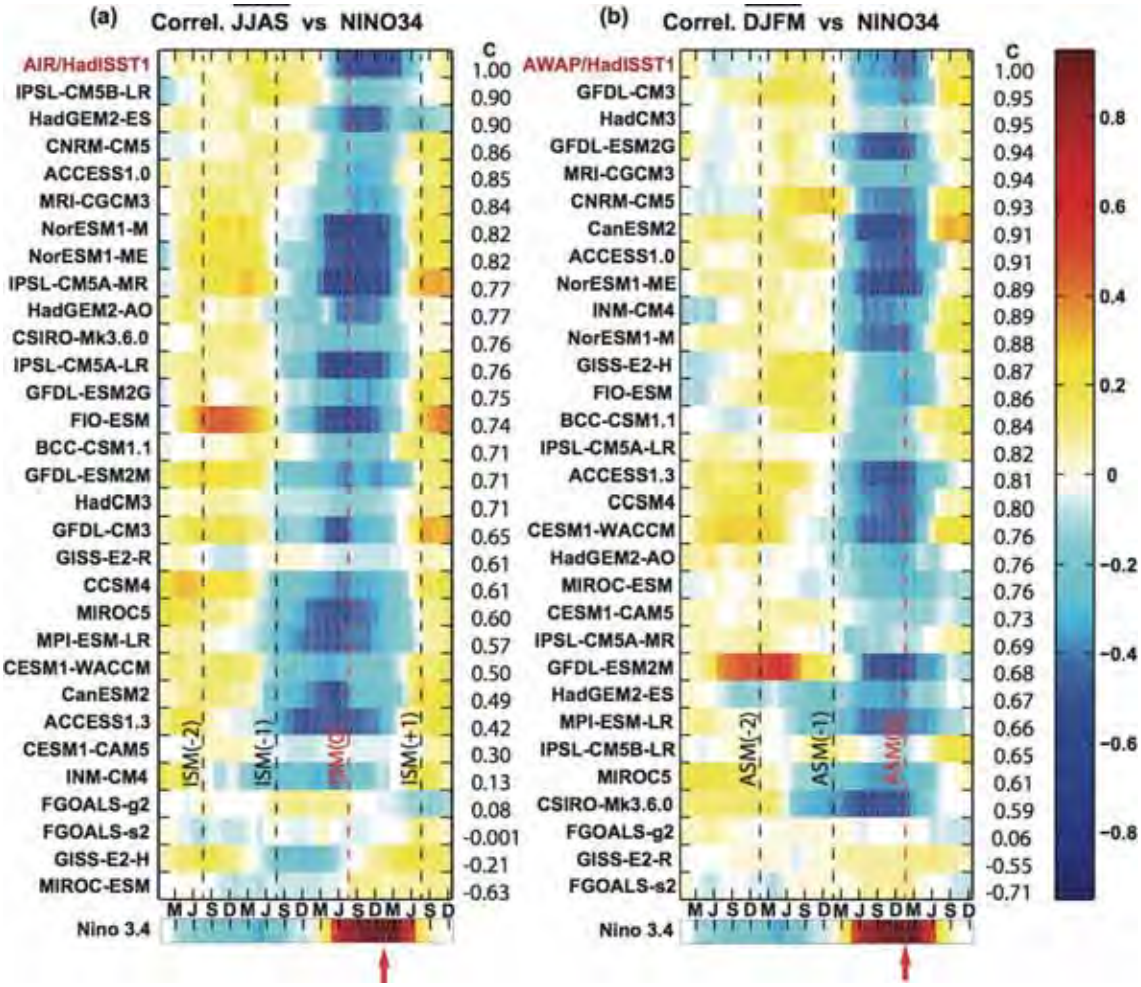

Figure 3.18 Lag correlation between (a) JJAS Indian land-only rainfall and monthly NINO3.4 indices, and lag correlation between (b) DJFM Australian land-only rainfall and monthly NINO3.4 indices for observation (top, red) and 30 CMIP5 models. The correlations between NINO3.4 averaged in DJFM and lagged monthly NINO3.4 values are shown at bottom of (a) and (b). Models are ranked according to the correlation with observation, with the values of correlation coefficient (r) listing on right. Months are labelled on x-axis (M, J, S and D represent March, June, September and December, respectively). ISM/ASM marks the Indian/Australian summer monsoon peak with the numbers in parentheses showing the years related to rainfall. The red arrows show the DJFM NINO3.4 SST of year(0) (modified from Figure 7&11 of *Jourdain et al.* [2013]).

Indian monsoon rainfall is highly negatively correlated with the developing ENSO that peaks a few months later between November and March in

observations. Most CMIP5 models show the negative correlation between JJAS rainfall and the NINO3.4 indices, however, with a range of timing and strength. For example, IPSL-CM58-LR and CNRM-CM5 have realistic timing, however, with weaker negative correlation than observation. In a number of models the maximum negative relationship occurs a few months early, i.e. NorESM1-ME, NorESM1-M, and IPSL-CM5A-MR with the maximum negative correlation starting from March in year(-1). For a number of models, the negative correlation relationship lasts too long, like ACCESS1.3 with correlation coefficients of less than -0.6 over a period of 15 months. Interestingly, the JJAS rainfall in model FIO-ESM not only show high negative lagged correlations with the NINO3.4 indices from December in year(-1) to December in year(0), but also a strong positive correlation with the NINO3.4 indices from July in year(-2) to July in year(-1). Some models exhibit strange behaviour in the correlations. For example, the negative correlations in INM-CM4 persist too long and also have biases in timing, while FGOALS-g2 shows completely the opposite correlation relationship to the observations. The most poorly performing models with lagged correlation time-series correlations less than 0.30, are INM-CM4, FGOALS-g2, FGOALS-s2, GISS-E2-H and MIROC-ESM.

The fact that minimum correlation occurs with the monsoon leading NINO3.4 by some months has lead some authors to suggest that the strength of the Indian monsoon may actually modulate the characteristics of the subsequent ENSO. *Kirtman and Shukla* [2000] revealed that the strongest negative correlation between Indian monsoon and ENSO appears approximately three to six months immediately following the Indian monsoon season. This is further supported by *Wu and Kirtman* [2003] in a coupled GCM. They concluded the monsoon-induced wind anomalies propagate eastwards and modulates SST in the western and central equatorial Pacific. *Mokhov et al.* [2011] also proposed a

linear monsoon-to-ENSO influence, such that the Indian monsoon can affect future behaviour of ENSO, and attributed this influence to the change of trade winds in the Pacific Ocean responding to the changes of monsoon system.

The lagged correlations shown in Figure 3.18b are calculated with the averaged DJFM Australian rainfall that leads the NINO3.4 index by 35 months to the averaged DJFM Australian rainfall that lags the NINO3.4 index by 9 months. Therefore, the Australian monsoon rainfall in year(0) occurs simultaneously with the peak of NINO3.4 indices. For the lag-lead correlation evolution between Australian monsoon rainfall and NINO3.4 indices (Figure 3.18b), the reference AMAP/HadISST1 observations demonstrate the simultaneous negative correlation between Australian monsoon rainfall and NINO3.4 indices. There are 27 out of 30 CMIP5 models that correctly show a negative correlation with three models showing no or slightly positive simultaneous correlation (FGOALS-g2, GISS-E2-R and FGOALS-s2). There are also amongst the models that perform the worst for the Indian monsoon. The strongly negative simultaneous correlations found in most CMIP5 models confirm that large influence of ENSO on Australian monsoon rainfall, which has been reported in numerous previous studies (e.g. *Joseph et al.* [1991]; *Power et al.* [1999]; *Yu and Janiga* [2007]). In a number of models, the negative correlations actually start a few months early and last to the end of Australian monsoon, such as GFDL-ESM2G with a negative correlation starting in June(0). Eleven models show negative correlation, but the magnitude is small. The GFDL-ESM2M also shows a strong positive correlation between the Australian monsoon rainfall and the NINO3.4 indices lagging by 24 months.

It is obvious that ENSO has a large influence over the two monsoon systems. As such we are interested in investigating how much of the TBO-like behaviour

in the models can be simply a passive response to ENSO. First, we correlate the *enhanced predictability* of 30 CMIP5 models with the corresponding correlation between monsoon rainfall and NINO3.4 indices for each of the transitions (Figure 3.19), to test if the strength of the ENSO-monsoon relationship can partially explain the *enhanced predictability*. In each plot, circles of one colour represent a set of CMIP5 models for one of the TBO transition.

Figure 3.19a shows a scatter pot of *enhance predictability* of each TBO transition against the correlation between the Australian monsoon rainfall and the NINO3.4 lagged by one year. The results for the Indian-Indian and the Australian-Australian monsoon out-of-phase transitions are significant (p-values are less than 0.1). For the Indian-Indian monsoon out-of-phase transition, the predictability appears to be somewhat dependent (25% of variance) on a relationship between the SST anomalies in the central Pacific and the Australian monsoon one year later. Also for the Australian-Australian monsoon out-of-phase transition, the SST anomalies in the central Pacific one-year early help the successful transition between two Australian monsoons.

With respect to the relationship of predictability with the simultaneous correlation between the NINO3.4 and the Australian monsoon rainfall (Figure 3.19b), the correlation coefficient is -0.48 with a p-value less than 0.1. This indicated that approximately 23% of the variance of the *enhanced predictability* in this transition is accounted for by the relationship between Australian monsoon rainfall and averaged DJFM SST anomalies in the central Pacific. This connection for other transitions is less clear.

A significant correlation (0.33) exists between predictability of the Indian-Indian

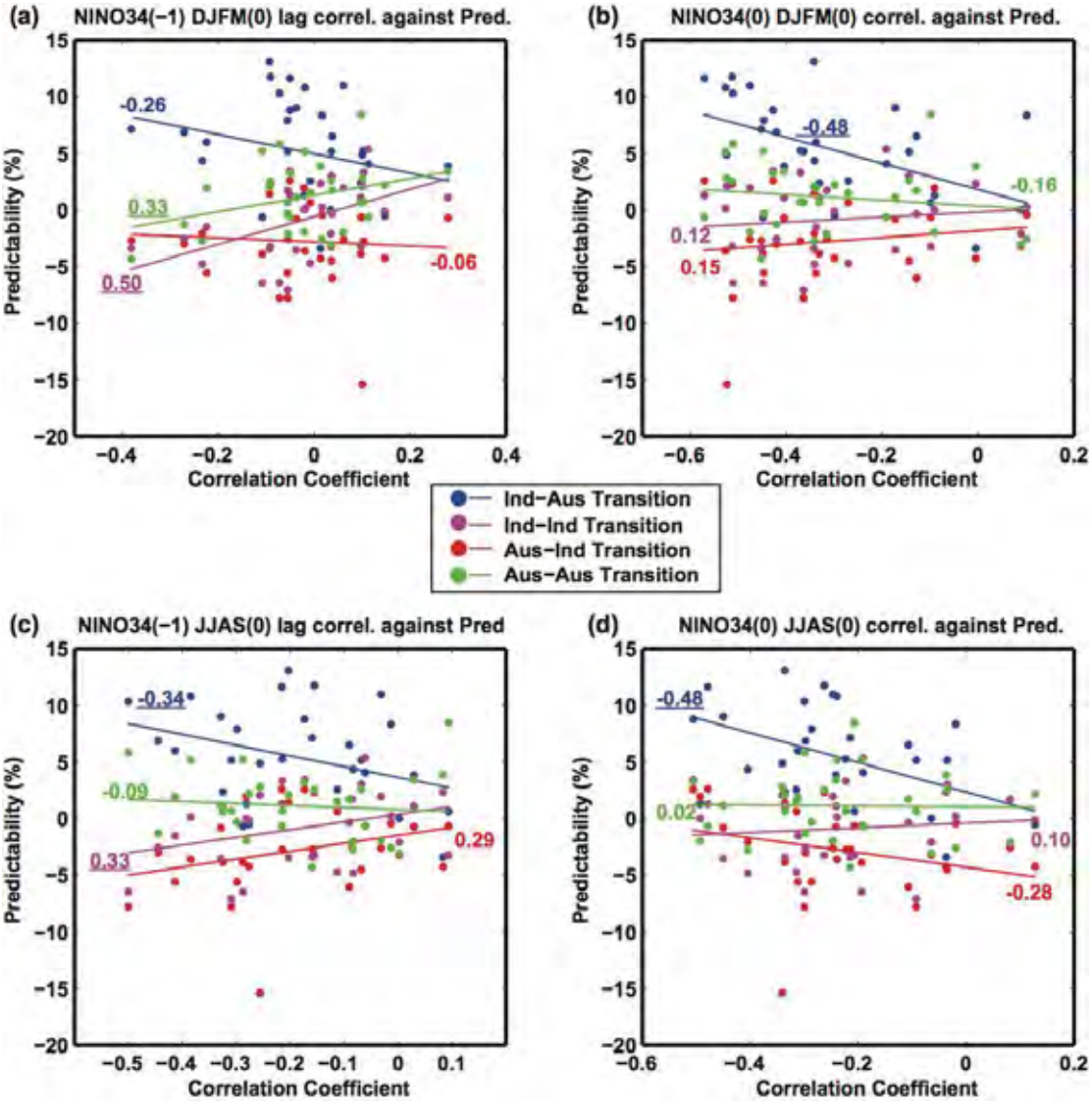

Figure 3.19 The scatter plots of averaged *enhanced predictability* of each CMIP5 model for four transitions (marked in different colours) against the lag correlation between (a) DJFM rainfall and (c) JJAS rainfall and NINO3.4 averaged SST in previous DJFM, the correlation between (b) DJFM rainfall and (d) JJAS rainfall and NINO3.4 averaged SST in DJFM. In each plot, the blue circles represent the Indian-Australian monsoon transitions, the red ones represent the Australian-Indian transitions, the magenta represents the Indian-Indian monsoon transitions and the green shows the Australian-Australian monsoon transitions. The line in each colour represents the best-fit liner regression with the value of correlation coefficient in corresponding colour. The significant correlation coefficient values are underscored.

monsoon out-phase transition and the relationship between DJFM NINO3.4

and the following Indian monsoon rainfall anomalies (Figure 3.19c). Conversely, we find a significant negative correlation (-0.34) between predictability of the Indian-Australian monsoon in-phase transition and the relationship between DJFM NINO3.4 and the following Indian monsoon rainfall anomalies (Figure 3.19c). In Figure 3.19d, the correlation for Indian-Australian monsoon in-phase transition is -0.48 with p-value less than 0.1, again indicating that approximately 23% of the variance of the *enhanced predictability* in this transition is accounted for by the relationship between Indian monsoon rainfall and the following DJFM NINO3.4.

The phase relationship between DJFM NINO3.4 SST anomalies and Indian/Australian monsoon rainfall described above is summarized in Figure 3.20 (only significant results are included). Based on the correlation analysis, SST anomalies in the Niño 3.4 region two seasons prior to Indian monsoon season appear to play some role in certain TBO transitions (Figure 3.20). The enhanced predictability of the Indian-Australian transition depends not only on the strength of the concurrent ENSO-Indian monsoon relationship (i.e. NINO3.4(0) and JJAS(0)) but also on the strength of the relationship between the Indian monsoon and ENSO activity prior to the Indian monsoon (i.e. NINO3.4(-1) and JJAS(0)).

We now investigate how in-phase (double El Niño or double La Niña) or out-of-phase (El Niño to La Niña or La Niña to El Niño) ENSO transitions affect the TBO transitions. We define in-phase ENSO transitions as when the averaged DJFM NINO3.4 standardized SST anomalies are greater/lower than +1/-1 SD for 2 successive years, while the out-of-phase ENSO transitions as when the averaged DJFM NINO3.4 standardized SST anomalies transition from greater/lower than +1/-1 SD to lower/greater than -1/+1 SD. Then, we

calculate the proportions of in-phase and out-of-phase ENSO transitions over the entire DJFM NINO3.4 SST time-series. The ratio difference is calculated by subtracting the proportion of in-phase ENSO transitions from that of out-of-phase. Thus, a negative ratio difference implies more out-of-phase ENSO transitions occur compared to in-phase ENSO transitions, while positive ratio difference implies more in-phase ENSO transitions occur.

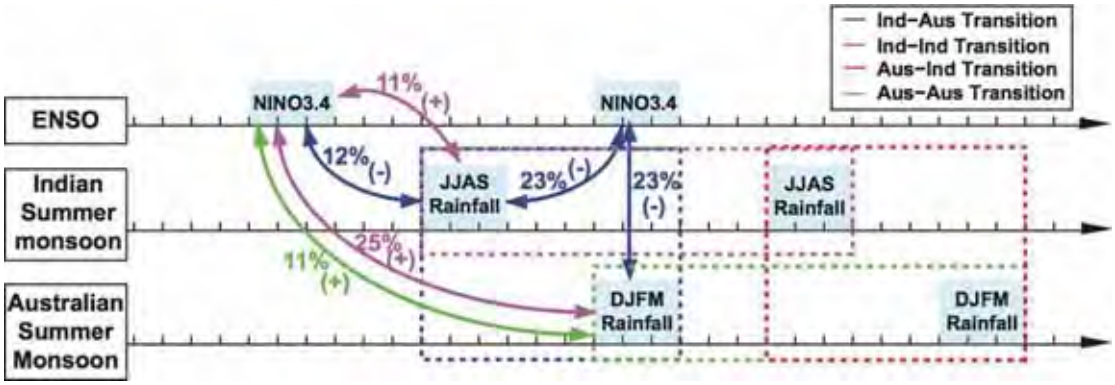

Figure 3.20 Schematic of the phase relationships between SST anomalies in NINO3.4 region and Indian/Australian monsoon rainfall drawn from Figure 3.19. Three parallel timeframes are used to represent the temporal relationship between ENSO, Indian summer monsoon and Australian summer monsoon. Double-headed arrows in corresponding colours show the transition where the relationship exists. The sign of (+)/(-) represents positive/negative correlation, and the squared correlation coefficient are represented as percentage.

Figure 3.21 shows the *enhanced predictability* for the different transitions against the ratio difference of ENSO for individual CMIP5 models. We remove seven bad models that have unrealistic low correlations, compared to observations, between ENSO and Indian and Australian monsoon rainfall (i.e. less than 0.40 for JJAS-NINO3.4 and DJFM-NINO3.4, respectively, see Figure 3.18). The seven bad models are CESM1-CAM5, INM-CM4, FGOALS-g2, FGOALS-s2, GISS-E2-H, GISS-E2-R and MIROC-ESM. Correlations between predictability and ratio difference are only significant for the Indian-Australian monsoon in-phase and Indian-Indian monsoon out-of-phase transitions (Figure

3.21a & b), with the correlation magnitudes increasing after removal of the bad models. For Indian-Australian monsoon in-phase transition, models, which have a higher proportion of consecutive El Niño or La Niña events, tend to have higher predictability (although the correlation is only significant after removal of the "bad" models). Particularly, for Indian-Indian monsoon out-of-phase transition, higher predictability tends to be associated with models that have more out-of-phase ENSO events. For the other two TBO transitions, the connection to the phase of ENSO is not that clear.

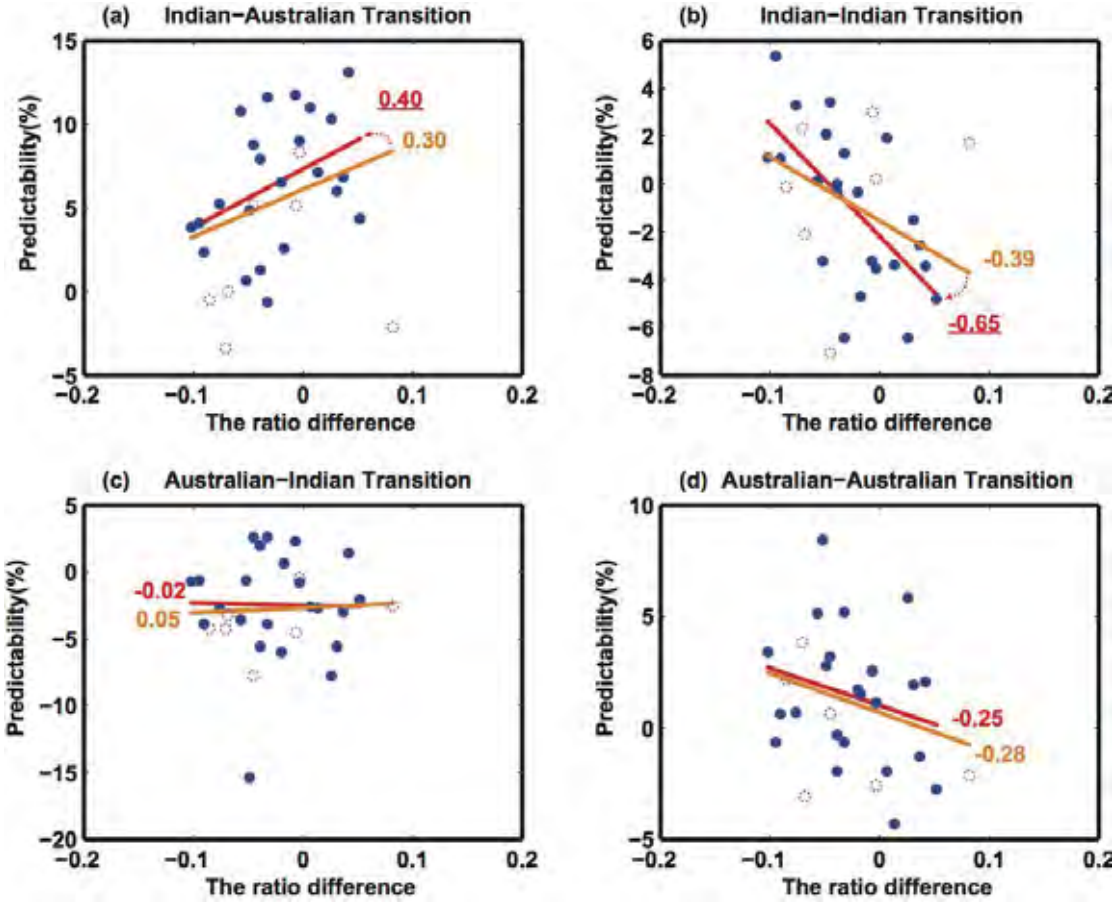

Figure 3.21 The scatter plots of the ENSO ratio difference against the percentage of predictability from (a) Indian-Australian Transition, (b) Indian-Indian Transition, (c) Australian-Indian Transition and (d) Australian-Australian Transition. The ratio difference is the incidence of in-phase ENSO events minus that of out-of-phase ENSO events. In this figure, the in-phase events are defined as the averaged DJFM NINO3.4 standardized SST anomalies is continuously greater/lower than 1/-1 SD for 2 successive years, while the out-of-phase events

are defined as the averaged DJFM NINO3.4 standardized SST anomalies transition from greater/lower than +1/-1 SD to lower/greater than -1/+1 SD. The orange/red lines show the best-fit regression before/after removing 7 bad models (shown in magenta dashed circles) that are unable to correctly simulate ENSO. The correlation coefficient is shown in each plot in corresponding orange/red with underscoring indicating the significant ones.

3.3 Predictability of transitions in future projections

A number of previous studies have indicated that monsoon characteristics are sensitive to the background state and Global warming. *Lee and Wang* [2012] investigated the global monsoon in the Representative Concentration Pathway RCP4.5 scenario and show that not only the monsoon domain but also monsoon duration will expend in the period of 2006-2100. *Hu et al.* [2000] investigated the Asian summer monsoon in a coupled model that is forced by increasing greenhouse gas and found the intensity and variability of Asian summer monsoon increased. They attributed such a change to the increasing corresponding SST variability in the tropical Pacific after the year of 2030. *Fan et al.* [2012] pointed out that the competing effects between convective latent heating and dry static stability are the possible influence on South Asian summer monsoon circulation when they examined the CMIP3 simulations responding to anthropogenic greenhouse gas. They also considered the change of ENSO as an important factor to modulate the monsoon circulation.

As such in the final part of our study, we also examine whether robust changes in *enhanced predictability* can be detected in future projections, based on 22 CMIP5 models under the RCP8.5 scenario (see Appendix Table A.3). For the purpose of comparison, we choose 50 years from the historical period of 1956-2005 and corresponding RCP8.5 period of 2051-2100. We use the same Monte Carlo technique for examining transition predictabilities for the historical

and future periods for both individual and concatenated ensemble members. Figure 3.22 shows differences of the predictability of four TBO transitions between historical records and corresponding RCP8.5 scenarios. Overall we find little evidence for any consistent future changes in predictability for any of the TBO transitions.

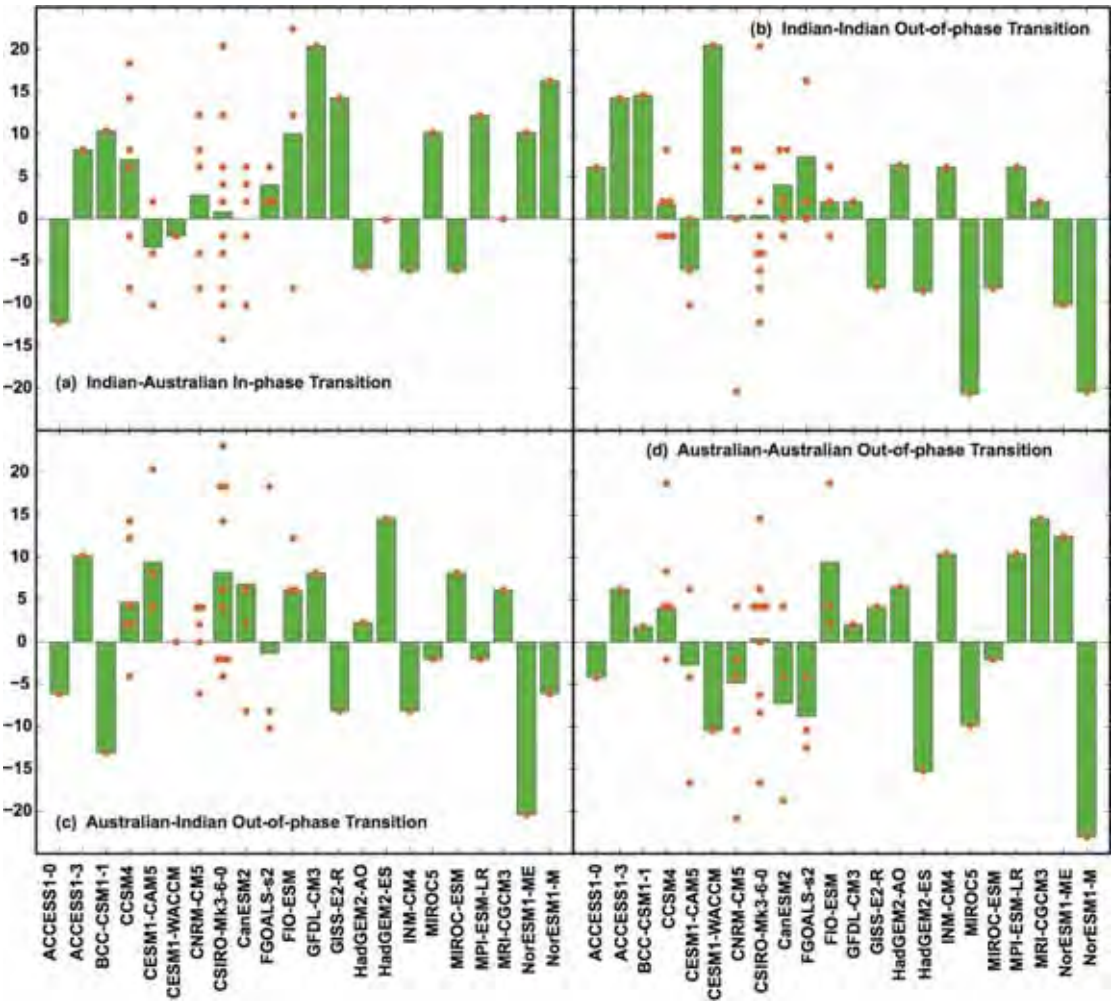

Figure 3.22 Differences of predictability between 50-year historical records and corresponding RCP8.5 scenarios (RCP8.5 minus historical) for (a) Indian-Australian in-phase transition, (b) Indian-Indian out-of-phase transition, (c) Australian-Indian out-of-phase transition and (d) Australian-Australian out-of-phase transition. Red circles represent individual ensemble members, and green bars show concatenated ensemble members.

For the Indian-Australian monsoon in-phase transition (Figure 3.22a), 13 out of 22 models show increased projected predictability for concatenated ensemble

members. For the models with large number of ensemble members, individual members show little consistency with projected increased and decrease in predictability (i.e. CSIRO-Mk3.6.0 and CanESM2). For the Indian-Indian monsoon out-of-phase transition (Figure 3.22b), there are 15 models showing increased projected predictability (based on concatenated ensemble members). CSIRO-Mk3.6.0 also shows a range of change of predictability for all ensemble members. For both Australian-Indian and Australian-Australian monsoon out-of-phase transitions (Figure 3.22c&d), 50% of models with increasing predictability in the projection. Models with multi-model ensemble members again show contrasting changes for individual ensemble members.

Chapter 4. Conclusion

This study examines the Indian-Australian summer monsoon system in four primary aspects:

1) Characteristics of the monsoon transitions, in particular, the predictability associated with these transitions;
2) Relationship between observed SST patterns and monsoon transitions;
3) Fidelity of CMIP3 and CMIP5 models in simulating the mean states and seasonality of this system;
4) Projected changes in the predictability of monsoon transitions

4.1 Improvement of simulated monsoon seasonality from CMIP3 to CMIP5

A necessary (but insufficient) condition for successful simulation of these transitions is some degree of realism in the simulation of the mean state and seasonality of the monsoons. We compared the seasonality of rainfall in land-only monsoon regions with that in the extended regions. For both

observations and models, the extended Indian region exhibits lower regional averaged monsoon precipitation in JJAS. In the extended Australian monsoon region, seasonality is relatively weak with considerable rainfall even outside of the monsoon season. The Maritime Continent that is included in the extended Australian monsoon region serves as the "land bridge" along which the maximum convection migrates from the Indian summer monsoon to the Australian summer monsoon. *Chang et al.* [2005] show that the Maritime Continent south of 5°S has wet season during January and April, with approximately 10 mm/d rainfall rate. In addition, this region contains substantial ocean area, where there is almost constant rain at all times of the year.

With respect to the simulated seasonality of rainfall in land-only monsoon regions, while all models produce at least some monsoon-like behaviour, there are very large spreads in average monsoonal rainfall in both CMIP3 and CMIP5 models, ranging from 40% to 140% of the observed total for Indian rainfall and from 30% to 130% for Australian rainfall. Multi-model means of Indian maximum rainfall are 6 mm/d for both CMIP3 and CMIP5 models, which underestimates the observational maximum rainfall (7-9 mm/d, depending on the datasets considered), while the multi-model means of Australian maximum rainfall for both CMIP3 and CMIP5 models are inside of the observational maximum rainfall range from 6 to 9 mm/d. Most models successfully reproduce the timing of the monsoons although phase shifts of up to two months are seen in a few models. Overall, there is no obvious improvement in the average strength of monsoon rainfall from CMIP3 to CMIP5. However, the CMIP5 models do show improved seasonality for both monsoons, in particular they are better at simulating the low levels of rainfall outside of the monsoon seasons.

4.2 Predictability for the Indian-Australian monsoon in-phase transitions

Using a Monte Carlo technique, we have presented the predictabilities associated with the four transitions that make up the Tropospheric Biennial Oscillation (TBO) for both land-only and extended monsoon regions. As the predictabilities calculated from extended monsoon regions are less clear for any TBO transitions, we mainly focus on predictability and the teleconnection of ENSO associated with the land-restricted regions. A significant *enhanced predictability* in the Indian-Australian transition is seen in all the observational/reanalysis produces with different periods ranging from approximately 13% to 28%. In particular, higher *enhanced predictability* is seen in the period of 1979-2008. The majority (13 of 24 CMIP3 and 20 of 30 CMIP5) models simulate significant *enhanced predictability*, with the ranges of 5%-30% for CMIP3 and 5%-15% for CMIP5 models. The results suggest that given the strength of the Indian monsoon we have approximately 10%-25% increased chance of correctly predicting whether the following Australian monsoon will be weaker or stronger than normal.

When investigating the relationship between predictability in the Indian-Australian monsoon transition and ENSO, higher predictability appears when the Indian monsoon is strongly negatively correlated with the subsequent ENSO and also when the Australian monsoon has a strong negative simultaneous correlation with ENSO (Figure 3.19 & 3.20). In addition, higher predictability tends to be obtained from models with consecutive El Niño or La Niña events (Figure 3.21). The consecutive ENSO events before and after the Indian monsoon play some roles in the Indian-Australian monsoon in-phase transition. In particular, the Indian monsoon rainfall and subsequent peak of

ENSO are highly negative correlated. The questions arise about how the SST anomalies in the central Pacific interact with Indian monsoon and facilitate the in-phase transition from Indian monsoon to Australian monsoon. Some previous studies revealed the negative correlation between Indian monsoon and ENSO after this Indian monsoon season and suggested that the Indian summer monsoon anomalies can influence the subsequent ENSO event (e.g. *Yasunari* [1990], *Kirtman and Shukla* [2000], *Mokhov et al.* [2011]). Such monsoon-to-ENSO influence is modulated by the anomalous surface winds caused by Indian anomalous monsoon over the central and eastern Pacific. However, some other studies argued that it is the SST anomalies in the tropical Pacific that provide certain "memory" from boreal summer (JJA) to boreal winter (DJF) and build up the in-phase transition from Indian summer monsoon to Australian summer monsoon (e.g. *Yu and Janiga* [2007]). Our results (see Figure 3.8) show that the SST anomalies in the Tropical Pacific start to become evident in the Indian monsoon season and persist to the Australian summer monsoon. However, before the Indian monsoon, no significant SST anomalies are shown in the tropical Pacific. During the Indian monsoon season, significant SST anomalies appear in the Pacific Ocean, which plays an important role in the onset of Indian monsoon. The Indian monsoon then might serve as a trigger to the subsequent anomalous ENSO [*Kirtman and Shukla*, 2000]. After the Indian monsoon season, some mechanisms help the persistent of SST anomalies until the Australian summer monsoon. Identifying the mechanisms of "memory" is beyond the scope of this study but is clearly important to our understanding of the impact of the SST anomalies in the tropical Pacific on the Indian-Australian monsoon in-phase transition.

4.3 Predictability for other TBO transitions

The *enhanced predictability* of ~8% for the Indian-Indian monsoon out-of-phase

transition is only captured in the long-term observational datasets (AIR and GPCC). When investigating the influence of ENSO on this out-of-phase transition in CMIP5 models, we found that the models that have more out-of-phase ENSO transitions (i.e. El Niño followed the next year by La Niña or La Niña followed by El Niño) tend to have higher predictability (Figure 3.21). *Fasullo* [2004] used observational datasets to investigate biennial characteristics of Indian monsoon rainfall and also found that during the Indian-Indian monsoon out-of-phase transition the strong Indian monsoon tends to be accompanied by La Niña and the preceding years are often associated with El Niño. While some models indicate significant *enhanced predictability*, many models actually show significantly reduced negative predictability. This suggests that in many models a strong Indian monsoon will tend to be followed by another strong monsoon in the subsequent year (opposite to the observations). Negative predictability is also evident in many models for the Australian-Indian transition. Indeed many of the models show common behaviour.

By splitting up observational rainfall dataset we find that some transitions are significant only over certain time periods. For example, the significant *enhanced predictability* of Australian-Australian monsoon out-of-phase transitions just appears in last 30 years. The Indian-Indian monsoon out-of-phase transitions experience a decreased predictability during the period of 1979-2007. There is no consistency in predictability of Australian-Indian monsoon out-of-phase transition across all observations during period of 1979-2007. For models with more than one ensemble members, individual ensemble members often show very different predictability for one transition. In some cases the sign of the *enhanced predictability* changes from member to member. This indicates a strong internal multi-decadal variability in the efficacy of the TBO transitions.

Given that climate models suggest that certain characteristics of the monsoon will change with Global warming, we also investigated the changes of predictability of monsoon transitions in RCP8.5 scenario. However, no consistent increase or decrease on the predictability of the TBO transitions is shown in CMIP5 RCP8.5 scenario. One reason for this could be that the CGCM models fail to project consistent changes in ENSO [*Collins et al.*, 2010], and ENSO life cycle is poorly simulated in CMIP5 [*Bellenger et al.* 2013, submitted].

In summary, while there is reasonable agreement between the observed and simulated Indian-Australian monsoon in-phase transition, the other transitions have a wide variety of behaviour in both the observations and the climate models. The results of predictability for land-only regions have been summarised in Table 3.4.

4.4 Future work

A number of questions remain unanswered that will be the focus of future work.

- Some of our results regarding the transition may relate to the definitions we have used. We would like to test the sensitivity of our results to different definitions, for example using the size of rainfall changes from one year to the next to select the relative strong or weak monsoons, rather than simply whether rainfall is anomalously positive or negative.
- In this study, the ENSO events are based on classification of *Ummenhofer et al.*[2009] whose definition filtered out the C-P type ENSO. In the future work, we will take into account all types of ENSO to explore the influence of ENSO behaviour on monsoon transitions.
- As shown in our results, ENSO characteristics in models can affect Australian-Indian and Indian-Indian monsoon transitions. Future work will try to determine why and how ENSO behaviour affects these two

transitions but not the other monsoon transitions.

- With respect to simulated predictability, by stratifying the models into those that show enhanced, average or reduced predictability we hope to identify common processes that lead to the success or failure of the various transition

Table 3.4 The percentage of predictability for all transitions based on observation/reanalysis, CMIP3 historical, CMIP5 historical and RCP 8.5. The enhanced predictabilities are marked in red while negative predictabilities are marked in blue.

		IND-AUS	IND-IND	AUS-IND	AUS-AUS
Observation & Reanalysis	AIR/AWAP	16.5%	7.3%	2.8%	1.9%
	GPCC	13.8%	5.5%	8.3%	4.6%
	GPCP	25.8%	0	0	13.3%
	CMAP	27.6%	-3.5%	3.6%	0
	NCEP/NCAR	14.3%	-1.6%	3.2%	0
CMIP3	cccma-cgcm3.1	6.00%	1.46%	0	3.60%
	cnrm-cm3	15.11%	7.91%	-13.67%	5.07%
	csiro-mk3.0	11.63%	-1.54%	0.39%	1.56%
	csiro-mk3.5	21.71%	-5.43%	-10.08%	-6.25%
	gfdl-cm2.0	8.63%	-2.8%	-3.60%	7.25%
	gfdl-cm2.1	14.63%	-5.96%	-6.49%	-1.44%
	giss-e-h	0.67%	0	-0.84%	0.34%
	giss-e-r	-0.81%	-2.42%	4.25%	0.09%

	iap-fgoals-g1.0	29.75%		10.47%		-4.48%		10.76%	
	ingv-echam4	-1.54%		-3.85%		-13.85%		9.30%	
	ipsl-cm4	3.57%		-5.00%		0.71%		12.23%	
	miroc3.2-hires	-5.00%		7.00%		8.00%		-3.03%	
	miub-echo-g	3.00%		4.69%		2.43%		8.87%	
	mpi-echam5	7.67%		-5.73%		-7.93%		1.44%	
	mri-cgcm2.3.2a	2.68%		-1.20%		0.13%		4.17%	
	ncar-ccsm3.0	1.65%		-2.02%		1.07%		-2.72%	
	ncar-pcm1	3.44%		2.96%		-3.45%		2.30%	
	ukmo-hadcm3	3.96%		-0.36%		-2.53%		2.53%	
CMIP5		**Historical**	**RCP8.5**	**Historical**	**RCP8.5**	**Historical**	**RCP8.5**	**Historical**	**RCP8.5**
	ACCESS1.0	10.97%	-2.04%	1.94%	12.24%	-3.23%	-2.08%	-1.95%	-2.13%
	ACCESS1.3	10.32%	12.24%	-6.45%	4.08%	-7.79%	4.08%	5.84%	12.50%
	BCC-CSM1.1	4.07%	10.4%	5.14%	14.58%	-0.64%	-4.17%	-0.64%	0
	CCSM4	7.96%	11.37%	-0.32%	0	-5.71%	-0.67%	-0.22%	2.35%
	CESM1-CAM5	5.14%	2.68%	3.00%	-4.03%	-4.72%	2.03%	2.58%	-1.35%

	CNRM-CM5	3.81%	4.82%	1.15%	-3.21%	-0.58%	-1.21%	3.55%	-1.21%
	CSIRO-Mk3.6.0	7.10%	6.01%	-3.40%	-3.01%	-2.58%	4.02%	-4.00%	1.41%
	CanESM2	10.71%	11.65%	0.13%	4.02%	-3.75%	4.03%	5.17%	-0.40%
	FGOALS-g2	-3.63%	—	2.55%	—	-4.07%	—	4.07%	—
	FGOALS-s2	8.35%	10.74%	0.21%	2.01%	-0.43%	-2.03%	-2.58%	-7.43%
	FIO-ESM	2.36%	5.37%	1.07%	2.68%	-3.86%	-0.68%	0.64%	6.08%
	GFDL-CM3	5.81%	12.24%	3.30%	6.12%	-2.77%	4.09%	0.83%	4.17%
	GFDL-ESM2G	11.57%	—	-2.99%	—	2.32%	—	2.78%	—
	GISS-E2-H	-0.39%	—	0	—	-4.39%	—	1.94%	—
	HadGEM2-AO	13.10%	14.58%	-3.45%	12.50%	1.39%	12.50%	2.08%	12.77%
	HadCM3	6.55%	—	-0.34%	—	-6.04%	—	1.90%	—
	IPSL-CM5A-LR	9.03%	—	-3.53%	—	-0.97%	—	0.97%	—
	IPSL-CM5B-LR	0	—	-3.23%	—	-0.65%	—	8.44%	—
	MIROC5	5.81%	2.04%	-1.50%	-22.45%	-5.39%	-2.04%	2.16%	-6.25%
	MPI-ESM-LR	7.10%	20.41%	-2.36%	-4.08%	-3.23%	0	-1.08%	6.25%
	MRI-CGCM3	2.37%	-4.08%	-4.50%	0	0.86%	8.16%	1.29%	4.17%

	NorESM1-M	8.82%	16.33%	3.64%	-6.12%	3.02%	-6.12%	3.45%	-2.08%
	NorESM1-ME	11.61%	20.41%	1.29%	-10.20%	2.58%	-4.08%	-0.65%	-8.33%

References

Adams, D. K., and A. C. Comrie (1997), The North American monsoon, *Bull. Amer. Meteor. Soc.*, *78*(10), 2197–2213.

Adler, R. F., G. J. Huffman, A. Chang, R. Ferraro, P.-P. Xie, J. Janowiak, B. Rudolf, U. Schneider, S. Curtis, and D. Bolvin (2003), The version-2 global precipitation climatology project (GPCP) monthly precipitation analysis (1979-present), *Journal of Hydrometeorology*, *4*(6), 1147–1167.

Adler, R. F., G. J. Huffman, D. T. Bolvin, S. Curtis, and E. J. Nelkin (2000), Tropical rainfall distributions determined using TRMM combined with other satellite and rain gauge information, *Journal of Applied Meteorology*, *39*(12), 2007–2023.

Arblaster, J. M., G. A. Meehl, and M. A (2002), Interdecadal modulation of Australian rainfall, *Clim Dyn*, *18*(6), 519–531, doi:10.1007/s00382-001-0191-y.

Ashok, K., S. K. Behera, S. A. Rao, H. Weng, and T. Yamagata (2007), El Niño Modoki and its possible teleconnection, *J. Geophys. Res.*, *112*(C11), C11007, doi:10.1029/2006JC003798.

Ashok, K., Z. Guan, and T. Yamagata (2001), Impact of the Indian Ocean dipole on the relationship between the Indian monsoon rainfall and ENSO, *Geophys. Res. Lett.*, *28*(23), 4499–4502.

Bellenger H., E. Guilyardi, J. Leloup, M. Lengaigne, J. Vialard (2013). ENSO representation in climate models: from CMIP3 to CMIP5. *Clim. Dyn.,* summited.

Boschat, G., P. Terray, and S. Masson (2010), Interannual relationships between Indian Summer Monsoon and Indo-Pacific coupled modes of variability during recent decades, *Clim Dyn*, *37*(5-6), 1019–1043, doi:10.1007/s00382-010-0887-y.

Chang, C.-P., and T. Li (2000), A theory for the tropical tropospheric biennial oscillation, *J. Atmos. Sci.*, *57*(14), 2209–2224.

Chang, C.-P., Z. Wang, J. McBride, and C.-H. Liu (2005), Annual cycle of Southeast Asia-Maritime Continent rainfall and the asymmetric monsoon transition, *J. Climate*, *18*(2), 287–301.

Chao, W. C., and B. Chen (2001), The origin of monsoons, *J. Atmos. Sci.*, *58*(22), 3497–3507.

Chowdary, J. S., and C. Gnanaseelan (2007), Basin-wide warming of the Indian Ocean during El Niño and Indian Ocean dipole years, *Int. J. Climatol.*, *27*(11), 1421–1438, doi:10.1002/joc.1482.

Clark, C. O., J. E. Cole, and P. J. Webster (2000), Indian Ocean SST and Indian summer rainfall: Predictive relationships and their decadal variability, *J. Climate*, *13*(14), 2503–2519.

Collins, M. et al. (2010), The impact of global warming on the tropical Pacific Ocean and El Niño, *Nature Geoscience*, *3*(6), 391–397, doi:10.1038/ngeo868.

Fan, F., M. E. Mann, S. Lee, and J. L. Evans (2012), Future Changes in the South Asian Summer Monsoon: An Analysis of the CMIP3 Multimodel Projections, *J. Climate*, *25*(11), 3909–3928, doi:10.1175/JCLI-D-11-00133.1.

Fasullo, J. T. (2004), Biennial characteristics of Indian monsoon rainfall, *J. Climate*, *17*(15), 2972–2982.

Hartmann, D. L., and M. L. Michelsen (1989), Intraseasonal periodicities in Indian rainfall, *J. Atmos. Sci.*, *46*(18), 2838–2862.

Hastenrath, S., L. Greischar, and J. van Heepden (1995), Prediction of the summer rainfall over South Africa, *J. Climate*, *8*, 1511–1518.

Hendon, H. H., and B. Liebmann (1990), The intraseasonal(30-50 day) oscillation of the Australian summer monsoon, *J. Atmos. Sci.*, *47*(24), 2909–2923.

Holland, G. J. (1986), Interannual variability of the Australian summer monsoon at Darwin: 1952-82, *Monthly Weather Review*, *114*(3), 594–604.

Hong, C.-C., T. Li, LinHo, and Y.-C. Chen (2010), Asymmetry of the Indian Ocean Basinwide SST Anomalies: Roles of ENSO and IOD*, *J. Climate*, *23*(13), 3563–3576, doi:10.1175/2010JCLI3320.1.

Hu, Z. Z., M. Latif, E. Roeckner, and L. Bengtsson (2000), Intensified Asian summer monsoon and its variability in a coupled model forced by increasing greenhouse gas concentrations, *Geophys. Res. Lett.*, *27*(17), 2681.

Jones, D. A., W. Wang, and R. Fawcett (2009), High-quality spatial climate data-sets for Australia, *Australian Meteorological and Oceanographic Journal*, *58*, 233–248.

Joseph, P. V., B. Liebmann, and H. H. Hendon (1991), Interannual variability of the Australian summer monsoon onset: Possible influence of Indian summer monsoon and El Niño, *J. Climate*, *4*, 529–538.

Jourdain, N. C., A. S. Gupta, A. S. Taschetto, C. C. Ummenhofer, A. F. Moise, and K. Ashok (2013), The Indo-Australian monsoon and its relationship to ENSO and IOD in reanalysis data and the CMIP3/CMIP5 simulations, *Clim Dyn*, doi:10.1007/s00382-013-1676-1.

Kalnay, E., M. Kanamitsu, R. Kistler, W. Collins, D. Deaven, L. Gandin, M. Iredell, S. Saha, G. White, and J. Woollen (1996), The NCEP/NCAR 40-year reanalysis project, *Bull. Amer. Meteor. Soc.*, *77*(3), 437–471.

Kawamura, R. (2002), A mechanism of the onset of the Australian summer monsoon, *J. Geophys. Res.*, *107*(D14), 4204, doi:10.1029/2001JD001070.

Kirtman, B. P., and J. Shukla (2000), Influence of the Indian summer monsoon on ENSO, *Q. J. R. Meteorol. Soc.*, *126*(562), 213–239.

Kumar, K. K., B. Rajagopalan, and M. A. Cane (1999), On the Weakening Relationship Between the Indian Monsoon and ENSO, *Science*, *284*(5423), 2156–2159, doi:10.1126/science.284.5423.2156.

Lee, J.-Y., and B. Wang (2012), Future change of global monsoon in the CMIP5, *Clim Dyn*, doi:10.1007/s00382-012-1564-0.

Li, T., and B. Wang (2005), A review on the western North Pacific monsoon: Synoptic-to-interannual variabilities, *Terr. Atmos. Ocean. Sci.*, *16*(2), 285–314.

Li, T., C. W. Tham, and C.-P. Chang (2001), A coupled air-sea-monsoon oscillator for the tropospheric biennial oscillation, *J. Climate*, *14*(5), 752–764.

Li, T., P. Liu, X. Fu, B. Wang, and G. A. Meehl (2006), Spatiotemporal Structures and Mechanisms of the Tropospheric Biennial Oscillation in the Indo-Pacific Warm Ocean Regions*, *J. Climate*, *19*(13), 3070–3087.

Loschnigg, J., G. A. Meehl, P. J. Webster, J. M. Arblaster, and G. P. Compo (2003), The Asian Monsoon, the Tropospheric Biennial Oscillation, and the Indian Ocean Zonal Mode in the NCAR CSM*, *J. Climate*, *16*(11), 1617–1642.

McCreary, J. P., K. E. Kohler, R. R. Hood, and D. B. Olson (1996), A four-component ecosystem model of biological activity in the Arabian Sea, *Progress in Oceanography*, *37*(3), 193–240.

Meehl, G. A. (1987), The annual cycle and interannual variability in the tropical Pacific and Indian Ocean regions, *Monthly Weather Review*, *115*(1), 27–50.

Meehl, G. A. (1993), A coupled air-sea biennial mechanism in the tropical Indian and Pacific regions: Role of the ocean, *J. Climate*, *6*(1), 31–41.

Meehl, G. A. (1994a), Coupled land-ocean-atmosphere processes and South Asian monsoon variability, *Science*, 263–263.

Meehl, G. A. (1994b), Influence of the land surface in the Asian summer monsoon: External conditions versus internal feedbacks, *J. Climate*, *7*, 1033–1049.

Meehl, G. A. (1997), The south Asian monsoon and the tropospheric biennial oscillation, *J. Climate*, *10*(8), 1921–1943.

Meehl, G. A., and J. M. Arblaster (1998), The Asian-Australian Monsoon and El Niño-Southern Oscillation in the NCAR Climate System Model*, *J. Climate*, *11*(6), 1356–1385.

Meehl, G. A., and J. M. Arblaster (2002), The tropospheric biennial oscillation and Asian-Australian monsoon rainfall, *J. Climate*, *15*(7), 722–744.

Meehl, G. A., and J. M. Arblaster (2011), Decadal Variability of Asian–Australian Monsoon–ENSO–TBO Relationships, *J. Climate*, *24*(18), 4925–4940, doi:10.1175/2011JCLI4015.1.

Meehl, G. A., and J. M. Arblaster (2012), Relating the strength of the tropospheric biennial oscillation (TBO) to the phase of the Interdecadal Pacific Oscillation (IPO), *Geophys. Res. Lett.*, *39*(20), L20716, doi:10.1029/2012GL053386.

Meyers, G. A., P. McIntosh, L. Pigot, and M. Pook (2007), The Years of El Niño, La Niña, and Interactions with the Tropical Indian Ocean, *J. Climate*, *20*(13), 2872–2880, doi:10.1175/JCLI4152.1.

Mohankumar, K., and P. A. Pillai (2008), Stratosphere–troposphere interaction associated with biennial oscillation of Indian summer monsoon, *Journal of Atmospheric and Solar-Terrestrial Physics*, *70*(5), 764–773, doi:10.1016/j.jastp.2007.12.001.

Mokhov, I. I., D. A. Smirnov, P. I. Nakonechny, S. S. Kozlenko, E. P. Seleznev, and J. Kurths (2011), Alternating mutual influence of El-Niño/Southern Oscillation and Indian monsoon, *Geophys. Res. Lett.*, *38*(8), n/a–n/a, doi:10.1029/2010GL045932.

Moss, R. H. et al. (2010), The next generation of scenarios for climate change research and assessment, *Nature*, *463*(7282), 747–756, doi:10.1038/nature08823.

Mujumdar, M., B. Preethi, T. P. Sabin, K. Ashok, S. Saeed, D. S. Pai, and R. Krishnan (2012), The Asian summer monsoon response to the La Niña event of 2010, edited by A. Ghelli, H. Cloke, and A. Kulkarni, *Met. Apps*, *19*(2), 216–225, doi:10.1002/met.1301.

Neale, R., and J. M. Slingo (2003), The maritime continent and its role in the global climate: A GCM study, *J. Climate*, *16*(5), 834–848.

Okumura, Y. M., and S.-P. Xie (2004), Interaction of the Atlantic Equatorial Cold Tongue and the African Monsoon*, *J. Climate*, *17*(18), 3589–3602.

Parthasarathy, B., A. A. Munot, and D. R. Kothawale (1994), All-India monthly and seasonal rainfall series: 1871–1993, *Theor Appl Climatol*, *49*(4), 217–224.

Power, S., T. Casey, C. Folland, A. Colman, and V. Mehta (1999), Inter-decadal modulation of the impact of ENSO on Australia, *Clim Dyn*, *15*(5), 319–324.

Rayner, N. A., D. E. Parker, E. B. Horton, C. K. Folland, L. V. Alexander, D. P. Rowell, E. C. Kent, and A. Kaplan (2003), Global analyses of sea surface temperature, sea ice, and night marine air temperature since the late nineteenth century, *J. Geophys. Res.*, *108*(D14), 4407.

Riahi, K., S. Rao, V. Krey, C. Cho, V. Chirkov, G. Fischer, G. Kindermann, N. Nakicenovic, and P. Rafaj (2011), RCP 8.5—A scenario of comparatively high greenhouse gas emissions, *Climatic Change*, *109*(1-2), 33–57, doi:10.1007/s10584-011-0149-y.

Rudolf, B., A. Becker, U. Schneider, A. Meyer-Christoffer, and M. Ziese (2010), The new “GPCC Full Data Reanalysis Version 5” providing high-quality gridded monthly precipitation data for the global land-surface is public available since December 2010, *GPCC Status Report December 2010*.

Saji, N. H., B. N. Goswami, P. N. Vinayachandran, and T. Yamagata (1999), A dipole mode in the tropical Indian Ocean, *Nature*, *401*, 360–363.

Schott, F. A., S.-P. Xie, and J. P. McCreary Jr. (2009), Indian Ocean circulation and climate variability, *Rev. Geophys.*, *47*(1), RG1002, doi:10.1029/2007RG000245.

Smith, I. N., L. Wilson, and R. Suppiah (2008), Characteristics of the Northern Australian Rainy Season, *J. Climate*, *21*(17), 4298–4311, doi:10.1175/2008JCLI2109.1.

Suhas, E., J. M. Neena, and B. N. Goswami (2012), Interannual Variability of Indian Summer Monsoon arising from Interactions between Seasonal Mean and Intraseasonal Oscillations, *J. Atmos. Sci.*, *69*(6), 1761–1774, doi:10.1175/JAS-D-11-0211.1.

Taschetto, A. S., A. Sen Gupta, H. H. Hendon, C. C. Ummenhofer, and M. H. England (2011), The Contribution of Indian Ocean Sea Surface Temperature Anomalies on Australian Summer Rainfall during El Niño Events, *J. Climate*, *24*(14), 3734–3747, doi:10.1175/2011JCLI3885.1.

Taschetto, A. S**.**, A. Sen Gupta, N. Jourdain, A. Santoso, C. C. Ummenhofer and M. H. England. 2012. Cold tongue and warm pool ENSO events in CMIP5: mean state and future projections. *J. Climate*, submitted.

Taylor, K. E. (2001), Summarizing multiple aspects of model performance in a single diagram, *J. Geophys. Res.*, *106*(D7), 7183–7192.

Trenberth, K. E. (1997), The definition of El Niño, *Bull. Amer. Meteor. Soc.*, *78*(12), 2771–2777.

Ummenhofer, C. C., A. Sen Gupta, Y. LI, A. S. Taschetto, and M. H. England (2011), Multi-decadal modulation of the El Niño–Indian monsoon relationship by Indian Ocean variability, *Environ. Res. Lett.*, *6*(3), 034006, doi:10.1088/1748-9326/6/3/034006.

Ummenhofer, C. C., M. H. England, P. C. McIntosh, G. A. Meyers, M. J. Pook, J. S. Risbey, A. S. Gupta, and A. S. Taschetto (2009), What causes southeast Australia's worst droughts? *Geophys. Res. Lett.*, *36*(4), L04706, doi:10.1029/2008GL036801.

Vernekar, A. D., J. Zhou, and J. Shukla (1995), The effect of Eurasian snow cover on the Indian monsoon, *J. Climate*, *8*(2), 248–266.

Wang, B. (1994), Climatic regimes of tropical convection and rainfall, *J. Climate*, *7*(7), 1109–1118.

Wang, B., and Q. Ding (2006), Changes in global monsoon precipitation over the past 56 years, *Geophys. Res. Lett.*, *33*(6), L06711, doi:10.1029/2005GL025347.

Wang, B., and Q. Ding (2008), Global monsoon: Dominant mode of annual variation in the tropics, *Dynamics of Atmospheres and Oceans*, *44*(3-4), 165–183, doi:10.1016/j.dynatmoce.2007.05.002.

Wang, B., J. Yang, T. Zhou, and B. Wang (2008a), Interdecadal Changes in the Major Modes of Asian–Australian Monsoon Variability: Strengthening Relationship with ENSO since the Late 1970s*, *J. Climate*, *21*(8), 1771–1789, doi:10.1175/2007JCLI1981.1.

Wang, B., Z. Wu, J. Li, J. Liu, C.-P. Chang, Y. Ding, and G. Wu (2008b), How to Measure the Strength of the East Asian Summer Monsoon, *J. Climate*, *21*(17), 4449–4463, doi:10.1175/2008JCLI2183.1.

Webster, P. J., and S. Yang (1992), Monsoon and ENSO: Selectively interactive systems, *Q. J. R. Meteorol. Soc.*, *118*(507), 877–926.

Webster, P. J., V. O. Maga a, T. N. Palmer, J. Shukla, R. A. Tomas, M. Yanai, and T. Yasunari (1998), Monsoons: Processes, predictability, and the prospects for prediction, *J. Geophys. Res.*, *103*(C7), 14451–14510.

Wu, R. (2008), Possible Role of the Indian Ocean in the In-Phase Transition of the Indian-to-Australian Summer Monsoon, *J. Climate*, *21*(21), 5727–5741, doi:10.1175/2008JCLI2354.1.

Wu, R. (2009), Possible Role of the Indian Ocean in the Out-of-Phase Transition of the Australian to Indian Summer Monsoon, *J. Climate*, *22*(7), 1834–1849, doi:10.1175/2008JCLI2602.1.

Wu, R., and B. P. Kirtman (2004), The tropospheric biennial oscillation of the monsoon-ENSO system in an interactive ensemble coupled GCM, *J. Climate*, *17*(8), 1623–1640.

Wu, R., and B. P. Kirtman (2003), On the impacts of the Indian summer monsoon on ENSO in a coupled GCM, *Q. J. R. Meteorol. Soc.*, *129*(595), 3439–3468, doi:10.1256/qj.02.214.

Wu, R., and B. P. Kirtman (2007), Role of the Indian Ocean in the Biennial Transition of the Indian Summer Monsoon, *J. Climate*, *20*(10), 2147–2164, doi:10.1175/JCLI4127.1.

Xie, P., and P. A. Arkin (1996), Analyses of global monthly precipitation using gauge observations, satellite estimates, and numerical model predictions, *J. Climate*, *9*(4), 840–858.

Xie, P., and P. A. Arkin (1997), Global precipitation: A 17-year monthly analysis based on gauge observations, satellite estimates, and numerical model outputs, *Bull. Amer. Meteor. Soc.*, *78*(11), 2539–2558.

Yasunari, T. (1990), Impact of Indian monsoon on the coupled atmosphere/ocean system in the tropical Pacific, *Meteorol. Atmos. Phys.*, *44*(1), 29–41.

Yu, J.-Y., and M. A. Janiga (2007), Changes in the in-phase relationship between the Indian and subsequent Australian summer monsoons during the past five decades, *Annales geophysicae*, *25*(9), 1929–1933.

Yu, J.-Y., S.-P. Weng, and J. D. Farrara (2003), Ocean roles in the TBO transitions of the Indian-Australian monsoon system, *J. Climate*, *16*(18), 3072–3080.

Zhou, J., and K. M. Lau (1998), Does a monsoon climate exist over South America? *J. Climate*, *11*(5), 1020–1040.

Appendix

Table A.1 Classification of years when positive or negative Indian Ocean Dipole was concurrent with El Niño or La Niña based on a technique designed to highlight independent ENSO and IOD years (*Ummenbofer et al*., 2009). Also shown are years of no event.

	Negative IOD	No event	Positive IOD
El Niño	1930	1877, 1888, 1899, 1905, 1911, 1914, 1918, 1925, 1940, 1941, 1965, 1972, 1986, 1987	1896, 1902, 1957, 1963, 1982, 1991, 1997
No event	1915, 1958, 1968, 1974, 1980, 1985, 1989, 1992	1880, 1881, 1882, 1883, 1884, 1895, 1898, 1900, 1901, 1904, 1907, 1908, 1912, 1920, 1921, 1927, 1929, 1931, 1932, 1934, 1936, 1937, 1939, 1943, 1947, 1948, 1951, 1952, 1953, 1959, 1960, 1962, 1966, 1967, 1969, 1971, 1976, 1977, 1979, 1983, 1990, 1993, 1995, 2001, 2002, 2003, 2005, 2006	1885, 1887, 1891, 1894, 1913, 1919, 1923, 1926, 1935, 1944, 1945, 1946, 1961, 1994, 2004
La Niña	1906, 1909, 1916, 1917, 1933, 1942, 1975	1878, 1879, 1886, 1889, 1890, 1892, 1893, 1897, 1903, 1910, 1922, 1924, 1928, 1938, 1949, 1950, 1954, 1955, 1956, 1964, 1970, 1973, 1978, 1981, 1984, 1988, 1996, 1998, 2000	1999

Table A.2 CMIP3 model I.D., available number of ensemble members and names of providing groups

CMIP3 Model I.D.	Ensemble Members	Originating Group, Country
bccr-bcm2.0	1	Bjerknes Centre for Climate Research, Norway
cccma-cgcm3.1	5	Canadian Centre for Climate Modelling and Analysis, Canada
cccma-cgcm3.1-t63	1	
cnrm-cm3	1	Météo-France/Centre National de Recherches Météorologiques, France
csiro-mk3.0	2	CSIRO Atmospheric Research, Australia

csiro-mk3.5	1	
gfdl-cm2.0	1	US Dept. of Commerce/NOAA/Geophysical Fluid Dynamics Laboratory (GFDL), USA
gfdl-cm2.1	3	
giss-aom	2	NASA/Goddard Institute for Space Studies, USA
giss-e-h	5	
giss-e-r	9	
iap-fgoals-g1.0	3	LASG/Institute of Atmospheric Physics, China
ingv-echam4	1	Instituto Nazionale di Geofisica e Vulcanologia, Italy
inm-cm3.0	1	Instituto Nazionale di Geofisica e Vulcanologia, Russia
ipsl-cm4	1	Institut Pierre - Simon Laplace, France
miroc3.2-hires	1	Center for Climate System Research (The University of Tokyo), National Institute for Environmental Studies, and Frontier Research Center for Global Change (JAMSTEC), Japan
miroc3.2-medres	3	
miub-echo-g	5	Meteorological Institute of the University of Bonn, Meteorological Research Institute of KMA, and Model and Data group, Germany/Korea
mpi-echam5	3	Max Planck Institute for Meteorology, Germany
mri-cgcm2.3.2a	5	Meteorological Research Institute, Japan
ncar-ccsm3.0	8	National Center for Atmospheric Research (NCAR), USA
ncar-pcm1	4	
ukmo-hadcm3	2	Hadley Centre for Climate Prediction and Research/Met Office, UK
ukmo-hadgem1	2	

Table A.3 CMIP5 model I.D., available number of ensemble members for historical simulations (before slash) and RCP8.5 scenario (if applicable, after slash), and names of providing groups (* the CMIP5 models also available for the RCP8.5 scenario)

CMIP5 model I.D.	Ensemble Members	Originating Group, Country
*ACCESS1.0	1/1	CSIRO and Bureau of Meteorology (BOM), Australia
*ACCESS1.3	1/1	
*BCC-CSM1.1	3/1	Beijing Climate Center, China Meteorological Administration, China
*CCSM4	6/6	University of Miami – RSMAS, USA
*CESM1-CAM5	3/3	Community Earth System Model Contributors, USA
*CESM1-WACCM	1/1	
*CNRM-CM5	10/5	Centre National de Recherches Météorologiques / Centre Européen de Recherche et Formation CERFACS Avancée en Calcul Scientifique, France

*CSIRO-Mk3.6.0	10/10	CSIRO/Queensland Climate Change Centre of Excellence, Australia
*CanESM2	5/5	Canadian Centre for Climate Modelling and Analysis, Canada
FGOAL-g2	3	LASG, Institute of Atmospheric Physics, Chinese Academy of Sciences and CESS, Tsinghua University, China
*FGOAL-s2	3/3	LASG, Institute of Atmospheric Physics, Chinese Academy of Sciences, China
*FIO-ESM	3/3	The First Institute of Oceanography, SOA, China
*GFDL-CM3	5/1	NOAA Geophysical Fluid Dynamics Laboratory, USA
GFDL-ESM2G	3	
GFDL-ESM2M	1	
GISS-E2-H	5	NASA Goddard Institute for Space Studies, USA
*GISS-E2-R	4/1	
*HadGEM2-AO	1/1	National Institute of Meteorological Research/Korea Meteorological Administration, Korea
HadCM3	4	Met Office Hadley Centre (additional HadGEM2-ES realizations contributed by INPE), UK
*HadGEM2-ES	3/1	
*INM-CM4	1/1	Institute for Numerical Mathematics, Russia
IPSL-CM5A-LR	4	Institut Pierre - Simon Laplace, France
IPSL-CM5A-MR	1	
IPSL-CM5B-LR	1	
*MIROC5	3/1	Atmosphere and Ocean Research Institute (The University of Tokyo), National Institute for Environmental Studies, and Japan Agency for Marine – Earth Science and Technology, Japan
*MIROC-ESM	3/1	
*MPI-ESM-LR	3/1	Max Planck Institute for Meteorology, Germany
*MRI-CGCM3	3/1	Meteorological Research Institute, Japan
*NorESM1-M	3/1	Norwegian Climate Centre, Norway
*NorESM1-ME	1/1	

Table A.4 The original Monte Carlo results of four TBO transitions based on land-restricted rainfall for 24 CMIP3 models. Second column (Ens. No.) shows numbers of ensemble members for each model. Obs. represents the percentage of observed successful TBO transition, while Pred. represents the percentage of *enhanced predictability*. Models shadowed in yellow show significant results at least in one ensemble member and one transition, which are plotted in bar chart in Section 3.2. Significant results are marked in red bold (More details see text).

CMIP3 models I.D.	Ens. No.	IND-AUS			IND-IND			AUS-IND			AUS-AUS		
		Obs. (%)	P-value	Pred. (%)	Obs. (%)	P-value	Pred. (%)	Obs. (%)	P-value	Pred. (%)	Obs. (%)	P-value	Pred. (%)
bccr-bcm2.0	1	51.33	0.43	1.33	54.00	0.18	4.00	**42.67**	**0.97**	**-7.33**	55.03	0.10	5.37
cccma-cgcm3.1	1	**69.33**	**0.00**	**19.33**	52.67	0.27	2.67	50.00	0.51	0.00	52.35	0.28	2.68
	2	51.33	0.40	1.33	53.33	0.23	3.33	48.67	0.67	-1.33	53.69	0.20	4.03
	3	54.00	0.20	4.00	48.00	0.71	-2.00	48.67	0.64	-1.33	**56.38**	**0.05**	**6.71**
	4	**56.67**	**0.06**	**6.67**	52.00	0.34	2.00	47.33	0.76	-2.67	52.35	0.25	3.36
	5	49.33	0.60	-0.67	51.33	0.39	1.33	54.00	0.18	4.00	53.02	0.26	2.68
cccma-cgcm3.1-t63	1	49.33	0.59	-0.67	52.00	0.34	2.00	52.00	0.35	2.00	50.34	0.42	1.34
cnrm-cm3	1	**64.75**	**0.0002**	**15.11**	**57.55**	**0.04**	**7.91**	**36.69**	**1.00**	**-13.67**	54.35	0.15	5.07
csiro-mk3.0	1	**61.24**	**0.01**	**10.85**	52.71	0.29	3.10	51.16	0.42	1.55	49.22	0.60	0.78
	2	**62.02**	**0.004**	**11.63**	**42.64**	**0.96**	**-6.98**	49.61	0.56	0.00	53.91	0.21	3.91
csiro-mk3.5	1	**71.32**	**0.00**	**21.71**	**44.19**	**0.92**	**-5.43**	**40.31**	**0.99**	**-10.08**	43.75	0.93	-6.25
gfdl-cm2.0	1	**58.99**	**0.02**	**8.63**	46.76	0.80	-2.88	46.04	0.84	-3.60	**56.52**	**0.05**	**7.25**
gfdl-cm2.1	1	**66.91**	**0.00**	**17.27**	46.04	0.81	-3.60	**41.73**	**0.98**	**-8.63**	44.93	0.89	-5.07
	2	**61.87**	**0.003**	**11.51**	**41.73**	**0.98**	**-7.91**	48.20	0.69	-1.44	52.17	0.33	2.17
	3	**64.75**	**0.00**	**15.11**	**42.45**	**0.96**	**-7.19**	**41.73**	**0.98**	**-8.63**	47.83	0.71	-2.17
giss-aom	1	52.00	0.34	2.00	46.00	0.86	-4.00	50.00	0.53	0.00	**40.94**	**0.99**	**-8.72**

	2	51.33	0.40	1.33	54.67	0.14	4.67	48.67	0.66	-1.33	47.65	0.74	-2.01
giss-e-h	1	47.06	0.77	-3.36	52.94	0.28	3.36	43.70	0.93	-5.88	54.24	0.20	4.24
	2	51.26	0.43	0.84	47.06	0.77	-2.52	50.42	0.49	0.84	48.31	0.62	-0.85
	3	53.78	0.22	4.20	48.74	0.63	-0.84	57.98	0.05	7.56	48.31	0.66	-1.69
	4	53.78	0.23	4.20	56.30	0.10	6.72	45.38	0.87	-5.04	49.15	0.58	-0.85
	5	47.90	0.71	-2.52	45.38	0.87	-5.04	48.74	0.64	-1.68	51.69	0.39	1.69
giss-e-r	1	47.15	0.77	-3.25	52.03	0.34	2.44	51.22	0.43	0.81	50.00	0.54	0.00
	2	51.22	0.43	1.63	42.28	0.96	-7.32	66.67	0.0001	16.26	47.54	0.73	-2.46
	3	47.97	0.67	-1.63	47.97	0.69	-1.63	51.22	0.47	0.81	50.00	0.44	0.82
	4	51.22	0.38	1.63	48.78	0.58	-0.81	58.54	0.04	8.13	51.64	0.36	1.64
	5	51.22	0.43	0.81	47.97	0.64	-1.63	52.85	0.29	3.25	50.82	0.46	0.82
	6	45.53	0.86	-4.07	48.78	0.64	-0.81	51.22	0.43	0.81	54.10	0.20	4.10
	7	57.72	0.05	7.32	52.85	0.29	3.25	49.59	0.57	0.00	50.00	0.50	0.00
	8	39.84	0.99	-9.76	45.53	0.85	-4.07	45.53	0.87	-4.88	47.54	0.72	-2.46
	9	50.41	0.48	0.81	40.65	0.98	-8.94	59.35	0.03	8.94	47.54	0.72	-2.46
iap-fgoals-g1.0	1	74.50	0.00	24.83	61.75	0.002	12.08	42.95	0.97	-7.38	60.81	0.01	10.81
	2	78.52	0.00	28.19	59.06	0.02	9.40	44.30	0.92	-5.37	60.81	0.004	10.81
	3	85.91	0.00	36.24	60.40	0.01	10.74	50.34	0.50	0.00	60.14	0.01	10.14
ingv-echam4	1	48.46	0.69	-1.54	46.15	0.82	-3.85	36.15	1.00	-13.85	58.91	0.02	9.30
inm-cm3.0	1	50.39	0.49	0.78	48.44	0.67	-1.56	47.29	0.76	-3.10	48.44	0.67	-1.56
ipsl-cm4	1	54.29	0.23	3.57	44.29	0.88	-5.00	50.00	0.46	0.71	61.87	0.003	12.23
miroc3.2-hires	1	45.00	0.87	-5.00	57.00	0.10	7.00	58.00	0.06	8.00	46.46	0.75	-3.03
miroc3.2-medres	1	51.00	0.47	1.00	42.00	0.96	-8.00	43.00	0.93	-7.00	54.55	0.20	5.05
	2	46.00	0.78	-3.00	47.00	0.67	-2.00	47.00	0.80	-4.00	52.53	0.32	3.03
	3	47.00	0.75	-3.00	49.00	0.61	-1.00	50.00	0.55	0.00	49.49	0.56	0.00

miub-echo-g	1	**42.86**	**0.96**	**-7.14**	45.00	0.88	-5.00	49.29	0.61	-0.71	**58.99**	**0.02**	**9.35**
	2	55.00	0.13	5.00	52.14	0.33	2.14	48.57	0.67	-1.43	54.68	0.15	5.04
	3	54.29	0.19	4.29	**60.00**	**0.01**	**10.00**	52.86	0.27	2.86	**58.99**	**0.02**	**9.35**
	4	52.86	0.28	2.86	**58.57**	**0.02**	**8.57**	52.86	0.27	2.86	**58.27**	**0.03**	**7.91**
	5	**60.00**	**0.01**	**10.00**	**57.14**	**0.05**	**7.14**	**58.57**	**0.03**	**8.57**	**62.59**	**0.002**	**12.95**
mpi-echam5	1	**58.27**	**0.03**	**8.63**	**39.57**	**0.99**	**-10.07**	45.32	0.88	-5.04	52.45	0.39	1.45
	2	**58.99**	**0.02**	**8.63**	45.32	0.86	-4.32	**43.17**	**0.95**	**-6.47**	49.28	0.59	-0.72
	3	**56.12**	**0.09**	**5.76**	46.76	0.79	-2.88	**38.85**	**1.00**	**-10.79**	53.62	0.22	3.62
mri-cgcm2.3.2a	1	**57.72**	**0.03**	**8.05**	49.66	0.55	0.00	51.68	0.38	1.34	51.35	0.40	1.35
	2	49.66	0.55	0.00	47.65	0.74	-2.68	48.32	0.70	-2.01	50.68	0.38	1.35
	3	54.36	0.16	4.03	45.64	0.86	-4.06	52.35	0.31	2.68	**59.46**	**0.01**	**9.46**
	4	52.35	0.31	2.01	51.01	0.43	1.34	48.99	0.62	-0.67	**56.76**	**0.06**	**6.76**
	5	48.99	0.64	-1.34	50.34	0.45	0.67	48.99	0.61	-0.67	52.03	0.34	2.03
ncar-ccsm3.0	1	55.81	0.12	5.43	**57.36**	**0.05**	**7.75**	48.84	0.62	-0.78	**39.06**	**0.99**	**-10.94**
	2	54.26	0.19	3.88	**44.19**	**0.92**	**-5.43**	51.16	0.43	0.78	**41.41**	**0.98**	**-8.59**
	3	54.26	0.18	4.65	51.94	0.35	2.33	49.61	0.58	-0.78	**40.63**	**0.99**	**-9.38**
	4	55.81	0.13	5.43	**43.41**	**0.92**	**-6.20**	50.39	0.46	0.78	52.34	0.31	2.34
	5	44.96	0.89	-5.43	47.29	0.75	-2.33	51.16	0.43	1.55	47.66	0.73	-2.34
	6	54.26	0.19	3.88	46.51	0.80	-3.10	**56.59**	**0.08**	**6.98**	48.44	0.67	-1.56
	7	45.74	0.87	-4.65	52.71	0.26	3.10	48.06	0.68	-1.55	50.00	0.53	0.00
	9	48.06	0.70	-2.33	**38.76**	**1.00**	**-10.85**	50.39	0.50	0.78	**59.38**	**0.02**	**9.38**
ncar-pcm1	1	48.62	0.65	-1.83	53.21	0.28	3.67	**40.37**	**0.98**	**-9.17**	55.56	0.15	5.56
	2	55.96	0.12	6.42	49.54	0.58	0.00	47.71	0.72	-1.83	52.78	0.31	2.78
	3	53.21	0.29	2.75	51.38	0.42	1.83	52.29	0.35	2.75	50.93	0.45	0.93
	4	55.96	0.12	5.50	**56.88**	**0.09**	**6.42**	**44.04**	**0.91**	**-6.42**	50.00	0.54	0.00

ukmo-hadcm3	1	**59.71**	**0.01**	**9.35**	50.36	0.50	0.72	47.48	0.75	-2.16	53.62	0.21	3.62
	2	48.20	0.71	-2.16	48.20	0.69	-1.44	46.76	0.79	-2.88	51.45	0.37	2.17
ukmo-hadgem1	1	53.96	0.19	4.32	**43.17**	**0.95**	**-6.47**	**44.60**	**0.91**	**-5.76**	50.00	0.53	0.00
	2	53.96	0.18	4.32	51.80	0.36	2.16	47.83	0.71	-2.17	49.64	0.51	0.00

Table A.5 The original Monte Carlo results of four TBO transitions based on land-restricted rainfall for 30 CMIP5 models. Second column (Ens. No.) shows numbers of ensemble members for each model. Obs. represents the percentage of observed successful TBO transition, while Pred. represents the percentage of *enhanced predictability*. Models shadowed in yellow show significant results at least in one ensemble member and one transition, which are plotted in bar chart in Section 3.2. Significant results are marked in red bold (More details see text).

CMIP5 models I.D.	Ens. No.	IND-AUS			IND-IND			AUS-IND			AUS-AUS		
		Obs. (%)	P-value	Pred. (%)	Obs. (%)	P-value	Pred. (%)	Obs. (%)	P-value	Pred. (%)	Obs. (%)	P-value	Pred. (%)
ACCESS1.0	1	**60.65**	**0.005**	**10.97**	51.61	0.37	1.94	47.10	0.80	-3.23	48.05	0.70	-1.95
ACCESS1.3	1	**60.65**	**0.006**	**10.32**	43.23	0.95	-6.45	**42.58**	**0.97**	**-7.10**	**55.84**	**0.08**	**5.84**
BCC-CSM1.1	1	48.39	0.69	-1.94	49.03	0.62	-0.65	**55.48**	**0.094**	**5.81**	48.05	0.70	-1.95
	2	**59.35**	**0.01**	**9.03**	**63.23**	**0.0007**	**13.55**	47.10	0.78	-2.58	46.10	0.71	-1.95
	3	54.19	0.17	4.52	53.55	0.21	3.23	**45.16**	**0.90**	**-5.16**	52.60	0.29	2.60
CCSM4	1	**56.13**	**0.08**	**5.81**	48.39	0.66	-1.29	**44.52**	**0.92**	**-5.16**	50.00	0.50	0.00
	2	**56.77**	**0.05**	**6.45**	48.39	0.68	-1.94	**42.58**	**0.97**	**-7.10**	50.65	0.47	0.65
	3	**58.06**	**0.02**	**8.39**	51.61	0.36	1.94	49.68	0.59	-0.65	44.81	0.89	-4.55
	4	**61.29**	**0.004**	**10.97**	52.90	0.24	3.23	49.03	0.62	-0.65	46.75	0.81	-3.25
	5	**56.77**	**0.04**	**7.10**	49.03	0.58	-0.65	**39.35**	**1.00**	**-10.97**	52.60	0.26	2.60
	6	**58.71**	**0.02**	**9.03**	47.74	0.73	-1.94	**38.96**	**1.00**	**-11.04**	52.94	0.21	3.92

CESM1-CAM5	1	54.19	0.17	3.87	50.32	0.49	0.65	47.10	0.78	-2.58	**55.84**	**0.08**	**5.84**
	2	50.97	0.46	0.65	53.55	0.20	3.87	45.81	0.86	-3.87	**44.16**	**0.93**	**-5.84**
	3	**60.00**	**0.008**	**9.68**	54.84	0.13	5.16	**43.23**	**0.96**	**-6.45**	**57.14**	**0.04**	**7.14**
CESM1-WACCM	1	49.03	0.62	-0.65	**43.23**	**0.96**	**-6.45**	46.45	0.83	-3.87	55.19	0.11	5.19
CNRM-CM5	1	51.61	0.37	1.94	50.32	0.50	0.65	49.68	0.57	-0.65	55.19	0.11	5.19
	2	52.90	0.26	3.23	50.32	0.49	0.65	48.39	0.69	-1.94	**62.34**	**0.001**	**12.34**
	3	54.19	0.17	3.87	54.84	0.13	4.52	46.45	0.83	-3.23	**55.84**	**0.08**	**5.84**
	4	**56.77**	**0.05**	**7.10**	47.10	0.78	-2.58	51.61	0.39	1.29	50.00	0.49	0.65
	5	54.84	0.13	5.16	49.03	0.62	-0.65	55.48	0.10	5.16	53.25	0.21	3.25
	6	54.19	0.17	4.52	**44.52**	**0.92**	**-5.16**	50.32	0.50	0.65	48.05	0.71	-1.95
	7	54.19	0.18	3.87	54.84	0.12	5.16	**43.87**	**0.94**	**-5.81**	50.65	0.46	0.65
	8	52.26	0.31	2.58	**60.00**	**0.01**	**9.68**	45.81	0.87	-4.52	**55.84**	**0.08**	**5.84**
	9	53.55	0.21	3.87	50.97	0.44	1.29	52.26	0.32	1.94	51.95	0.31	2.60
	10	53.55	0.21	3.23	49.68	0.56	0.00	49.68	0.56	0.00	52.60	0.28	2.60
CSIRO-Mk3.6.0	1	52.26	0.33	1.94	46.45	0.83	-3.23	47.74	0.72	-1.94	53.90	0.17	3.90
	2	52.26	0.30	2.58	**44.52**	**0.92**	**-5.16**	45.81	0.88	-4.52	**42.86**	**0.97**	**-7.14**
	3	**58.06**	**0.03**	**7.74**	**43.23**	**0.94**	**-6.45**	54.19	0.16	4.52	50.65	0.46	0.65
	4	**56.13**	**0.07**	**5.81**	49.68	0.55	0.00	**38.06**	**1.00**	**-11.61**	50.00	0.53	0.00
	5	**59.35**	**0.01**	**9.68**	47.74	0.74	-1.94	53.55	0.21	3.23	**40.91**	**0.99**	**-9.09**
	6	**58.71**	**0.02**	**8.39**	50.32	0.41	1.29	**36.13**	**1.00**	**-13.55**	**44.16**	**0.94**	**-5.84**
	7	**63.23**	**0.001**	**13.55**	49.68	0.52	0.00	50.32	0.52	0.00	47.40	0.76	-2.60
	8	**63.23**	**0.001**	**12.90**	**41.29**	**0.99**	**-8.39**	48.39	0.68	-1.29	**42.21**	**0.98**	**-7.79**
	9	53.55	0.21	3.87	**44.52**	**0.92**	**-5.16**	49.68	0.56	-0.65	46.10	0.85	-3.90
	10	54.84	0.13	4.52	46.45	0.81	-3.23	49.03	0.62	-0.65	**41.56**	**0.99**	**-8.44**
CanESM2	1	**56.77**	**0.08**	**5.81**	52.90	0.22	3.23	**41.94**	**0.97**	**-7.10**	**64.29**	**0.00**	**15.58**

	2	63.87	0.0003	13.55	47.74	0.74	-1.94	47.74	0.74	-1.94	53.90	0.16	4.55
	3	60.65	0.01	10.97	50.97	0.44	0.65	43.87	0.95	-6.45	53.90	0.17	3.90
	4	59.35	0.01	9.03	51.61	0.37	1.94	50.97	0.43	1.29	54.55	0.15	4.55
	5	63.23	0.001	13.55	47.10	0.79	-2.58	46.45	0.83	-3.23	48.05	0.71	-1.95
FGOALS-g2	2	46.15	0.85	-3.85	43.59	0.95	-6.41	48.72	0.65	-1.28	52.90	0.26	3.23
	3	48.72	0.65	-1.28	56.41	0.06	6.41	46.15	0.85	-3.85	54.84	0.12	5.16
	4	44.23	0.94	-5.77	56.41	0.06	6.41	41.67	0.98	-8.33	54.84	0.13	5.16
FGOALS-s2	1	60.00	0.008	10.32	52.26	0.32	2.58	53.55	0.21	3.23	48.70	0.65	-1.30
	2	56.77	0.05	7.10	51.61	0.37	1.94	48.39	0.69	-1.94	48.05	0.70	-1.95
	3	58.71	0.02	9.03	45.81	0.87	-3.87	47.10	0.79	-3.23	46.10	0.85	-3.90
FIO-ESM	1	56.77	0.05	6.45	52.26	0.31	2.58	46.45	0.83	-3.23	52.60	0.29	2.60
	2	47.74	0.73	-1.94	47.10	0.78	-2.58	45.16	0.90	-5.16	51.30	0.37	1.95
	3	52.26	0.31	2.58	53.55	0.21	3.87	45.81	0.87	-4.52	48.05	0.71	-1.95
GFDL-CM3	1	52.41	0.31	2.07	46.21	0.82	-3.45	48.28	0.69	-2.07	51.39	0.40	1.39
	2	54.48	0.17	4.14	48.97	0.58	-0.69	53.10	0.24	3.45	45.14	0.89	-4.86
	3	53.79	0.20	4.14	55.86	0.09	6.21	44.14	0.93	-6.21	54.17	0.17	4.17
	4	58.33	0.03	8.33	59.72	0.01	9.72	44.44	0.92	-5.56	55.24	0.12	5.59
	5	58.33	0.03	8.33	55.56	0.10	5.56	45.83	0.86	-4.17	46.85	0.80	-2.80
GFDL-ESM2G	1	59.03	0.02	9.03	45.83	0.86	-4.17	49.31	0.60	-0.69	44.76	0.91	-4.90
	2	65.28	0.0001	15.28	46.53	0.82	-3.47	53.47	0.23	3.47	58.74	0.02	9.09
	3	60.42	0.01	10.42	47.92	0.72	-2.08	54.17	0.18	4.17	55.24	0.11	5.59
GFDL-ESM2M	1	54.86	0.14	4.86	51.39	0.36	2.08	35.42	1.00	-14.58	52.45	0.31	2.10
GISS-E2-H	1	47.74	0.75	-2.58	44.52	0.89	-4.52	42.58	0.97	-7.10	54.55	0.15	4.55
	2	50.97	0.51	0.00	49.64	0.50	0.00	49.68	0.49	0.65	49.35	0.50	0.65
	3	51.61	0.45	0.65	45.81	0.85	-3.87	43.87	0.92	-5.16	48.05	0.54	0.00

	4	55.48	0.17	4.52	50.32	0.43	1.29	43.23	0.93	-5.81	51.95	0.18	3.90
	5	46.45	0.89	-4.52	57.42	0.03	7.74	43.87	0.92	-5.16	50.00	0.35	1.95
GISS-E2-R	1	50.97	0.46	0.65	49.68	0.41	1.29	48.39	0.67	-1.29	45.45	0.89	-4.55
	3	54.84	0.16	4.52	44.52	0.92	-5.16	44.52	0.91	-5.16	46.10	0.77	-2.60
	4	51.61	0.52	0.00	46.45	0.75	-2.58	40.65	0.98	-7.74	44.16	0.85	-3.90
	5	45.81	0.88	-4.52	48.38	0.67	-1.29	50.97	0.41	1.29	50.00	0.48	0.65
HadGEM2-AO	1	62.76	0.001	13.10	46.21	0.83	-3.45	51.72	0.39	1.38	52.08	0.32	2.08
HadCM3	1	57.93	0.03	8.28	45.52	0.88	-4.14	50.34	0.50	0.69	52.08	0.34	2.08
	3	61.38	0.004	11.03	52.41	0.31	2.76	40.00	0.99	-9.66	51.39	0.37	1.39
	5	48.97	0.63	-1.38	50.34	0.49	0.69	42.07	0.98	-7.59	48.61	0.66	-1.39
	8	57.93	0.03	8.28	50.34	0.50	0.69	42.76	0.97	-7.59	54.86	0.13	4.86
HadGEM2-ES	1	54.48	0.16	4.14	46.90	0.80	-2.76	48.28	0.69	-1.38	50.00	0.53	0.00
	2	54.48	0.16	4.83	44.83	0.90	-4.83	44.83	0.91	-4.83	47.22	0.77	-2.78
	3	54.48	0.16	4.83	44.14	0.93	-5.52	51.03	0.44	0.69	43.75	0.93	-6.25
INM-CM4	1	54.84	0.12	5.16	42.58	0.97	-7.10	42.58	0.98	-7.74	50.65	0.45	0.65
IPSL-CM5A-LR	1	56.77	0.05	7.10	49.68	0.56	0.00	49.03	0.64	-1.29	45.45	0.86	-3.90
	2	60.00	0.01	9.68	44.52	0.92	-5.16	43.23	0.96	-6.45	51.95	0.30	2.60
	3	58.71	0.01	9.03	49.68	0.55	0.00	56.13	0.09	5.81	53.90	0.14	4.55
	4	60.00	0.01	10.32	40.65	0.99	-9.03	48.39	0.70	-1.94	51.95	0.34	1.95
IPSL-CM5A-MR	1	50.97	0.42	1.29	49.68	0.56	0.00	52.26	0.33	1.94	47.40	0.71	1.95
IPSL-CM5B-LR	1	50.32	0.50	0.00	46.45	0.80	-3.23	49.68	0.57	-0.65	58.44	0.02	8.44
MIROC5	1	56.77	0.05	7.10	47.74	0.70	-1.94	48.39	0.70	-1.94	52.60	0.28	2.60
	2	60.65	0.01	10.32	45.16	0.86	-3.87	44.52	0.93	-5.81	51.95	0.34	1.95
	3	49.68	0.58	-0.65	49.68	0.47	0.65	39.35	1.00	-10.32	51.30	0.40	1.30
MIROC-ESM	1	47.74	0.74	-2.58	56.13	0.07	6.45	43.87	0.94	-5.81	50.00	0.53	0.00

	2	45.81	0.87	-3.87	46.45	0.82	-3.23	49.03	0.63	-1.29	**41.56**	**0.99**	**-8.44**
	3	50.32	0.50	0.00	52.90	0.24	3.23	48.39	0.68	-1.29	52.60	0.29	2.60
MPI-ESM-LR	1	**57.42**	**0.04**	**7.10**	45.16	0.88	-4.52	47.74	0.73	-1.94	48.05	0.71	-1.95
	2	**56.13**	**0.07**	**6.45**	49.03	0.63	-0.65	46.45	0.83	-3.87	52.60	0.28	2.60
	3	**58.06**	**0.03**	**7.74**	47.74	0.74	-1.94	47.10	0.78	-2.58	46.75	0.80	-3.25
MRI-CGCM3	1	53.55	0.22	3.23	50.32	0.46	0.65	52.90	0.25	3.23	**56.49**	**0.06**	**6.49**
	2	47.10	0.78	-2.58	**42.58**	**0.97**	**-7.10**	49.03	0.63	-1.29	**43.51**	**0.95**	**-6.49**
	3	**56.13**	**0.07**	**6.45**	**41.94**	**0.97**	**-7.74**	49.68	0.57	-0.65	53.90	0.19	3.90
NorESM1-M	1	**58.06**	**0.03**	**7.74**	**56.13**	**0.07**	**6.45**	52.90	0.24	3.23	54.55	0.14	4.55
	2	**57.42**	**0.04**	**7.74**	53.55	0.21	3.87	53.55	0.22	3.23	50.65	0.45	0.65
	3	**61.29**	**0.003**	**10.97**	49.68	0.54	0.00	50.97	0.43	1.29	55.19	0.11	5.19
NorESM1-ME	1	**61.94**	**0.002**	**11.61**	50.97	0.43	1.29	52.90	0.26	2.58	49.35	0.59	-0.65

Table A.6 The original Monte Carlo results of four TBO transitions based on rainfall over extend regions for 24 CMIP3 models. Second column (Ens. No.) shows numbers of ensemble members for each model. Obs. represents the percentage of observed successful TBO transition, while Pred. represents the percentage of *enhanced predictability*. Models shadowed in yellow show significant results at least in one ensemble member and one transition, which are plotted in bar chart in Section 3.2. Significant results are marked in red bold (More details see text).

CMIP3 models I.D.	Ens. No.	IND-AUS			IND-IND			AUS-IND			AUS-AUS		
		Obs. (%)	P-value	Pred. (%)	Obs. (%)	P-value	Pred. (%)	Obs. (%)	P-value	Pred. (%)	Obs. (%)	P-value	Pred. (%)
BCCR-BCM2.0	1	**41.33**	**0.98**	**-8.00**	49.33	0.56	0.00	**56.00**	**0.095**	**5.33**	52.35	0.29	2.68
CGCM3.1-T47	1	**57.33**	**0.05**	**7.33**	47.33	0.73	-2.00	54.00	0.17	4.00	50.34	0.49	0.67
	2	53.33	0.23	3.33	49.33	0.60	-0.67	46.67	0.82	-3.33	**55.70**	**0.095**	**5.37**

	3	57.33	0.04	7.33	49.33	0.58	-0.67	44.00	0.94	-6.00	46.98	0.79	-2.68
	4	50.67	0.47	0.67	48.00	0.71	-2.00	52.00	0.34	2.00	49.66	0.57	-0.67
	5	52.67	0.28	2.67	52.67	0.28	2.67	41.33	0.99	-8.67	51.68	0.37	2.01
CGCM3.1-T63	1	54.67	0.14	4.67	54.67	0.12	5.33	41.33	0.99	-8.67	51.01	0.43	1.34
CNRM-CM3	1	51.80	0.36	2.16	54.68	0.15	5.04	59.71	0.01	9.35	44.20	0.92	-5.80
CSIRO-Mk3.0	1	49.61	0.57	0.00	51.16	0.43	1.55	47.29	0.76	-3.10	36.72	1.00	-13.28
	2	48.84	0.65	-1.55	44.19	0.92	-5.43	50.39	0.49	0.78	53.91	0.20	3.91
CSIRO-Mk3.5	1	68.22	0.00	18.60	42.64	0.96	-6.98	49.61	0.61	-0.78	43.75	0.89	-4.69
GFDL-CM2.0	1	63.31	0.001	13.67	55.40	0.10	5.76	51.80	0.42	1.44	54.35	0.13	5.07
GFDL-CM2.1	1	53.96	0.20	4.32	44.60	0.91	-5.04	60.43	0.01	10.07	50.00	0.53	0.00
	2	61.87	0.004	11.51	52.52	0.30	2.88	47.48	0.72	-2.16	43.48	0.88	-5.07
	3	48.92	0.66	-1.44	45.32	0.88	-4.32	47.48	0.73	-2.16	41.30	0.96	-7.25
GISS-AOM	1	49.33	0.61	-0.67	47.33	0.75	-2.67	46.00	0.85	-4.00	44.97	0.90	-4.70
	2	46.00	0.86	-4.00	46.67	0.79	-3.33	59.33	0.01	9.33	52.35	0.31	2.68
GISS-EH	1	49.58	0.59	-0.84	51.26	0.40	1.68	47.90	0.69	-1.68	44.07	0.91	-5.93
	2	56.30	0.098	6.72	53.78	0.23	4.20	47.06	0.77	-3.36	49.15	0.59	-0.85
	3	52.94	0.31	2.52	46.22	0.80	-3.36	51.26	0.41	1.68	49.15	0.60	-0.85
	4	43.70	0.93	-5.88	51.26	0.40	1.68	45.38	0.87	-5.04	50.00	0.54	0.00
	5	49.58	0.57	0.00	42.22	0.82	-3.36	36.13	1.00	-14.29	47.46	0.74	-2.54
GISS-ER	1	56.10	0.10	6.50	50.41	0.50	0.00	37.40	1.00	-13.01	59.84	0.02	9.84
	2	48.78	0.60	-0.81	47.15	0.72	-2.44	43.09	0.96	-7.32	48.36	0.65	-1.64
	3	47.15	0.77	-3.25	52.03	0.34	2.44	52.85	0.29	3.25	53.28	0.26	3.28
	4	53.66	0.23	4.07	50.41	0.50	0.00	52.85	0.30	2.44	49.18	0.59	-0.82
	5	43.09	0.95	-7.32	43.09	0.95	-6.50	47.97	0.71	-2.44	57.38	0.06	7.38
	6	52.03	0.36	2.44	53.66	0.23	4.07	47.97	0.71	-2.44	53.28	0.27	3.28

	7	55.28	0.16	4.88	50.41	0.46	0.81	51.22	0.40	1.63	59.84	0.02	9.84
	8	51.22	0.42	1.63	40.65	0.98	-8.94	52.03	0.36	1.63	50.82	0.46	0.82
	9	46.34	0.81	-3.25	48.78	0.63	-0.81	48.78	0.65	-1.63	51.64	0.39	1.64
FGOALS-g1.0	1	72.48	0.00	22.82	59.06	0.02	9.40	47.65	0.77	-2.68	54.05	0.14	4.73
	2	75.17	0.00	24.83	59.06	0.02	8.72	50.34	0.50	0.67	60.81	0.004	11.49
	3	76.51	0.00	26.17	60.40	0.01	10.07	53.02	0.25	3.36	53.38	0.14	4.73
INGV-ECHAM4	1	50.77	0.48	0.77	43.08	0.95	-6.92	43.08	0.95	-6.92	47.29	0.74	-2.33
INM-CM3.0	1	51.94	0.36	2.33	53.49	0.24	3.88	50.39	0.50	0.00	46.88	0.73	-2.34
IPSL-CM4	1	44.29	0.93	-5.71	52.14	0.33	2.14	50.71	0.46	0.71	48.20	0.69	-1.44
MIROC3.2-hires	1	42.00	0.96	-8.00	53.00	0.31	3.00	57.00	0.10	7.00	45.45	0.81	-4.04
MIROC3.2-medres	1	46.00	0.82	-4.00	49.00	0.59	-1.00	49.00	0.62	-1.00	46.46	0.79	-3.03
	2	50.00	0.50	1.00	44.00	0.81	-4.00	50.00	0.58	0.00	49.49	0.57	0.00
	3	47.00	0.76	-3.00	45.00	0.86	-5.00	50.00	0.54	0.00	52.53	0.34	3.03
ECHO-G	1	55.71	0.10	5.71	50.71	0.46	0.71	50.71	0.46	0.71	57.55	0.04	7.91
	2	56.43	0.07	6.43	46.43	0.80	-2.86	52.86	0.28	2.86	52.52	0.31	2.16
	3	50.71	0.46	0.71	55.00	0.12	5.71	57.14	0.06	7.14	53.96	0.20	4.32
	4	56.43	0.08	6.43	51.43	0.40	1.43	55.00	0.13	5.00	66.19	0.0001	16.55
	5	60.71	0.01	10.71	53.57	0.21	3.57	55.71	0.10	5.71	45.32	0.87	-4.32
ECHAM5/MPI-OM	1	54.68	0.15	5.04	42.45	0.97	-7.19	51.80	0.37	1.44	51.45	0.39	1.45
	2	53.24	0.24	3.60	41.73	0.97	-7.91	52.52	0.31	2.16	40.58	0.99	-9.42
	3	43.17	0.94	-6.47	46.76	0.79	-2.88	50.36	0.55	0.00	50.72	0.35	2.17
MRI-CGCM2.3.2	1	49.66	0.58	-0.67	52.35	0.28	2.68	47.65	0.74	-2.01	44.59	0.92	-5.41
	2	56.38	0.07	6.04	53.69	0.21	4.03	50.34	0.50	0.00	49.32	0.57	-0.68
	3	55.70	0.09	6.04	51.01	0.44	0.67	44.30	0.93	-6.04	47.97	0.68	-1.35
	4	54.36	0.18	4.03	50.34	0.45	0.67	48.99	0.60	-0.67	51.35	0.39	1.35

	5	50.34	0.50	0.00	53.02	0.25	3.36	46.31	0.84	-4.03	**43.24**	**0.96**	**-6.76**
NCAR-CCSM3	1	52.71	0.30	3.10	**61.24**	**0.01**	**11.63**	54.26	0.19	3.88	48.44	0.67	-1.56
	2	49.61	0.56	0.00	48.06	0.70	-1.55	**44.19**	**0.92**	**-6.20**	**43.75**	**0.93**	**-6.25**
	3	48.84	0.64	-1.55	50.39	0.50	0.78	48.84	0.64	-0.78	46.09	0.84	-3.91
	4	53.49	0.25	3.10	**44.19**	**0.92**	**-5.43**	51.94	0.36	2.33	45.31	0.87	-4.69
	5	51.16	0.44	0.78	48.06	0.69	-1.55	47.29	0.75	-2.33	49.22	0.59	-0.78
	6	54.26	0.19	4.65	46.51	0.81	-3.88	50.39	0.50	0.00	55.47	0.12	5.47
	7	55.04	0.15	5.43	51.16	0.43	0.78	46.51	0.81	-3.88	**42.78**	**0.97**	**-7.81**
	9	51.16	0.42	1.55	**43.41**	**0.94**	**-6.20**	**41.09**	**0.98**	**-9.30**	50.78	0.45	0.78
NCAR-PCM	1	46.79	0.75	-2.75	49.54	0.56	0.00	45.87	0.85	-4.59	53.70	0.19	4.63
	2	**61.47**	**0.01**	**11.93**	48.62	0.65	-0.92	44.95	0.88	-5.50	47.22	0.72	-2.78
	3	51.38	0.41	1.83	**56.88**	**0.09**	**7.34**	**61.47**	**0.01**	**11.01**	54.63	0.17	4.63
	4	55.05	0.17	4.59	53.21	0.29	2.75	44.95	0.87	-4.59	51.85	0.34	2.78
UKMO-HadCM3	1	**58.99**	**0.02**	**9.35**	53.96	0.20	4.32	47.48	0.77	-2.88	**38.41**	**0.99**	**-10.14**
	2	53.24	0.23	3.60	53.24	0.24	3.60	52.52	0.33	2.16	47.10	0.75	-2.17
UKMO-HadGEM1	1	**43.88**	**0.93**	**-5.76**	48.20	0.68	-1.44	46.76	0.82	-3.60	55.07	0.12	5.07
	2	**43.17**	**0.94**	**-6.47**	49.64	0.55	0.00	51.45	0.40	1.45	**42.34**	**0.96**	**-7.30**

Table A.7 The original Monte Carlo results of four TBO transitions based on rainfall over extend regions for 30 CMIP5 models. Second column (Ens. No.) shows numbers of ensemble members for each model. Obs. represents the percentage of observed successful TBO transition, while Pred. represents the percentage of *enhanced predictability*. Models shadowed in yellow show significant results at least in one ensemble member and one transition, which are plotted in bar chart in Section 3.2. Significant results are marked in red bold (More details see text).

CMIP5 models I.D.	Ens. No.	IND-AUS			IND-IND			AUS-IND			AUS-AUS		
		Obs. (%)	P-value	Pred. (%)	Obs. (%)	P-value	Pred. (%)	Obs. (%)	P-value	Pred. (%)	Obs. (%)	P-value	Pred. (%)
ACCESS1.0	1	50.32	0.47	0.65	51.61	0.34	1.94	50.97	0.46	0.65	56.49	0.06	6.49
ACCESS1.3	1	63.23	0.001	13.55	43.23	0.96	-6.45	47.40	0.76	-2.60	50.33	0.44	1.31
BCC-CSM1.1	1	47.74	0.74	-2.58	49.03	0.62	-0.65	47.10	0.79	-2.58	51.95	0.34	1.95
	2	54.84	0.13	5.16	59.35	0.01	9.68	49.03	0.63	-1.29	59.74	0.01	9.74
	3	58.06	0.03	8.39	50.97	0.44	0.65	52.90	0.26	2.58	59.74	0.01	9.74
CCSM4	1	58.06	0.04	7.74	49.68	0.54	0.00	58.06	0.02	8.39	50.00	0.41	1.30
	2	59.35	0.02	9.03	50.32	0.49	0.65	50.97	0.40	1.29	50.65	0.34	1.95
	3	60.00	0.01	9.68	45.16	0.89	-4.52	45.16	0.88	-4.52	55.19	0.05	7.14
	4	64.52	0.0004	13.55	50.32	0.47	0.65	48.39	0.60	-0.65	48.05	0.51	0.00
	5	63.87	0.0001	14.84	45.16	0.87	-4.52	45.16	0.93	-5.81	49.35	0.50	0.00
	6	63.87	0.0004	13.55	55.48	0.097	5.81	49.03	0.60	-0.65	49.35	0.56	0.00
CESM1-CAM5	1	49.03	0.65	-1.29	52.90	0.25	3.23	52.26	0.29	2.58	47.40	0.66	-1.30
	2	45.16	0.88	-4.52	58.71	0.02	9.03	51.61	0.42	1.29	46.10	0.78	-2.60
	3	45.16	0.88	-4.52	47.74	0.73	-1.94	57.42	0.05	7.10	46.75	0.72	-1.95
CESM1-WACCM	1	55.48	0.09	5.81	52.26	0.32	1.94	55.48	0.10	5.16	47.40	0.49	0.65
CNRM-CM5	1	54.84	0.14	4.52	50.97	0.43	1.29	49.68	0.55	0.00	51.30	0.39	1.30
	2	60.00	0.01	9.68	55.48	0.098	5.81	50.32	0.50	0.00	50.00	0.53	0.00
	3	52.90	0.27	2.58	50.32	0.50	0.65	50.97	0.42	1.29	54.55	0.15	4.55
	4	58.06	0.03	7.74	52.26	0.29	2.58	59.35	0.01	9.68	48.05	0.71	-1.95
	5	54.19	0.19	3.87	45.81	0.85	-3.87	56.77	0.05	7.10	53.90	0.19	3.90
	6	63.23	0.0004	13.55	52.90	0.23	3.23	57.42	0.04	7.10	55.84	0.08	5.84
	7	49.03	0.66	-1.29	56.13	0.07	6.45	56.77	0.04	7.10	45.45	0.86	-3.90

	8	46.45	0.83	-3.87	50.97	0.42	1.29	50.32	0.50	0.00	47.40	0.76	-2.60
	9	52.90	0.23	3.23	47.10	0.77	-2.58	47.74	0.77	-2.58	53.90	0.15	4.55
	10	54.19	0.17	4.52	49.68	0.56	-0.65	51.61	0.38	1.29	49.35	0.59	-0.65
CSIRO-Mk3.6.0	1	49.03	0.63	-0.65	49.03	0.63	-0.65	**48.52**	**0.93**	**-5.81**	**40.91**	**0.99**	**-9.09**
	2	45.81	0.86	-3.87	**44.52**	**0.92**	**-5.16**	53.55	0.22	3.23	43.51	0.95	-6.49
	3	53.55	0.16	4.52	50.32	0.43	1.29	51.61	0.44	0.65	51.95	0.29	2.60
	4	49.68	0.57	-0.65	48.39	0.69	-1.29	49.68	0.56	0.00	46.10	0.85	-3.90
	5	50.32	0.47	0.65	**43.25**	**0.96**	**-6.45**	51.61	0.40	1.29	44.16	0.88	-4.55
	6	52.90	0.26	2.58	49.68	0.52	0.00	**60.65**	**0.01**	**10.32**	48.70	0.65	-1.30
	7	52.26	0.31	2.58	49.03	0.62	-0.65	54.19	0.17	3.87	48.05	0.70	-1.95
	8	49.68	0.56	0.00	**43.87**	**0.95**	**-5.81**	**43.87**	**0.95**	**-5.81**	51.30	0.40	1.30
	9	**42.58**	**0.96**	**-6.45**	54.84	0.10	5.16	51.61	0.46	0.65	51.30	0.30	2.60
	10	**55.48**	**0.099**	**5.81**	48.39	0.69	-1.94	51.61	0.38	1.29	50.00	0.53	0.00
CanESM2	1	**64.52**	**0.0003**	**14.19**	51.61	0.37	1.94	48.39	0.68	-1.94	48.70	0.65	-1.30
	2	**61.29**	**0.003**	**10.97**	**42.58**	**0.97**	**-7.10**	52.90	0.26	2.58	**57.14**	**0.04**	**7.14**
	3	**58.06**	**0.03**	**7.74**	49.68	0.57	-0.65	50.32	0.50	0.65	46.10	0.77	-2.60
	4	**61.29**	**0.003**	**11.61**	49.03	0.61	-0.65	46.45	0.84	-3.87	53.90	0.18	3.90
	5	**61.94**	**0.002**	**11.61**	49.03	0.62	-0.65	52.26	0.31	2.58	48.70	0.63	-1.30
FGOALS-g2	2	**39.74**	**1.00**	**-10.26**	51.28	0.40	1.28	46.15	0.86	-3.85	49.68	0.49	0.65
	3	**34.62**	**1.00**	**-15.38**	46.79	0.80	-3.21	50.64	0.49	0.64	**58.71**	**0.01**	**9.03**
	4	**42.95**	**0.97**	**-7.05**	**58.33**	**0.02**	**8.33**	**42.31**	**0.98**	**-7.69**	54.84	0.13	5.16
FGOALS-s2	1	**58.71**	**0.02**	**9.03**	52.26	0.30	2.58	**44.52**	**0.93**	**-5.81**	48.05	0.71	-1.95
	2	54.84	0.13	5.16	**45.16**	**0.90**	**-4.52**	46.45	0.83	-3.23	53.25	0.23	3.25
	3	49.68	0.56	0.00	**43.87**	**0.94**	**-5.81**	47.74	0.74	-2.58	51.30	0.40	1.30
FIO-ESM	1	**60.65**	**0.01**	**10.32**	54.84	0.11	5.16	**42.58**	**0.97**	**-7.10**	**56.49**	**0.06**	**6.49**

	2	65.16	0.0001	15.48	54.84	0.13	5.16	49.68	0.57	-0.65	50.65	0.46	0.65
	3	58.06	0.02	8.39	48.39	0.68	-1.29	40.00	1.00	-10.32	53.25	0.21	3.90
GFDL-CM3	1	48.97	0.64	-1.38	48.28	0.68	-1.38	46.90	0.79	-2.76	46.85	0.80	-2.80
	2	54.48	0.15	4.83	47.59	0.74	-2.07	55.86	0.09	5.52	44.76	0.91	-4.90
	3	46.90	0.80	-3.45	53.10	0.25	3.45	51.03	0.43	1.38	52.45	0.30	2.80
	4	48.61	0.67	-1.39	62.50	0.001	12.50	59.72	0.01	9.72	53.85	0.20	4.20
	5	53.47	0.23	3.47	58.33	0.03	8.33	45.14	0.90	-4.86	52.45	0.28	2.80
GFDL-ESM2G	1	36.11	1.00	-13.89	56.94	0.06	6.94	52.78	0.27	2.78	49.65	0.56	0.00
	2	49.31	0.59	-0.69	51.39	0.40	1.39	56.25	0.08	6.25	44.76	0.88	-4.90
	3	50.69	0.49	0.69	51.39	0.39	1.39	47.92	0.70	-2.08	45.45	0.86	-4.20
GFDL-ESM2M	1	54.86	0.14	4.86	50.00	0.53	0.00	54.86	0.14	4.86	47.55	0.71	-2.10
GISS-E2-H	1	52.26	0.30	2.58	52.90	0.23	3.23	60.65	0.01	10.32	48.05	0.70	-1.95
	2	54.84	0.12	5.16	56.13	0.07	6.45	54.84	0.14	4.52	49.35	0.57	-0.65
	3	57.42	0.04	7.10	54.19	0.17	4.52	52.90	0.26	2.58	51.95	0.34	1.95
	4	57.42	0.04	7.10	57.42	0.04	7.74	45.81	0.87	-3.87	48.05	0.71	-1.95
	5	54.19	0.17	3.87	56.13	0.08	5.81	52.90	0.26	3.23	51.30	0.39	1.30
GISS-E2-R	1	56.77	0.05	7.10	52.90	0.26	3.23	48.39	0.69	-1.94	49.35	0.57	-0.65
	3	55.48	0.11	5.16	52.90	0.24	3.23	49.68	0.55	0.00	53.90	0.18	3.90
	4	51.61	0.38	1.29	49.68	0.55	0.00	51.61	0.37	1.94	50.65	0.47	0.65
	5	61.29	0.002	11.61	47.74	0.69	-1.94	50.32	0.52	0.00	45.45	0.88	-4.55
HadGEM2-AO	1	55.86	0.08	6.21	47.59	0.73	-2.07	48.97	0.66	-1.38	56.25	0.07	6.25
HadCM3	1	51.03	0.44	0.69	45.52	0.88	-4.14	47.59	0.74	-2.07	47.92	0.68	-1.39
	3	51.72	0.37	1.38	50.34	0.50	0.69	47.59	0.75	-2.07	42.36	0.97	-7.64
	5	51.03	0.43	1.38	51.03	0.43	1.38	46.21	0.85	-4.14	47.92	0.71	-2.08
	8	48.97	0.68	-1.38	50.34	0.42	1.38	42.07	0.97	-7.59	47.22	0.75	-2.78

HadGEM2-ES	1	52.41	0.28	2.76	48.28	0.69	-1.38	53.47	0.22	3.47	52.45	0.28	2.80
	2	54.48	0.16	4.83	49.66	0.57	-0.69	49.66	0.56	0.00	50.00	0.52	0.00
	3	51.39	0.40	1.39	53.47	0.20	4.17	45.52	0.86	-4.14	46.53	0.82	-3.47
INM-CM4	1	60.65	0.005	10.32	49.68	0.56	0.00	41.29	0.99	-9.03	48.70	0.66	-1.30
IPSL-CM5A-LR	1	34.19	1.00	-16.13	48.39	0.69	-1.94	48.39	0.68	-1.94	53.25	0.23	3.25
	2	39.35	1.00	-10.32	43.87	0.95	-5.81	56.77	0.06	6.45	53.90	0.18	3.90
	3	40.00	0.99	-9.68	49.68	0.53	0.00	52.90	0.26	2.58	53.90	0.19	3.90
	4	41.29	0.99	-9.03	37.42	1.00	-12.26	58.71	0.02	9.03	46.75	0.81	-3.25
IPSL-CM5A-MR	1	45.81	0.87	-3.87	50.97	0.43	1.29	53.55	0.22	3.23	52.60	0.28	2.60
IPSL-CM5B-LR	1	56.77	0.06	6.45	43.87	0.94	-5.81	53.55	0.20	3.87	51.95	0.34	1.95
MIROC5	1	58.06	0.03	7.74	45.81	0.87	-4.52	49.03	0.62	-0.65	48.70	0.54	0.00
	2	60.00	0.01	10.32	54.19	0.16	4.52	46.45	0.84	-3.87	48.70	0.65	-1.30
	3	57.42	0.04	7.10	52.90	0.26	3.23	49.03	0.61	-0.65	44.81	0.87	-4.55
MIROC-ESM	1	49.03	0.61	-0.65	45.81	0.87	-3.87	46.45	0.84	-3.87	45.45	0.86	-3.90
	2	55.48	0.11	5.16	47.74	0.72	-1.94	44.52	0.92	-5.16	47.40	0.76	-2.60
	3	60.00	0.01	9.68	49.68	0.56	0.00	47.10	0.78	-2.58	52.60	0.26	3.25
MPI-ESM-LR	1	44.52	0.93	-5.81	51.61	0.38	1.29	50.32	0.50	0.65	50.00	0.53	0.00
	2	50.97	0.45	0.65	52.26	0.31	2.58	48.39	0.68	-1.29	50.65	0.42	1.30
	3	53.55	0.21	3.87	49.03	0.62	-0.65	47.74	0.75	-2.58	46.75	0.81	-3.25
MRI-CGCM3	1	47.10	0.78	-2.58	45.16	0.90	-4.52	54.19	0.17	3.87	44.81	0.91	-5.19
	2	42.58	0.97	-7.10	47.74	0.73	-1.94	56.13	0.08	5.81	45.45	0.84	-3.90
	3	48.39	0.68	-1.29	40.00	0.99	-9.68	46.45	0.83	-3.87	47.40	0.75	-2.60
NorESM1-M	1	72.26	0.00	21.94	57.42	0.03	7.74	54.19	0.15	4.52	53.25	0.21	3.90
	2	66.45	0.00	16.77	58.71	0.02	9.03	53.55	0.23	3.23	50.65	0.44	0.65
	3	70.97	0.00	20.65	49.68	0.52	0.00	42.58	0.97	-7.10	42.21	0.98	-7.79

NorESM1-ME	1	**61.94**	**0.003**	**11.61**	**57.42**	**0.04**	**7.74**	50.32	0.46	0.65	49.35	0.49	0.65

Evaluation of monsoon seasonality and the tropospheric biennial oscillation transitions in the CMIP models

Yue Li,[1] Nicolas C. Jourdain,[1] Andréa S. Taschetto,[1] Caroline C. Ummenhofer,[2] Karumuri Ashok,[3] and Alexander Sen Gupta[1]

Received 31 July 2012; revised 17 September 2012; accepted 25 September 2012; published 26 October 2012.

[1] Characteristics of the Indian and Australian summer monsoon systems, their seasonality and interactions are examined in a variety of observational datasets and in the Coupled Model Intercomparison Project Phase 3 and 5 (CMIP3 and CMIP5) climate models. In particular, it is examined whether preferred monsoon transitions between the two regions and from one year to another, that form parts of the Tropospheric Biennial Oscillation, can lead to improved predictive skill. An overall improvement in simulation of seasonality for both monsoons is seen in CMIP5 over CMIP3, with most CMIP5 models correctly simulating very low rainfall rates outside of the monsoon season. The predictability resulting from each transition is quantified using a Monte Carlo technique. The transition from strong/weak Indian monsoon to strong/weak Australian monsoon shows ∼15% *enhanced predictability* in the observations, in estimating whether the following monsoon will be stronger/weaker than the climatology. Most models also successfully simulate this transition. However, *enhanced predictability* for other transitions is less clear.
Citation: Li, Y., N. C. Jourdain, A. S. Taschetto, C. C. Ummenhofer, K. Ashok, and A. Sen Gupta (2012), Evaluation of monsoon seasonality and the tropospheric biennial oscillation transitions in the CMIP models, *Geophys. Res. Lett.*, *39*, L20713, doi:10.1029/2012GL053322.

1. Introduction

[2] The Indian - Australian monsoon system affects approximately one-fourth of the world's population. As such, a thorough understanding of the monsoon variability is of vital importance for the population living in those areas. Both Indian and Australian monsoons undergo large year-to-year variations. Previous studies have suggested that this variability can be partly understood in terms of a quasi-biennial oscillation, whereby a relatively strong Indian monsoon is followed by a strong Australian monsoon half a year later and relatively weak Indian monsoon in the subsequent year (and vice versa) [*Meehl*, 1987]. This monsoonal see-saw is often referred to as Tropospheric Biennial Oscillation (TBO) [*Meehl*, 1997]. Large-scale atmospheric circulation change and ocean-land temperature gradient are key ingredients of the TBO, with modulation by remote modes of variability, such as the El Niño-Southern Oscillation (ENSO) [*Meehl and Arblaster*, 2002].

[3] Previous studies have examined the possible mechanisms for the TBO and the individual transitions that make up the TBO. *Meehl* [1987] and *Meehl and Arblaster* [2002], for example examine the Indian-Australian in-phase transition when a strong (weak) Indian monsoon is followed by a strong (weak) Australian monsoon. They show that a direct forcing by ENSO tends to reinforce the transition, as an El Niño (La Niña) tends to suppress (enhance) both monsoons. According to *Wu* [2008] however, this transition can also occur independently of any ENSO influence via interactions confined to the Indian Ocean and Maritime Continent. A number of complementary mechanisms have also been proposed for the out-of-phase transition, i.e., from a strong (weak) Australian monsoon to a weak (strong) Indian monsoon. When the phase of ENSO changes just after an Australian monsoon season, it can directly drive the out-of-phase transition [e.g., *Meehl and Arblaster*, 2002]. In another mechanism, cool Indian Ocean SST anomalies resulting from a combined strong Indian monsoon and La Niña conditions may persist through to the next year to produce a weak Indian monsoon [*Meehl and Arblaster*, 2002]. At the same time the persistence of La Niña drives a strong Australian monsoon. Thus we see a strong Australian monsoon followed by a weak Indian monsoon, although the strong Australian monsoon is not the cause of the Indian monsoon anomaly. Finally, *Wu* [2009] also proposes a mechanism that is independent of ENSO in which the Australian monsoon generates SST anomalies in the north Indian Ocean, which in turn influence the subsequent Indian monsoon. TBO-like variability has been successfully reproduced in both simple box models [e.g., *Chang and Li*, 2000] and coupled climate models [*Nanjundiah et al.*, 2005]. Previous studies have shown considerable decadal variability in the presence of the TBO (e.g., K. Ashok et al., Decadal changes in the relationship between the Indian and Australian summer monsoons, submitted to *Climate Dynamics*, 2012).

[4] Using a Monte Carlo sampling of observed monsoon rainfall, *Fasullo* [2004] examined the Indian-Indian monsoon transition. He found that the success of this transition was highly dependent on the co-occurrence of ENSO events, suggesting that ENSO-related mechanisms are a necessary condition for the existence of a TBO. In this study we use a similar approach to *Fasullo* [2004] to examine all monsoon transitions in several observational products and in the CMIP3 and CMIP5 historical simulations. In particular, we quantify the enhanced predictive skill, resulting from each of the

[1]Climate Change Research Centre, University of New South Wales, Sydney, New South Wales, Australia.
[2]Department of Physical Oceanography, Woods Hole Oceanographic Institution, Woods Hole, Massachusetts, USA.
[3]Centre for Climate Change Research, Indian Institute of Tropical Meteorology, Pune, India.

Corresponding author: Y. Li, Climate Change Research Centre, University of New South Wales, Sydney, NSW 2052, Australia. (yue.li@student.unsw.edu.au)

0094-8276/12/2012GL053322

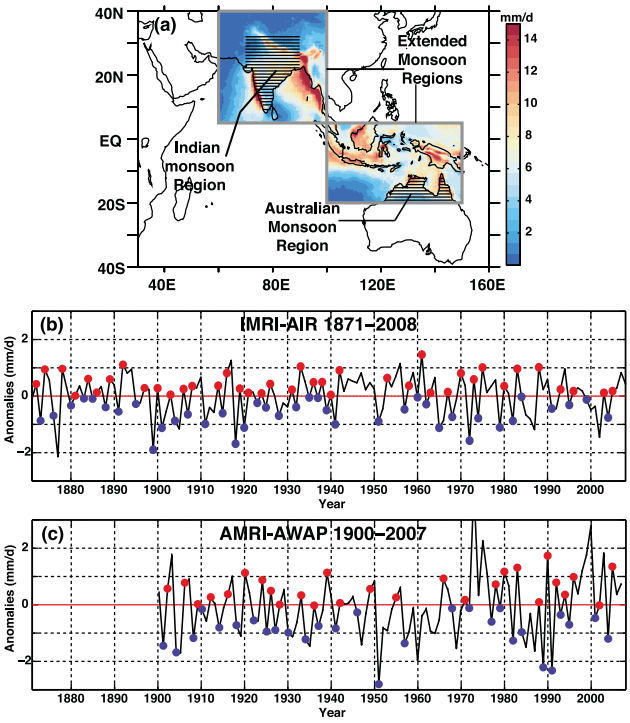

Figure 1. (a) The map showing the continental Indian and Australian monsoon regions (shaded) used to calculated the IMRI and AMRI, and the extended monsoon regions (boxes: 5°N–40°N, 60°E–100°E and 20°S–5°N, 100°E–150°E), including the ocean based on *Meehl and Arblaster* [2002]. (b) The IMRI-AIR is the anomaly derived from average JJAS rainfall over the Indian subcontinent, and (c) the AMRI-AWAP is the anomaly averaged from DJFM rainfall over North Australia. Red/blue circles in Figures 1b and 1c represent the successful positive/negative transition years, respectively, relating to Indian-Indian and Australian-Australian transitions.

transitions, i.e., the probability that the following monsoon rainfall will be stronger or weaker than the climatological average.

2. Methodology

[5] In order to examine Indian and Australian monsoon variability, we define the Indian Monsoon Rainfall Index (IMRI) and the Australian Monsoon Rainfall Index (AMRI). The reference IMRI is based on mean JJAS (June to September) All-Indian Monsoon Rainfall (AIR) computed by *Parthasarathy et al.* [1995] (1871–2008, referred to as IMRI-AIR, see Figure 1a). Other IMRIs are similarly defined using other observational datasets (see below) for the shaded area shown in Figure 1a. These indices differ from the IMRI-AIR in that the Himalaya is entirely included in our domain in order to be consistent with various coarse model grids. The Australian Monsoon Rainfall Index (AMRI) is defined as the mean DJFM (December to March) rainfall anomaly over northern Australia (Figure 1a). In this paper, the reference AMRI is derived from the high-quality daily rainfall data from the Australian Water Availability Project (AWAP) (1900–2007; resolution 0.1° × 0.1° [*Jones et al.*, 2009]) (referred to as AMRI-AWAP). In order to test the sensitivity of our results to the choice of dataset, we also calculate the IMRI and AMRI from two global gridded precipitation datasets: the Climate Prediction Center Merged Analysis of Precipitation dataset (CMAP; resolution 2.5° × 2.5°; 1979–2008) [*Xie and Arkin*, 1996] and the Global Precipitation Climatology Centre dataset (GPCC; resolution 1° × 1°; 1901–2010) [*Rudolf et al.*, 2010]. The IMRI and AMRI are also calculated for 24 CMIP3 models simulations (20c3m experiment) covering approximately 1860–2000, and for 23 CMIP5 simulations (historical experiment) covering 1850–2005 (some models contain more than one member).

3. Results

3.1. Seasonality

[6] For all three observed Indian rainfall datasets, the four wettest months extend from June to September with maximum rainfall in July (Figure 2a). The CMIP models show a range of behaviors. Eleven out of 24 CMIP3 models (Figure 2a) and 11 out of 23 CMIP5 models (Figure 2c) correctly simulate peak rainfall in July, with several models with peak rainfall delayed by one month. Three CMIP3 models have large timing biases: the mpi_echam5 and csiro_mk3.5/ipsl-cm4 peak two months early and late respectively. There is also considerable spread in the amplitude of the seasonal cycle. While rainfall in the peak monsoon month ranges from 7.2 to 9.1 mm/d across observations, both CMIP3 and CMIP5 models range from ∼3 to 10 mm/d. The multi-model means (±1 standard deviation) for CMIP3 and CMIP5 models are similar with a maximum of ∼6 ± 2 mm/d in August, indicating that in general the monsoon rainfall in the models is too weak. For a few models (particularly for CMIP3), there is too much rainfall outside of the monsoon season (e.g., cnrm_cm3 and inmcm3_0).

[7] Over Australia maximum observed rainfall occurs in February, ranging between 5.9 to 8.6 mm/d across the three observational datasets (Figure 2b) with most rainfall from December to March. Again there is a considerable range in monsoon strength across the models (2 to 11 mm/d), although the multi-model means (7.5 ± 3/7.0 ± 3 mm/d for CMIP3/CMIP5) lie within the observational range. The giss_aom and ipsl_cm4 CMIP3 models have essentially no monsoon season. Most CMIP3 and CMIP5 models simulate maximum rainfall in the correct month with a few of models peaking one month early and others with an overly long rainy season (e.g., bccr_bcm2_0).

[8] In general, for both CMIP3 and CMIP5 and for both regions the range in monsoon strength across the models is about the same. However, there is a clear overall improvement in the seasonality of both monsoons from CMIP3 to CMIP5, with most CMIP5 models better simulating the monsoon timing and very low rainfall rates outside of the monsoon season.

3.2. TBO Transitions Assessment

[9] A Monte Carlo technique is used to assess the significance of *enhanced predictability* associated with the TBO. In particular we assess the success rate of the four transitions that are thought to be important for the TBO tendency starting from a given year t: (1) Successful Indian-Indian out-of-phase transition is defined as IMRI(t) > 0 and IMRI(t + 1) < 0 or IMRI(t) < 0 and IMRI(t + 1) > 0; (2) Successful Australian-

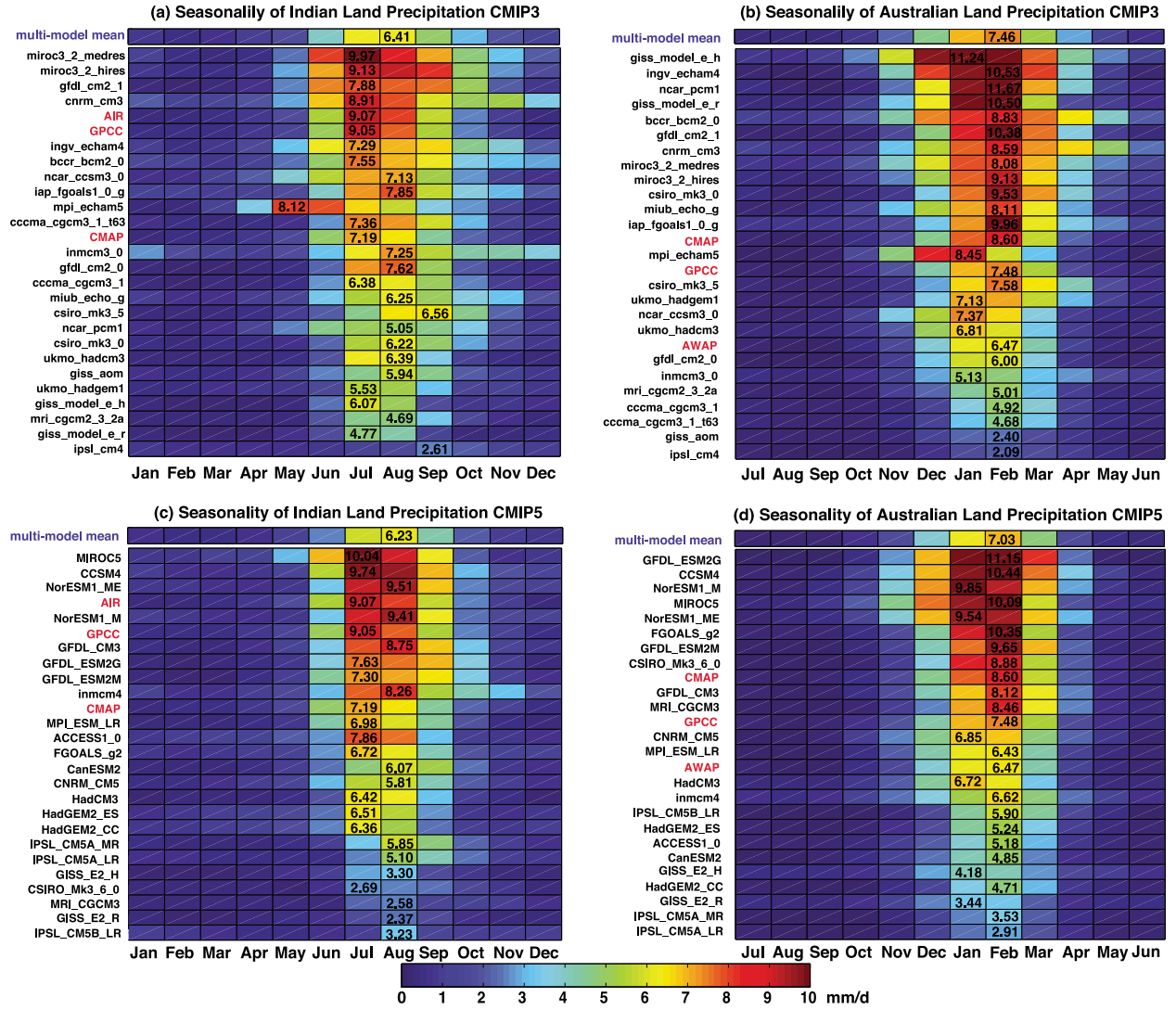

Figure 2. Seasonal cycle of the (a, c) Indian and (b, d) Australian land-restricted rainfall for observed and CMIP3 (Figures 2a and 2b) and CMIP5 (Figures 2c and 2d) models over. Models (names in black) and observations (names in red) are sorted according to the average monsoon rainfall amount (JJAS rainfall for Indian monsoon and DJFM rainfall for Australian monsoon). The top row shows the multi-model mean (names in blue) of CMIP3 or CMIP5 models for Indian and Australian rainfall. Internal numbers show the maximum rainfall (mm/d) in the month of greatest rainfall.

Australian out-of-phase transition is defined as AMRI(t) > 0 and AMRI(t + 1) < 0 or AMRI(t) < 0 and AMRI(t + 1) > 0; (3) Successful Indian-Australian in-phase transition is defined as IMRI(t) > 0 and AMRI(t) > 0 or IMRI(t) < 0 and AMRI(t) < 0; and, (4) Successful Australian-Indian out-of-phase transition is defined as AMRI(t) > 0 and IMRI(t + 1) < 0 or AMRI(t) < 0 and IMRI(t + 1) > 0.

[10] To determine the observed predictability associated with a given transition, we count the number of successful transitions in the timeseries (Figures 1b and 1c), relative to the total number of possible successful transitions. This is then repeated 100,000 times by randomly resampling the observed timeseries (with replacement). The predictability of the monsoon resulting from a given transition is considered enhanced if the observed or simulated percentage of successful transitions is significantly higher than the median of the randomized distribution. Moreover, the *enhanced predictability* is considered significant if the observed or simulated percentage of successful transitions lies in the upper decile of the randomized distributions (i.e., there is only a 10% probability of getting the *enhanced predictability* by chance).

[11] In the IMRI-AIR and AMRI-AWAP, only two of the four transitions show a significantly *enhanced predictability* over the random distribution: the Indian-Indian out-of-phase transition and the Indian-Australian in-phase transition, where the *enhanced predictability* from the median is 8.8% ($p \sim 0.1$) and ~15% ($p \sim 0.001$), respectively (Figure S1 in the auxiliary material).[1] This means that if the Indian monsoon is anomalously strong (weak) in a given year there is a ~59% probability that the subsequent Indian monsoon will be anomalously weak (strong) and a ~65% probability that the subsequent Australian monsoon will be anomalously strong (weak).

[1] Auxiliary materials are available in the HTML. doi:10.1029/2012GL053322.

[12] To test the sensitivity of these results to the datasets, we compute predictability based on different datasets and time periods: CMAP (1979–2008) and GPCC (1901–2010) over the same spatial land areas (Figure 1a). Indices from both datasets show significant *enhanced predictability* ($p \sim 0.1$) of 27.6% and 13.8%, respectively, for the Indian to Australian transition. However, for the Indian-Indian out-of-phase transition, only GPCC shows an *enhanced predictability* of 6.4% ($p \sim 0.12$). Given the relative shortness of the CMAP datasets, the lack of significant results might arise from multi-decadal variability of the TBO. To examine this, we divided the IMRI-AIR into a CMAP-like period (1979–2008) and pre-CMAP period (1871–1978). The pre-CMAP period shows significantly *enhanced predictability* (10.3%, $p \sim 0.1$). The predictability for over the later CMAP-like period is not significant. This suggests that the biennial tendency for the Indian-Indian out-of-phase transition has deceased in the past 30-yrs, consistent with the recent weakening of the El Niño-Indian monsoon relationship [*Ummenhofer et al.*, 2011; *Meehl and Arblaster*, 2011].

[13] Figure 3 shows the *enhanced predictability* for the different observational datasets and selected CMIP3 and CMIP5 models for the four transitions. We only show models for which at least one ensemble member shows a significantly *enhanced predictability* in any of the transitions. Twelve CMIP3 and 15 CMIP5 models have at least one ensemble member with significantly *enhanced predictability* for the Indian-Australian in-phase transition (Figure 3a), consistent with the observations. For the CMIP5 models the range of *enhanced predictability* is relatively small (5%–15%, for significant results only). As such the models generally underestimate the observed *enhanced predictability* of ~15%. For the CMIP3 models the range is larger (5–35%). For the models with multiple ensemble members, many show contrasting results for different members, indicating a substantial multi-decadal variability in the efficacy of this transition. Nevertheless, when considering concatenated ensemble members, the Indian- Australian transition has *enhanced predictability* in 11 of 24 (14 of 23) CMIP3 (CMIP5) models.

[14] As noted above, the only other transition that provides significantly *enhanced predictability* using the long-term reference observations is the Indian-Indian out-of-phase transition, although it is mostly associated with the earlier part of the record (see discussion above). For this transition (Figure 3b), seven CMIP3 and five CMIP5 models show *enhanced predictability* for at least one ensemble member. In the case of models with multiple ensemble members, only a small number of members are significant (e.g., CNRM_CM5, GISS_E2_H and NorESM_M). As such, only four CMIP3 and two CMIP5 models show *enhanced predictability* when considering the multi-ensemble concatenation for each model.

[15] For the Australian-Indian out-of-phase transition (Figure 3c), one of the longer observational timeseries suggests a multi-decadal period when there was *enhanced predictability* associated with this transition. Five CMIP3 and only one CMIP5 models have ensemble members with significantly *enhanced predictability*, despite conflicting results within each ensemble set. Surprisingly, a large number of models actually show significant *negative predictability*, in particular when considering concatenated ensemble members. Negative predictability suggests that a strong (weak) Australian monsoon would tend to be followed by a strong (weak) Indian monsoon. Such behavior is not found in the observations, and might be related to bias in the simulated ENSO seasonal cycle, e.g., where La Niña events tend to persists too long this would lead to a strong Australian monsoon followed by a strong Indian monsoon (N. C. Jourdain et al., The Indo-Australian monsoon and its relationship to ENSO and IOD in reanalysis data and the CMIP3/CMIP5 simulations, submitted to *Climate Dynamics*, 2012). Finally for the Australian-Australian out-of-phase transition (Figure 3d), for which there is no observational evidence of *enhanced predictability*, eight of the CMIP3 and five of the CMIP5 models have ensemble members with significantly *enhanced predictability.*

[16] While the impacts of the monsoon are primarily over land, the teleconnections associated with global modes of variability can involve larger domains. To assess the effect of the monsoon in a larger context, we also derived similar rainfall indices over extended Indian and Australian regions (including the oceanic regions, Figure 1a, see methods) used in previous analysis of the TBO [e.g., *Meehl and Arblaster*, 2002]. Applying the Monte Carlo analysis to these indices for both CMIP3 and CMIP5 models, we find that for the Indian-Australian transition, most models show significant *enhanced predictability* independent of the index definition (Figure S2). For the other transitions there is little consistency with regards to predictability across the models. For the Australian-Indian transition, fewer models show the negative predictability seen with the land-only based indices. In addition for the Australian-Australian transition there are more CMIP3 models that exhibit *enhanced predictability* using the more inclusive index. As such, overall we do not find that the sequence of events that combine to make up the TBO is more obvious when examining a larger land-ocean area.

4. Conclusion

[17] This study examines the fidelity of climate models in simulating the mean state and seasonality of the Indian and Australian monsoons and the various transitions that play a role in the TBO. While almost all models produce at least some monsoon-like behavior, there are very large spreads in maximum monthly rainfall: 33% to 110% (50% to 170%) of the AIR/AWAP observational dataset for Indian (Australian) rainfall. The multi-model means of Indian maximum rainfall are underestimated for both CMIP3 and CMIP5 models (6 ± 2 mm/d as compared to 7–9 mm/d), while multi-model means of Australian maximum rainfall are within the observed range (6–9 mm/d). Most models successfully reproduce the timing of the monsoons although phase shifts of up to 2 months are evident in a few models. Overall, while there is no obvious improvement in the average summer monsoon rainfall from CMIP3 to CMIP5, in general, the CMIP5 models do show improved seasonality for both monsoons.

[18] In the observations and in the majority of the models (13 of 24 CMIP3 and 15 of 23 CMIP5), we find significantly *enhanced predictability* in the Indian-Australian in-phase transition. The observations suggest that given the strength of the Indian monsoon we have a ~65% chance of correctly estimating whether the following Australian monsoon will be weaker or stronger than normal. The *enhanced predictability* in CMIP models is probably related to the fact that the models correctly reproduce an ENSO-monsoon link, such that an

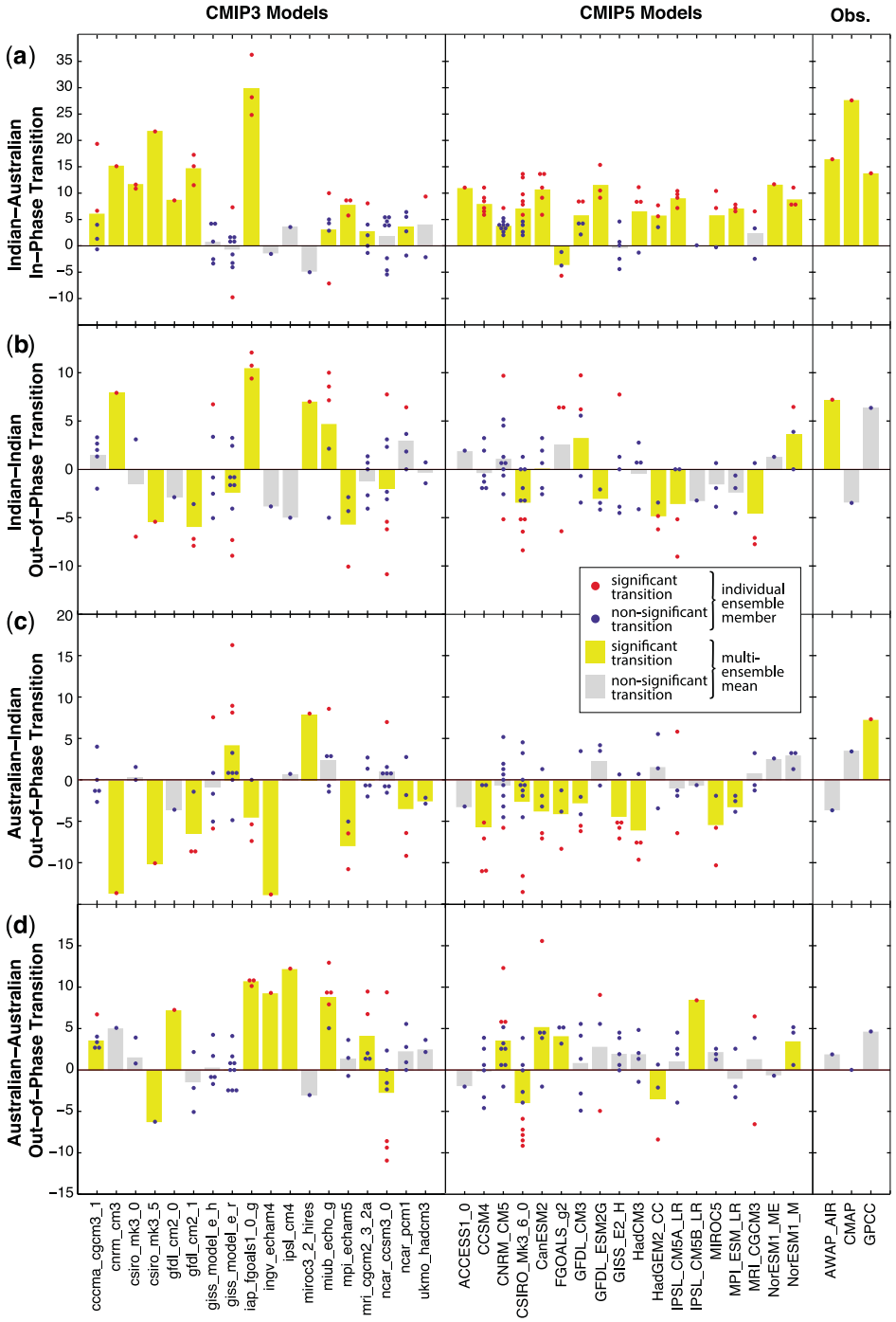

Figure 3. Percentage *enhanced predictability* for the (a) Indian-Australian, (b) Indian-Indian, (c) Australian-Indian and (d) Australian-Australian transitions for observations and CMIP3 and CMIP5 models for which at least one ensemble member for that model and for at least one of the transitions shows a significant increase in predictability. Circles represent individual ensemble members (marked in red are significant, $p < 0.1$). Bars represent the multi-ensemble mean percentage *enhanced predictability* for each model with yellow indicating significant changes. The multi-ensemble mean predictability was calculated by concatenating time series for all ensemble members prior to Monte Carlo resampling.

El Niño (La Niña) is associated with both a weak (strong) Indian and Australian monsoon [*Webster et al.*, 1998].

[19] The Indian-Indian out-of-phase transition is only significant in the long AIR dataset, providing *enhanced predictability* of ~8% (Figure 3b), however it varies over certain time periods. For CMIP3 and CMIP5 models with multiple ensemble members, only some of the ensemble members show successful transitions. This suggests a high-degree of multi-decadal variability in this transition. This is consistent with previous studies looking at the observational records [e.g., *Fasullo*, 2004; *Meehl and Arblaster*, 2011]. While some models indicate significantly *enhanced*

predictability, many models actually show significantly reduced predictability for the Indian-Indian and Australian-Indian out-of-phase transitions. Future work will examine the reasons behind these inter-model differences.

[20] In summary, this study examines four different TBO transitions, for which a number of different mechanisms have been proposed [e.g., *Meehl and Arblaster*, 2002]. Our study demonstrates that while for both observations and models the India-Australia link seems to be robust, the other transitions are both dataset and time period dependent, with a range of contrasting behaviors exhibited in the climate models. In particular there seems to be little evidence that the Australian monsoon can directly influence the subsequent Indian monsoon.

[21] **Acknowledgments.** We acknowledge the WCRP's Working Group on Coupled Modelling, which is responsible for CMIP, and the climate modeling groups for their model output. The U.S. DoE's PCMDI provides coordinating support for CMIP in partnership with the GOESSP. This project was supported by funding from the Australian Research Council (DP110100601) and the Centre of Excellence for Climate System Science. This work was also supported by an award under the Merit Allocation Scheme on the NCI National Facility at the ANU. Two anonymous reviewers provided helpful comments on the paper.

[22] The Editor thanks two anonymous reviewers for their assistance in evaluating this paper.

References

Chang, C.-P., and T. Li (2000), A theory for the tropical tropospheric biennial oscillation, *J. Atmos. Sci.*, *57*, 2209–2224, doi:10.1175/1520-0469(2000)057<2209:ATFTTT>2.0.CO;2.

Fasullo, J. (2004), Biennial characteristics of all India rainfall, *J. Clim.*, *17*, 2972–2982, doi:10.1175/1520-0442(2004)017<2972:BCOIMR>2.0.CO;2.

Jones, D. A., W. Wang, and R. Fawcett (2009), High-quality spatial climate data-sets for Australia, *Aust. Meteorol. Oceanogr. J.*, *58*, 233–248.

Meehl, G. A. (1987), The annual cycle and interannual variability in the tropical Pacific and Indian Ocean regions, *Mon. Weather Rev.*, *115*, 27–50, doi:10.1175/1520-0493(1987)115<0027:TACAIV>2.0.CO;2.

Meehl, G. A. (1997), The South Asian monsoon and the tropospheric biennial oscillation, *J. Clim.*, *10*, 1921–1943, doi:10.1175/1520-0442(1997)010<1921:TSAMAT>2.0.CO;2.

Meehl, G. A., and J. M. Arblaster (2002), The tropospheric biennial oscillation and Asian-Australian monsoon rainfall, *J. Clim.*, *15*, 722–744, doi:10.1175/1520-0442(2002)015<0722:TTBOAA>2.0.CO;2.

Meehl, G. A., and J. M. Arblaster (2011), Decadal variability of Asian–Australian monsoon–ENSO–TBO relationships, *J. Clim.*, *24*, 4925–4940, doi:10.1175/2011JCLI4015.1.

Nanjundiah, R. S., V. Vidyunmala, and J. Srinivasan (2005), The impact of increase in CO_2 on the simulation of tropical biennial oscillations (TBO) in 12 coupled general circulation models, *Atmos. Sci. Lett.*, *6*(3), 183–191, doi:10.1002/asl.115.

Parthasarathy, B., A. A. Munot, and D. R. Kotawale (1995), Monthly and seasonal rainfall series for all-India homogeneous regions and meteorological sub-divisions: 1871–1994, *Res. Rep. 65*, Indian Inst. of Trop. Meteorol., Pune.

Rudolf, B., A. Becker, U. Schneider, A. Meyer-Christoffer, and M. Ziese (2010), GPCC Status Report, December 2010, report, 7 pp., Global Precip. Climatol. Cent., Boulder, Colo.

Ummenhofer, C. C., A. Sen Gupta, Y. Li, A. S. Taschetto, and M. H. England (2011), Multi-decadal modulation of the El Niño-Indian monsoon relationship by Indian Ocean variability, *Environ. Res. Lett.*, *6*, 034006, doi:10.1088/1748-9326/6/3/034006.

Webster, P. J., V. O. Magaña, T. N. Palmer, J. Shukla, R. A. Tomas, M. Yanai, and T. Yasunari (1998), Monsoons: Processes, predictability, and the prospects for prediction, *J. Geophys. Res.*, *103*(C7), 14,451–14,510, doi:10.1029/97JC02719.

Wu, R. (2008), Possible role of the Indian Ocean in the in-phase transition of the Indian to Australian summer monsoon, *J. Clim.*, *21*, 5727–5741, doi:10.1175/2008JCLI2354.1.

Wu, R. (2009), Possible role of the Indian Ocean in the out-of-phase transition of the Australian to Indian summer monsoon, *J. Clim.*, *22*, 1834–1849, doi:10.1175/2008JCLI2602.1.

Xie, P., and P. A. Arkin (1996), Analyses of global monthly precipitation using gauge observations, satellite estimates, and numerical model predictions, *J. Clim.*, *9*, 840–858, doi:10.1175/1520-0442(1996)009<0840:AOGMPU>2.0.CO;2.

Environ. Res. Lett. **6** (2011) 034006 (8pp) doi:10.1088/1748-9326/6/3/034006

Multi-decadal modulation of the El Niño–Indian monsoon relationship by Indian Ocean variability

Caroline C Ummenhofer, Alexander Sen Gupta, Yue Li, Andréa S Taschetto and Matthew H England

Climate Change Research Centre, University of New South Wales, Sydney, Australia

E-mail: c.ummenhofer@unsw.edu.au

Received 13 March 2011
Accepted for publication 20 June 2011
Published 5 July 2011
Online at stacks.iop.org/ERL/6/034006

Abstract

The role of leading modes of Indo-Pacific climate variability is investigated for modulation of the strength of the Indian summer monsoon during the period 1877–2006. In particular, the effect of Indian Ocean conditions on the relationship between the El Niño–Southern Oscillation (ENSO) and the Indian monsoon is explored. Using an extended classification for ENSO and Indian Ocean dipole (IOD) events for the past 130 years and reanalyses, we have expanded previous interannual work to show that variations in Indian Ocean conditions modulate the ENSO–Indian monsoon relationship also on decadal timescales. El Niño events are frequently accompanied by a significantly reduced Indian monsoon and widespread drought conditions due to anomalous subsidence associated with a shift in the descending branch of the zonal Walker circulation. However, for El Niño events that co-occur with positive IOD (pIOD) events, Indian Ocean conditions act to counter El Niño's drought-inducing subsidence by enhancing moisture convergence over the Indian subcontinent, with an average monsoon season resulting. Decadal modulations of the frequency of independent and combined El Niño and pIOD events are consistent with a strengthened El Niño–Indian monsoon relationship observed at the start of the 20th century and the apparent recent weakening of the El Niño–Indian monsoon relationship.

Keywords: climate variability, Indian monsoon, drought, decadal variability, El Nino–Southern Oscillation, Indian Ocean dipole

1. Introduction

Indian monsoon variability is intricately linked to Pacific Ocean conditions, in particular the El Niño–Southern Oscillation (ENSO). In fact, failure of the Indian monsoon and ensuing droughts and famines at the turn of the 20th century led to the discovery of ENSO by Sir Gilbert Walker. When looking for atmospheric precursors to predict the strength of the Indian monsoon in the 1920s, he identified and recognized the importance of the Southern Oscillation [1, and references therein]. Indian monsoon rainfall is negatively correlated with sea surface temperatures (SST) in the central and eastern equatorial Pacific, with El Niño events generally accompanying a weakening of the Indian summer monsoon (i.e., June–September; JJAS). The teleconnection from the tropical Pacific to India is due to anomalous subsidence, associated with changes in the zonal Walker circulation, occurring over the Indian subcontinent during El Niño events [2, and references therein].

However, the relationship between El Niño events and the strength of the Indian monsoon is far from perfect, nor is it stationary in time. While generally accounting for 30% of interannual Indian monsoon rainfall variability, ENSO's impact on the Indian monsoon varies on decadal timescales [1]. Furthermore, [3] reports a weakening of the relationship between the Indian monsoon and ENSO over recent decades. The authors link this to a southeastward shift of the subsiding branch of the anomalous Walker circulation

during recent El Niño events, which allows for normal monsoon development. It has been suggested that the change in the ENSO teleconnection to the Indian monsoon is due to enhanced warming of the Eurasian continent and an amplified land–sea temperature gradient that favours a strengthened Indian monsoon [3]. Alternatively, recent changes in the characteristics of El Niño events have been used to explain the complex ENSO–Indian monsoon relationship. In [2] the authors found that the location of maximum warming along the equatorial Pacific during El Niño events seems to be key for understanding whether drought-producing subsidence occurs over the Indian subcontinent with subsequent monsoon failure: enhanced SST in the central tropical Pacific, rather than the eastern Pacific, more effectively reduces Indian monsoon rainfall. Such modulation of ENSO teleconnections is particularly noteworthy, as the location of maximum El Niño warming has been occurring more frequently in the central Pacific in recent decades [4].

Apart from remote forcing from the Pacific Ocean, SST from the adjacent Indian Ocean also exerts a considerable influence on Indian monsoon variability [5, for example, and references therein]. Pacific and Indian Ocean variability is intricately linked, as manifest in the frequent co-occurrence of ENSO events with the Indian Ocean's tropical mode of climate variability, the Indian Ocean dipole (IOD) [6, 7]. Several studies [8–10] have explored how the Indian Ocean modulates the ENSO–Indian monsoon teleconnection.

Using the atmospheric general circulation model (AGCM) experiments forced with composite SST anomalies during independent and co-occurring El Niño and positive IOD (pIOD) events, [9] demonstrated that a coincident pIOD event counteracted the monsoon reduction expected from the El Niño-related anomalous subsidence over the Indian subcontinent due to anomalous convergent flow enhancing monsoonal rainfall over the region. Similarly, [10] described negative zonal wind anomalies in the equatorial Indian Ocean related to pIOD events to be associated with above-average monsoon rainfall, despite simultaneous El Niño events occurring. Focusing on conditions early in the Indian monsoon season, [11] found that in some combined pIOD and El Niño years drought may still occur during July (although the rest of the monsoon season returned to more normal rainfall levels). The authors suggested that the occurrence of such a July drought depends upon the timing of the onset of the pIOD, which acts to offset an El Niño-related deficiency in monsoon rainfall during subsequent months. In contrast, analysis by [12] using an index, which combines both ENSO and atmospheric variability in the Indian Ocean basin, found a reinforcing effect of Indian and Pacific Ocean variability on the strength of the Indian summer monsoon for the period 1958–2003.

Recent changes in the Asian monsoon have been reported [13, for example, and references therein] and climate model projections demonstrate the sensitivity of the monsoon to a warming climate. Observed trends in the Indian monsoon have been linked to atmospheric circulation changes associated with low-level divergence and the Somali Jet [13], observed changes in land-use and agricultural intensification [14], and aerosols inducing changes in radiative forcing and in the local Hadley circulation [15, and references therein], amongst others. Here, we look at how Indo-Pacific conditions have impacted the Indian monsoon over the last 130 years. Over recent decades, non-uniform warming of Indian Ocean temperatures has been reported [16, for example, and references therein], with the eastern Indian Ocean warming less than the west. Consistent with this pIOD-like trend, increasing frequencies of pIOD events have been found in 20th century observations [17]. Given these Indian Ocean trends, the question arises whether a recent weakening of the ENSO–Indian monsoon relationship is in fact driven by changes in ENSO characteristics [2] or in the land–sea temperature contrast [3], or whether increased co-occurrence of pIOD events with El Niño events might be sufficient to explain the weakening relationship. The latter hypothesis is explored here and offers a novel explanation for long-term variations in the ENSO–Indian monsoon teleconnection over the last 130 years due to decadal Indo-Pacific variability.

Drought can have major societal effects over the Indian subcontinent. However, it is subsurface water deficits, more than rainfall itself, that exert stress on agriculture and natural ecosystems. This highlights the importance of focusing on (sub)surface water availability to assess societal impacts associated with drought [18]. The Palmer drought severity index (PDSI), used here as an indicator of drought severity, combines information from both rainfall and surface temperature variability and thus provides an integrative measure of water availability within the ground, being highly correlated with subsurface soil moisture and streamflow conditions [19]. In a review of drought indices, the PDSI has been described to be only of limited use as a short-term monitoring tool for assessing moisture changes on the timescale of several weeks, with questions remaining about its utility in extremely seasonal climates dominated by monsoon dynamics [20, and references therein]. However, the PDSI is used widely and successfully for reconstructing annually resolved drought conditions associated with the summer monsoon across Southeast Asia [21, for example, and references therein], including India. This suggests that it can offer useful insights into the region's drought conditions associated with Indo-Pacific climate variability across the timescales investigated here.

We expand here on past work [8, 9, in particular] to assess Indian monsoon variability, as well as drought conditions there, during independent and combined pIOD and El Niño events, using a recent classification for ENSO and IOD events over the last 130 years [22, 23]. In particular, decadal modulation of the ENSO–Indian monsoon relationship by Indian Ocean conditions is explored. Thus, our focus on the multi-decadal timescale bridges previous work on interannual variability [8, 9, 12, 10] and recent trends [2, 3]. We also examine how the Indian monsoon variation is linked to large-scale climate anomalies across the Indo-Pacific region.

2. Observations and reanalysis products

For observed Indian precipitation, we use monthly data from the Indian regional/subdivisional monthly rainfall data set by the Indian Institute of Tropical Meteorology [24]. The analyses

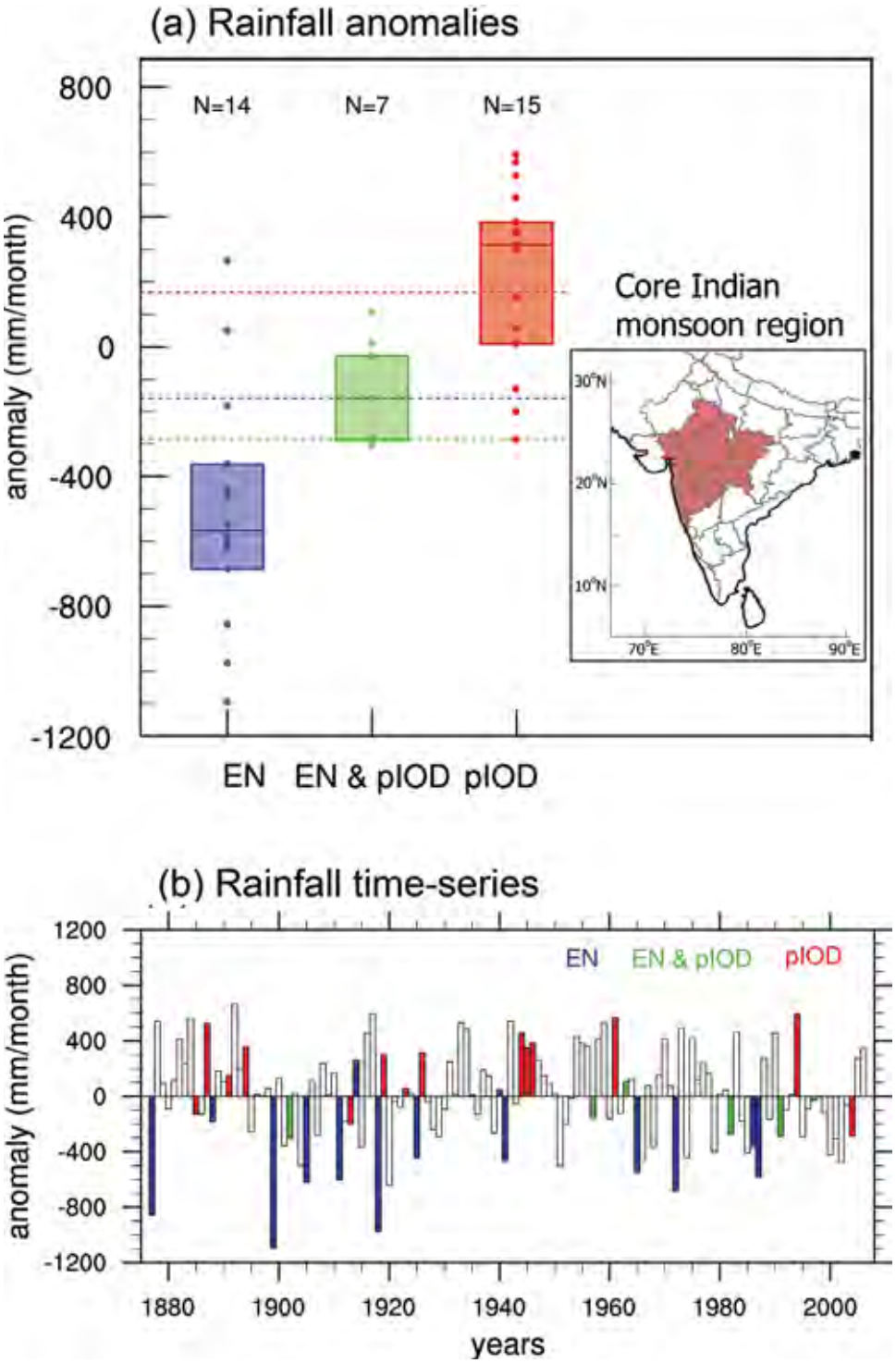

Figure 1. Rainfall anomalies (mm month^{-1}) for the different ENSO/IOD categories for the core Indian monsoon region (see map inset; definition according to IITM; http://www.tropmet.res.in/IITM/region-maps.html) during the June–September months for the period 1877–2006: (a) rainfall anomalies shown as dots for El Niño (blue), co-occurring El Niño and pIOD (green), and pIOD (red) events. The colored boxes are delimited by the upper and lower quartiles, with the middle bar denoting the median rainfall in the respective category. Dashed lines indicate the 90% confidence level (as estimated by Monte Carlo testing) for the medians for the different categories (indicated in color), with only the lower threshold shown for the El Niño and co-occurring El Niño with pIOD events and the upper threshold for pIOD events. The number of years (N) in each category is indicated at the top. (b) Time-series of rainfall anomalies with the associated ENSO/IOD categories indicated in color.

here focus on the Indian core monsoon region (see highlighted region in figure 1(a)) for the period 1877–2006 during the summer monsoon (JJAS). To explore the relationship between Indian monsoon variability and the large-scale circulation associated with ENSO and the IOD we use the classification based on [22], which has been more recently updated in [23].

To investigate large-scale conditions during ENSO/IOD events atmospheric circulation anomalies are assessed with the National Center for Environmental Prediction and the National Center for Atmospheric Research reanalysis (NNR) [25]. Monthly data was used for the period 1948–2006, though all analyses were checked for robustness by using the shorter period 1957–2006 with improved data quality. In addition, rainfall composites were also examined with the Climate Prediction Center Merged Analysis of Precipitation (CMAP) data (1979–2006) [26]. For winds, the 20th century NNR product [27] was also used for the period 1877–2006. SST are taken from the HadISST gridded data set for the period 1877–2006 [28], and the drought index is based on the gridded Dai PDSI for the period 1877–2005 [19]. Given the limitations in the PDSI as a short-term monitoring tool [20], future work could also incorporate more responsive drought indices. Here, however, we are mainly interested in variations of the Indian summer monsoon on multi-decadal timescales, for which the PDSI is suitable and has successfully been applied previously [21, and references therein]. All figures present the analysis with the longest record available to maximize the number of events in the respective categories.

3. Monsoon variability in relation to El Niño and pIOD events

For the Indian core monsoon region (inset figure 1(a)), rainfall anomalies during the summer monsoon (JJAS) for the period 1877–2006 are investigated. To assess the influence of the dominant Indo-Pacific modes of climate variability, anomalous rainfall during El Niño, pIOD, and co-occurring El Niño with pIOD events is presented (figure 1(a)). During El Niño events, median rainfall was significantly reduced by close to 600 mm month^{-1}. Only two El Niño events recorded weakly positive rainfall anomalies, while in excess of 85% of El Niño events showed anomalous dry conditions. More than 20% of El Niño events recorded rainfall deficits in excess of 800 mm month^{-1}. In contrast, El Niño events that co-occurred with a pIOD generally experienced normal rainfall conditions during the summer monsoon. Significantly enhanced rainfall with a median of 300 mm month^{-1} was recorded for 'pure' pIOD events.

A time-series of summer monsoon rainfall between 1877 and 2006, with the different ENSO/IOD events highlighted, confirms these results (figure 1(b)): the majority of 'pure' El Niño events coincided with large deficits in Indian monsoonal rainfall, while 'pure' pIOD events were generally associated with anomalous wet conditions. Co-occurring El Niño and pIOD years showed normal levels of rainfall. Severe monsoon failures during El Niño events occurred between 1899 and 1925 (figure 1(b)). In contrast, the period 1926–64 only experienced two El Niño events, one of which was associated with a large deficit in monsoonal rainfall, while a similarly dry year (1920) occurred independent of ENSO or IOD events. During this same period, several consecutive pIOD events coincided with anomalous wet conditions for the Indian core monsoon region. These results highlight the presence of considerable decadal variability across the tropical Indo-Pacific region [29, for example].

Table 1. Number of independent and combined El Niño and pIOD events and mean JJAS Indian monsoon rainfall (in mm), ±1 standard deviation (SD) during four separate multi-decadal periods of the observational record. Bold type numbers indicate values that are significant at the 90% confidence level for the number of events and at the 75% confidence level for rainfall, based on Monte Carlo analyses. Over the period 1877–2006, mean JJAS rainfall was 2200 mm, with an SD of 356 mm.

	Number of events			
	EN and pIOD	EN	pIOD	Rainfall (±1 SD)
1877–1910	2	4	4	2202 (±387)
1911–42	**0**	**6**	5	2173 (±374)
1943–74	2	**2**	4	**2267** (±352)
1975–2006	**3**	**2**	**2**	2155 (±310)

Given the decadal modulation in the tropical Indo-Pacific modes of variability, it is of interest to explore whether this contributes to modulations in the strength of the ENSO–Indian monsoon relationship. Table 1 presents the number of independent and co-occurring El Niño and pIOD events over the last 130 years during four multi-decadal periods, as well as mean JJAS Indian monsoon rainfall and its standard deviation over the four periods. Using a Monte Carlo test, random multi-decadal periods are compared with these four observed periods. This was repeated 25 000 times to determine whether the numbers of El Niño and pIOD events (mean rainfall) recorded in each multi-decadal period were unusual. Despite obtaining some statistically significant results, we would still caution that the analysis relies on relatively few events.

Over the last three decades, there were three incidents of co-occurring pIOD and El Niño events, while only two independent El Niño and pIOD events each occurred (table 1). This indicates a significantly enhanced occurrence of combined events during this period and a significantly reduced incidence in the number of independent events. The latter contributes to the lowest standard deviation (SD; 310 mm) in mean rainfall recorded for any of the four periods (table 1). The period 1943–74 is characterized by a significant reduction in El Niño, but with twice as many pIOD events. This is manifest as a significantly increased mean JJAS rainfall. The two earlier periods do not show significant anomalies in mean rainfall, most likely due to a compensating increase in the frequency of wet pIOD and dry El Niño events, as reflected in the high SD. During the period 1911–42, six independent El Niño events occurred and remarkably no combined event. This is unprecedented during any part of the 130 year record. The period without any single co-occurring El Niño and pIOD event actually extends from 1903 to 1956 (cf figure 1(b)). This is in marked contrast to the latter half of the historical record, when 5 combined events have occurred post-1957. Multi-decadal Indian Ocean variability, as manifest in the frequency of IOD events, could potentially play an important role in controlling the Indian monsoon through modulation of the ENSO–Indian monsoon relationship.

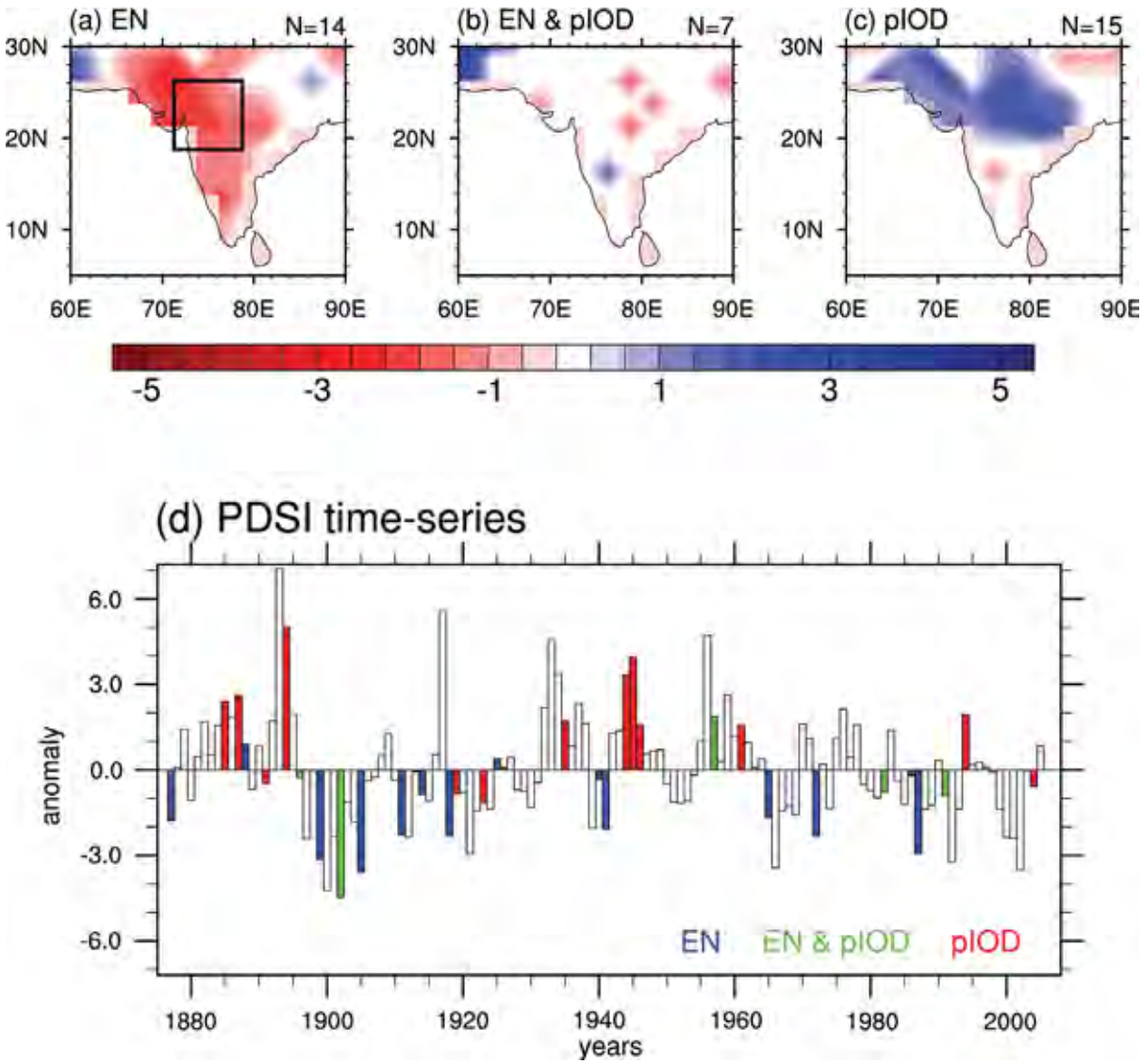

Figure 2. Composite PDSI anomalies during (a) El Niño, (b) combined El Niño and pIOD, and (c) pIOD events averaged for the June–September months for the period 1877–2005. Only anomalies are shown that are significant at the 80% confidence level as estimated by a two-tailed *t*-test. (d) Time-series of PDSI anomalies spatially averaged over the core monsoon region (black box in (a) indicated) with the associated ENSO/IOD categories indicated in color.

4. Drought variability in relation to El Niño and pIOD events

Composites of PDSI for El Niño, pIOD, and co-occurring events highlight the distinct impacts of the two modes on drought across the Indian subcontinent (figures 2(a)–(c)). During El Niño events, much of India suffers drought conditions (figure 2(a)). This is particularly apparent in the centre and northwest regions that make up the core monsoon region (cf inset figure 1(a)): PDSI values are in excess of -3 indicating severe drought conditions. In contrast, no consistent large-scale features in drought incidence are observed during co-occurring El Niño and pIOD events (figure 2(b)). Anomalous wet conditions with a PDSI in excess of $+2$ are found during pIOD events for the northern half of the Indian subcontinent (figure 2(c)).

The PDSI time-series spatially averaged over the Indian core monsoon region (see box in figure 2(a)) for the period 1877–2006 shows that more than 85% of El Niño events were associated with negative PDSI values (figure 2(d)). About 50% of El Niño events were associated with very severe drought conditions, while more than 60% of pIOD events had PDSI values in excess of $+1$. Decadal variability in the PDSI time-series related to changes in the numbers of ENSO and IOD events matches that seen from the rainfall time-series (cf table 1 and figure 1).

5. Climate conditions during El Niño and pIOD events

For a better understanding of the contrasting rainfall and drought responses associated with the different mode phases,

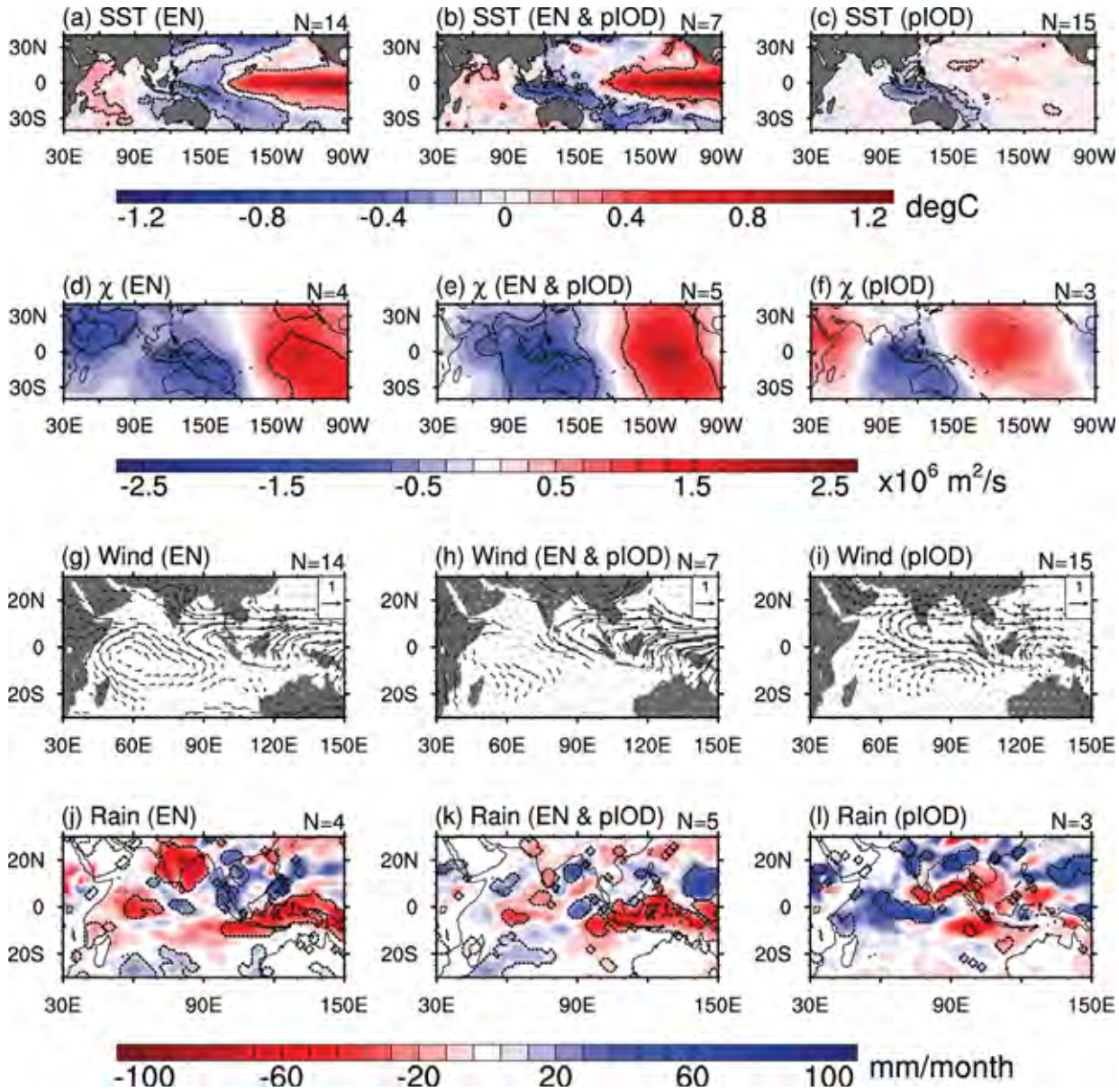

Figure 3. Composite anomalies during (left) El Niño, (middle) combined El Niño and pIOD, and (right) pIOD events averaged for the June–September months for (a)–(c) SST (°C), (d)–(f) 850 hPa velocity potential χ ($m^2\ s^{-1}$), (g)–(i) 850 hPa winds ($m\ s^{-1}$), and (j)–(l) rainfall (mm $month^{-1}$). Anomalies for χ and rainfall are based on the period 1948–2006, SST and winds on 1877–2006. The number of members (N) in each category is indicated. The area enclosed by the dashed contours and the black arrows denote anomalies that are significant as estimated by a two-tailed t-test at the following confidence levels: 90% for SST and χ, and 80% for winds and rainfall.

the anomalous large-scale circulation features across the Indo-Pacific region are explored for El Niño, pIOD, and the co-occurrence of these events (figure 3). For the three respective event categories, composite anomalies are shown for SST, velocity potential χ, winds, and rainfall. A higher number of events in the composites exist for SST and winds, as the analysis is over the 1877–2006 period, while the shorter period 1948–2006 is used for the other variables due to the constraints in data availability (cf section 2). The larger spatial extent of significant anomalies in figures 3(a)–(c) and (g)–(i) can largely be attributed to this fact. The winds are presented at the 850 hPa level, which is well suited to the study of monsoon dynamics [30]. Velocity potential, which provides an indication of subsidence associated with the large-scale circulation, is shown at the same level for consistency. Anomalies in the velocity potential at 200 hPa (figure not shown) highlight a comparable pattern, but of opposite sign, confirming the low-level results.

Pure El Niño events are characterized by warm SST anomalies, exceeding 1.5 °C, in the eastern equatorial Pacific, surrounded by cold anomalies in the classical 'horseshoe' pattern in the subtropics and western tropical Pacific (figure 3(a)). In the Indian Ocean, warm (cold) SST anomalies are observed in the western (eastern) tropical region. The cold SST anomalies in the eastern Indian Ocean are mainly located off the northwest shelf of Australia, south of the

IOD eastern pole of [6]. The velocity potential shows anomalous rising motion over the eastern Pacific, while anomalous subsidence occurs over the western Pacific warm pool region, the Maritime Continent, and the Australian region (figure 3(d)). In addition, an anticyclonic anomaly associated with anomalous subsidence is also observed over the Indian subcontinent extending west across the Indian Ocean towards East Africa. The regional winds at 850 hPa are consistent with the anomalous subsidence over India, with easterly anomalies over the Arabian Sea (5°–20°N) extending from India to the East African coastline (figure 3(g)). The easterly wind anomalies represent a weakening of the moisture-bearing onshore westerlies during the Indian summer monsoon, and this is consistent with the anomalous dry conditions during El Niño years (figure 3(j)).

For pIOD events, the cold SST anomalies around the Maritime Continent dominate (figure 3(b)) due to enhanced upwelling and southeasterly anomalies in the equatorial eastern Indian Ocean (figure 3(i)). There is a suggestion of moderate anomalous subsidence over the Australian region, flanked by two regions of anomalous ascent over eastern Africa and the central Pacific (figure 3(f)), however, the values are not statistically significant. Significantly enhanced westerly winds are, however, observed over the northern Indian Ocean, including the Arabian Sea, Bay of Bengal, and India (figure 3(i)), accounting for anomalous wet conditions across western India and the core monsoon region during pIOD events (figure 3(l)).

During co-occurring El Niño and pIOD years, the warm equatorial SST anomalies in the eastern Pacific are enhanced relative to pure El Niño events (cf figures 3(a) and (b)). The cold anomalies are clearly apparent in the eastern tropical Indian Ocean, around the Maritime Continent, and western Pacific warm pool region (figure 3(b)), while only a localized area of above-average SST can be seen to the west of the Indian subcontinent. Consistent with the SST anomaly pattern, anomalous ascending motion is observed over the eastern Pacific. Anomalous subsidence dominates across the western Pacific and eastern Indian Ocean, with the centre of subsidence located over the Maritime Continent and India at the western edge of the anomalous vertical motion (figure 3(e)). Consequently over India, the winds at 850 hPa do not show any significant changes during co-occurring El Niño and pIOD events (figure 3(h)), nor are there any significant rainfall anomalies except in a few very localized regions (figure 3(k)).

6. Discussion and conclusions

We have assessed the impact of El Niño and pIOD events, both individually and in combination, on the Indian summer monsoon season (JJAS) for the period 1877–2006. The majority of pure El Niño events are associated with significant reductions in monsoon rainfall and widespread drought conditions due to anomalous subsidence over the Indian subcontinent, associated with changes in the zonal Walker circulation and weakening of the onshore monsoon circulation over India. This is consistent with previous work detailing the mechanisms for Indian monsoon failure during El Niño events [3, 9, 2, for example]. In contrast, during pure pIOD events increased rainfall generally occurs due to an intensified monsoon circulation, resulting in anomalously enhanced positive PDSI values. During co-occurring pIOD and El Niño events, the El Niño-modulation of Indian monsoon rainfall is absent and normal rainfall levels are maintained. During combined events there is anomalous subsidence associated with the Indo-Pacific SST anomaly pattern centered over the Maritime Continent, as also shown by [9] in AGCM simulations.

Using a classification for ENSO and IOD events for the past 130 years, we have expanded on previous observational studies [8, for example] and shown that decadal variations in Indian Ocean conditions modulate the ENSO–Indian monsoon relationship. In the first half of the 20th century, six El Niño events were accompanied by severe Indian monsoon failures; this period is notable for a prolonged absence of co-occurring pIOD and El Niño events and high JJAS monsoon rainfall variability. In contrast, a trend towards more frequent pIOD events has occurred over recent decades [17]; this is reflected in a significantly enhanced incidence of co-occurring pIOD and El Niño events post-1975, the lowest interannual monsoon variability observed over the last 130 years, and a reduced frequency of pure El Niño events. Recent trends in tropical Indian Ocean variability are therefore able to help explain the weakening relationship between ENSO and the Indian monsoon, adding to previous explanations of changing land–sea temperature gradients [3] and the characteristics of El Niño events [2]. The role of the Pacific Ocean in forcing recent Indian Ocean trends, as well as modulating decadal variability within that basin, remains to be assessed.

In summary, whether an El Niño event causes a failure of the Indian monsoon and resulting drought conditions can largely be determined by the state of the Indian Ocean. Earlier work has demonstrated that the modulation of the monsoon by El Niño depends on the location of maximum warming in the equatorial Pacific [2]. Here, we demonstrate that changes in Indian Ocean variability play an important role in modulating the ENSO-related monsoon rainfall response on multi-decadal timescales.

Acknowledgments

We are grateful for the following data sets: Indian regional/subdivisional Monthly Rainfall by the Indian Institute of Tropical Meteorology; HadISST by the UK Met Office; PDSI, CMAP, and NNR provided by NOAA/OAR/ESRL PSD, Boulder, Colorado, USA. Two anonymous reviewers are gratefully acknowledged for their helpful comments. This work was supported by the Australian Research Council.

References

[1] Webster P J and Hoyos C D 2010 Beyond the spring barrier? *Nat. Geosci.* **3** 152–3

[2] Krishna Kumar K, Rajagopalan B, Hoerling M P, Bates G and Cane M 2006 Unraveling the mystery of Indian monsoon failure during El Niño *Science* **314** 115–9

[3] Krishna Kumar K, Rajagopalan B and Cane M A 1999 On the weakening relationship between the Indian monsoon and ENSO *Science* **284** 2156–9
[4] Ashok K, Behera S K, Rao S A, Weng H and Yamagata T 2007 El Niño Modoki and its possible teleconnection *J. Geophys. Res.* **112** C11007
[5] Schott F A, Xie S-P and McCreary J P 2009 Indian Ocean variability and climate variability *Rev. Geophys.* **47** RG1002
[6] Saji N H, Goswami B N, Vinayachandran P N and Yamagata T 1999 A dipole mode in the tropical Indian Ocean *Nature* **401** 360–3
[7] Webster P J, Moore A M, Loschnigg J P and Leben R R 1999 Coupled ocean–atmosphere dynamics in the Indian Ocean during 1997–98 *Nature* **401** 356–60
[8] Ashok K, Guan Z and Yamagata T 2001 Impact of the Indian Ocean dipole on the relationship between the Indian monsoon rainfall and ENSO *Geophys. Res. Lett.* **28** 4499–502
[9] Ashok K, Guan Z, Saji N H and Yamagata T 2004 Individual and combined influences of the ENSO and Indian Ocean dipole on the Indian summer monsoon *J. Clim.* **17** 3141–55
[10] Ihara C, Kushnir Y, Cane M A and De la Pena V H 2007 Indian summer monsoon rainfall and its link with ENSO and Indian Ocean climate indices *Int. J. Climatol.* **27** 179–87
[11] Ihara C, Kushnir Y and Cane M A 2008 July droughts over homogeneous Indian Monsoon region and Indian Ocean dipole during El Niño events *Int. J. Climatol.* **28** 1799–805
[12] Gadgil S, Vinaychandran P N, Francis P A and Gadgil S 2004 Extremes of the Indian summer monsoon rainfall, ENSO and equatorial Indian Ocean oscillation *Geophys. Res. Lett.* **31** L12213
[13] Turner A G and Hannachi A 2010 Is there regime behaviour in monsoon convection in the late 20th century? *Geophys. Res. Lett.* **37** L16706
[14] Niyogi D, Kishtawal C, Tripathi S and Govindaraju R S 2010 Observational evidence that agricultural intensification and land use change may be reducing the Indian summer monsoon rainfall *Water Resour. Res.* **46** W03533
[15] Ji Z, Kang S, Zhang D, Zhu C, Wu J and Xu Y 2011 Simulation of the anthropogenic aerosols over South Asia and their effects on Indian summer monsoon *Clim. Dyn.* **36** 1633–47
[16] Ihara C, Kushnir Y and Cane M A 2008 Warming trend of the Indian Ocean SST Indian Ocean dipole from 1880 to 2004 *J. Clim.* **21** 2035–46
[17] Cai W, Cowan T and Sullivan A 2009 Recent unprecedented skewness towards positive Indian Ocean dipole occurrences and their impact on Australian rainfall *Geophys. Res. Lett.* **36** L11705
[18] LeBlanc M J, Tregoning P, Ramillien G, Tweed S O and Fakes A 2009 Basin-scale, integrated observations of the early 21st century multiyear drought in southeast Australia *Water Resour. Res.* **45** W04408
[19] Dai A, Trenberth K E and Qian T 2004 A global data set of Palmer drought severity index for 1870–2002: relationship with soil moisture and effects of surface warming *J. Hydrometeorol.* **5** 1117–30
[20] Smakhtin V U and Hughes D A 2004 Review, automated estimation and analyses of drought indices in South Asia *Working Paper 83* (Colombo, Sri Lanka: International Water Management Institute) p 24
[21] Cook E R, Anchukaitis K J, Buckley B M, D'Arrigo R D, Jacoby G C and Wright W E 2010 Asian monsoon failure and megadrought during the last millennium *Science* **328** 486–9
[22] Meyers G, McIntosh P, Pigot L and Pook M 2007 The years of El Niño, La Niña and interactions with the tropical Indian Ocean *J. Clim.* **20** 2872–80
[23] Ummenhofer C C, England M H, Meyers G A, McIntosh P C, Pook M J, Risbey J S, Sen Gupta A and Taschetto A S 2009 What causes Southeast Australia's worst droughts? *Geophys. Res. Lett.* **36** L04706
[24] Parthasarathy B, Munot A A and Kothawale D R 1994 All India monthly and seasonal rainfall series: 1871–1993 *Theor. Appl. Climatol.* **49** 217–24
[25] Kistler R *et al* 2001 The NCEP-NCAR 50-year reanalysis: monthly means CD-ROM and documentation *Bull. Am. Meteorol. Soc.* **82** 247–67
[26] Xie P and Arkin P A 1996 Analyses of global monthly precipitation using gauge observations, satellite estimates, and numerical model predictions *J. Clim.* **9** 840–58
[27] Compo G P, Whitaker J S and Sardeshmukh P D 2006 Feasibility of a 100 year reanalysis using only surface pressure data *Bull. Am. Meterol. Soc.* **87** 175–90
[28] Rayner N A, Parker D E, Horton E B, Folland C K, Alexander L V and Rowell D P 2003 Global analyses of SST, sea ice and night marine air temperature since the late nineteenth century *J. Geophys. Res.* **108** 4407–35
[29] D'Arrigo R, Abram N, Ummenhofer C, Palmer J and Mudelsee M 2011 Reconstructed streamflow for Citarum River, Java, Indonesia: linkages to tropical climate dynamics *Clim. Dyn.* **36** 451–62
[30] Webster P J, Magana V O, Palmer T N, Shukla J, Tomas R A, Yanai M and Yasunari T 1998 Monsoons: processes, predictability, and the prospects for prediction *J. Geophys. Res.* **103** 14451–510